2021-01-15

Fundamental Understanding of Warm Lime Softening Process to Improve Steam Assisted Gravity Drainage Produced Water Treatment Performance

Zhang, Lu

UNIVERSITY OF CALGARY

Fundamental Understanding of Warm Lime Softening Process to Improve Steam Assisted Gravity Drainage Produced Water Treatment Performance

by

Lu Zhang

A THESIS

SUBMITTED TO THE FACULTY OF GRADUATE STUDIES

IN PARTIAL FULFILMENT OF THE REQUIREMENTS FOR THE

DEGREE OF MASTER OF ENGINEERING

GRADUATE PROGRAM IN CHEMICAL AND PETROLEUM ENGINEERING

CALGARY, ALBERTA

JANUARY, 2021

Abstract

Since the commercialization of the first steam assisted gravity drainage (SAGD) enhanced oil recovery facility in 2001, the warm lime softening (WLS) process has been commonly deployed as part of a SAGD central processing facility (CPF) water treatment plant. The principal process goal of the WLS process is to remove dissolved hardness (e.g. calcium and magnesium ions) and silica by the addition of lime ($Ca(OH)_2$), magnesium oxide (MgO), soda ash (Na_2CO_3), coagulant, and flocculant. Although the WLS process has been operated for almost 30 years in the oil sands industry, the fundamental electrokinetic properties of the particles generated are not thoroughly investigated. The high temperature, high silica and dissolved organic concentrations also make the WLS unique compared to the traditional cold lime softening process used in municipal water treatment and other industrial water treatment. The understanding of the electrokinetic properties of particle suspensions is of paramount importance as it directly relates to the performance of sedimentation and clarification, as well as the selection of chemicals and doses. Furthermore, the understanding of the impact of feed water chemistry deviations on the charge behaviors of the particle suspensions and on the coagulant dose is of significant practical implications for the WLS operations. This research was undertaken to investigate the surface charges of the two most common softening particles, calcium carbonate ($CaCO_3$) and magnesium hydroxide ($Mg(OH)_2$), under SAGD WLS conditions from zeta potential perspective. A number of experimental conditions (pH, temperature, presence of other ions, additions of other chemicals) were varied to exam the impact on the zeta potential of two softening particles. Visual MINTEQ modelling was utilized to predict chemical speciation under various conditions and was used to assist with data interpretation. High temperature (65°C) jar tests were also performed using synthetic SAGD produced water (PW) samples to simulate the WLS process and assess the impact of feed water

deviations (silica, clay, humic acid, $Ca(OH)_2$, MgO, Na_2CO_3, $NaHCO_3$, $CaCl_2$, and $MgCl_2$) on the dose of a polyamine-based cationic coagulant. The electrokinetic study revealed that pH, and the type of ions and functional groups present in solution are the main impacting factors on the zeta potential of softening particles. The coagulation study revealed that the coagulant dose was significantly influenced by humic acid and silica. The findings of this research can provide insightful knowledge to SAGD operators regarding process monitoring, approaches to onsite chemical optimization, possible controls during an influent water off-specification event.

Keywords: Steam assisted gravity drainage; warm lime softening; thermodynamic modeling; calcium carbonate; magnesium hydroxide; potential determining ions; coagulation; flocculation

Preface

Chapter 3 of this thesis has been published as **Lu Zhang**, Dinesh Mishra, Kailun Zhang, Basil Perdicakis, David Pernitsky, and Qingye Lu, "Electrokinetic Study of Calcium Carbonate and Magnesium Hydroxide Particles in Lime Softening" in Water Research, 2020, 186, 116415 (doi.org/10.1016/j.watres.2020.116415).

Chapter 4 of this thesis includes a manuscript to be submitted as **Lu Zhang**, Dinesh Mishra, Kailun Zhang, Basil Perdicakis, David Pernitsky, and Qingye Lu, "Impact of Solution Feed Deviations on Polymer Coagulant Dose in Synthetic SAGD Produced Water".

The work in Chapter 3 and Chapter 4 was also presented as "Charge Characteristics of Particles in SAGD Warm Lime Softeners" at the International Water Conference on November 9, 2020.

Acknowledgments

First and foremost, I would like to express my sincere gratitude to my supervisor, Dr. Qingye (Gemma) Lu, for giving me the opportunity to conduct research in her group, as well as for her continuous support, invaluable guidance, encouragement, and mentoring during the course of my graduate study. I would also like to thank my thesis committee members, Dr. Simon Park and Dr. Maen Husein, for their constructive feedback.

I am extremely grateful for the enormous support and assistance provided by Dr. Dinesh Mishra and Kailun Zhang throughout my research project. Also, many thanks to Dr. David Pernitsky and Dr. Basil Perdicakis for offering industrial insights that helped produce two quality manuscripts.

I would also like to express my deep gratitude for the support from the Natural Sciences and Engineering Research Council of Canada (NSERC) Discovery Grant, the Start-up Fund and the Seed Grant from the University of Calgary, NSERC-Engage Grant, the Alberta Innovates Water Innovation Program, Suncor Energy, Stantec Consulting Ltd., the Canada First Research Excellence Fund (CFREF) for its Global Research Initiative in Sustainable Low Carbon Unconventional Resources, and Canada Foundation of Innovation (CFI).

Finally, I would like to thank my lovely wife, Carrie, and my little girl, Everly, who have been my champion and blessed me with a ray of sunshine.

Table of Contents

List of Tables

List of Figures and Illustrations

List of Abbreviations

Abbreviation	Definition
BBD	Boiler Blowdown
BFW	Boiler Feed Water
BS&W	Bottom Sediments and Water
CLS	Cold Lime Softening
CPF	Central Processing Facility
DMA	Dimethylamine
DOM	Dissolved Organic Matter
EPA	Environmental Protection Agency
EPI	Epichlorohydrin
ESEM	Environmental Scanning Electron Microscopy
HA	Humic Acid
ICP-OES	Inductively Coupled Plasma Optical Emission Spectrometer
LEED	Low Energy Electron Diffraction
MUW	Make-up Water
OTSG	Once Through Steam Generator
PDI	Potential Determine Ion
polyDDA	Polydiallyldimethylammonium
PW	Produced Water
PZC	Point Zero Charge
SAGD	Steam Assisted Gravity Drainage
SI	Saturation Index

TDS	Total Dissolved Solids
TIC	Total Inorganic Carbon
TOC	Total Organic Carbon
WAC	Weak Acid Cation
WLS	Warm Lime Softening
XPS	X-ray Photoelectron Spectroscopy
TOC	Total Organic Carbon

List of Nomenclature and Symbols

Symbol	Definition
$F(ka)$	Henry Function
U_E	Electrophoretic Mobility
$\psi_{\sigma\tau}$	Stern Potential
ζ	Zeta Potential
ε	Dielectric Constant of Water
η	Water Viscosity

Chapter 1 Introduction

1.1 Overview of Steam Assisted Gravity Drainage Operation

Canada has the world's third-largest oil reserves, 97% of which is Alberta's oil sands (Natural Resouces Canada 2020). Alberta's oil sands mainly consist of sand, clay or other minerals, water, and bitumen, and can be found in three (3) deposits: Athabasca, Peace River, and Cold Lake, with proven reserves of 166 billion barrels (Natural Resouces Canada 2020). The bitumen is typically of very high viscosity, therefore enhanced oil recovery methods are needed to produce oil. Approximately, 20% of oil sands is adjacent to the surface and can be mined; the reminder (in situ oil sands) is too deep for the mining operation and often recovered by either steam assisted gravity drainage (SAGD) or cyclic steam stimulation (CSS). The SAGD enhanced oil recovery is commonly used in the Athabasca deposit and requires the drilling of two horizontal wells - an injector (injection well) and a producer (production well) that is typically located five (5) meters below the injector. Steam is injected into the injection well with the goal to reduce bitumen viscosity and have a manageable flow. Bitumen, also commonly referred to as emulsion in the field, drains to the production well primarily due to the gravitational force. A central processing facility (CPF), which typically consists of an oil treating facility, a de-oiling facility, a water treatment facility, a steam generation facility, and a disposal water treatment facility (**Figure 1.1**). The produced emulsion from the production well pads proceeds to the oil treating facility where oil and residual gas are separated from the water. The purpose is to produce oil with a bottom sediments and water (BS&W) content less than 0.5 wt%. The oily produced water (PW) then enters the de-oiling facility where the bitumen-in-water content is lowered to 5 ppm (hexane extraction method). The PW from the de-oiling facility flows to the water treatment facility, where silica, calcium, magnesium, iron, and suspends solids are removed to meet the typical once-through

steam generator (OTSG) feed water specifications. The treated water or the boiler feed water (BFW) is heated up in the steam generation facility to produce high temperature and pressure steam, which is about 80% steam quality. A portion (depends on the upstream PW quality) of the boiler blowdown (BBD) generated from the OTSGs is typically recycled to the water treatment facility and the rest is sent to the disposal water treatment facility where the high concentration brine is injected into disposal wells after pH adjustment for silica removal.

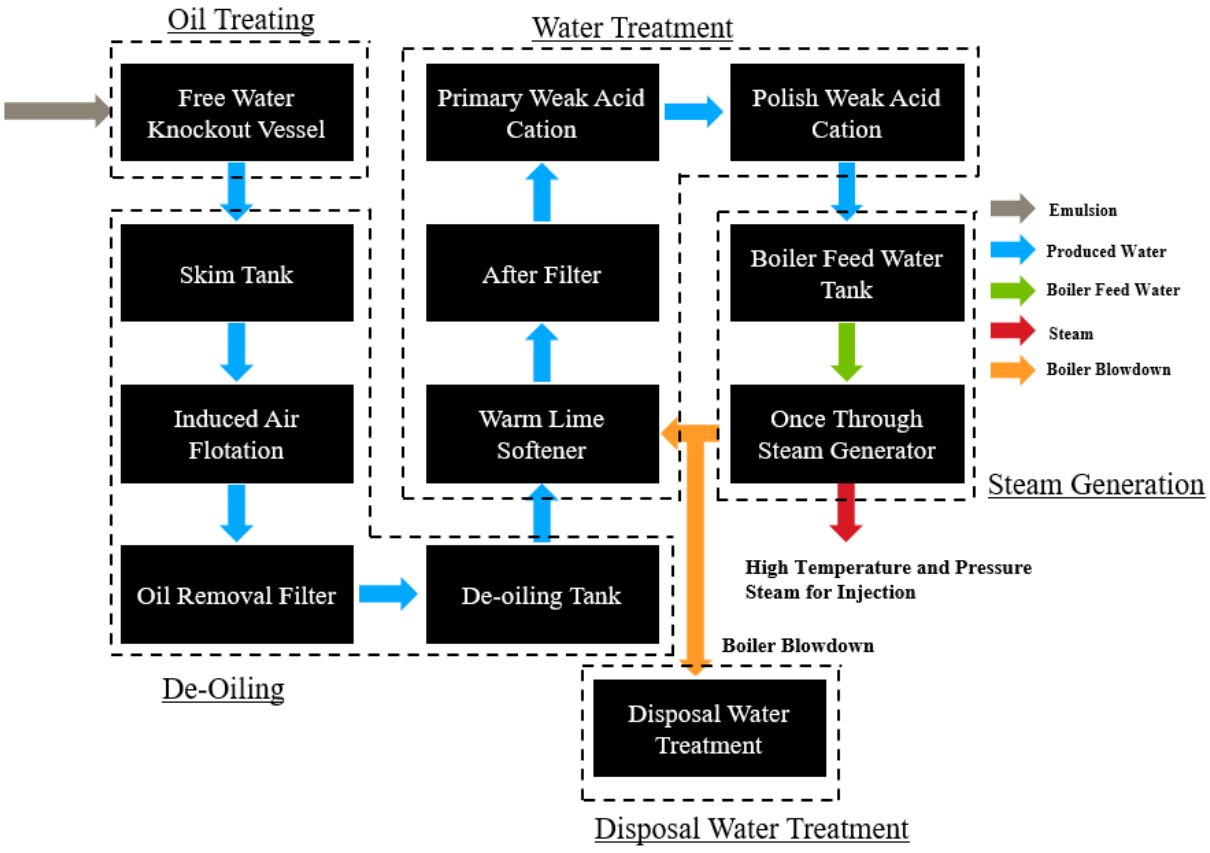

Figure 1.1. Block flow diagram of simplified SAGD central processing facility.

1.2 Warm Lime Softening

In a SAGD CPF, there are two types of water treatment processes: chemical reaction based and heat transfer based. The heat transfer based water treatment process utilizes evaporative

technology to produce condensate which is collected and used as BFW. Due to the process nature of the heat transfer based process, the BFW generated is generally low in total dissolved solids (TDS) and hardness, and is of higher quality compared to the BFW generated from the chemical reaction based process. Because of the better qualify of BFW, the BBD generate also has a less load of concentrated contaminates and can even be recycled directly back to a BFW storage tank. The major drawback of using the heat transfer-based water treatment process is the high energy consumption (W. Heins and Peterson 2005). The chemical-based water treatment process starts with a warm lime softener followed by after filters, primary weak acid cation (WAC) units, and polishing WAC units. The main disadvantages of employing a WLS are the high chemical dosing (W. Heins and Peterson 2005) and the complexity of the process. As mentioned above, the BBD generated is partially recirculated back to the WLS which adds additional complexity to the process. Nevertheless, the goals of both processes are to produce BFW that meets the influent specifications of the OTSGs' and to maintain the integrity of the downstream equipment.

As shown in **Figure 1.2**, the WLS unit typically receives PW from the deoiling facility and BBD from the steam generation facility. Other plant miscellaneous streams such as condensate, backwash recycled from after filter and WACs, and even tailings water may go to the WLS depending on the plant configuration and operational strategy. The generated sludge is partially recirculated back to the rapid mixing zone for seeding and settling enhancement. The main process goals of the WLS are: 1. reduce the soluble calcium and magnesium hardness to 5 ppm as $CaCO_3$ (typical) and 2. reduce the dissolved silica content to as least 50 ppm (typical).

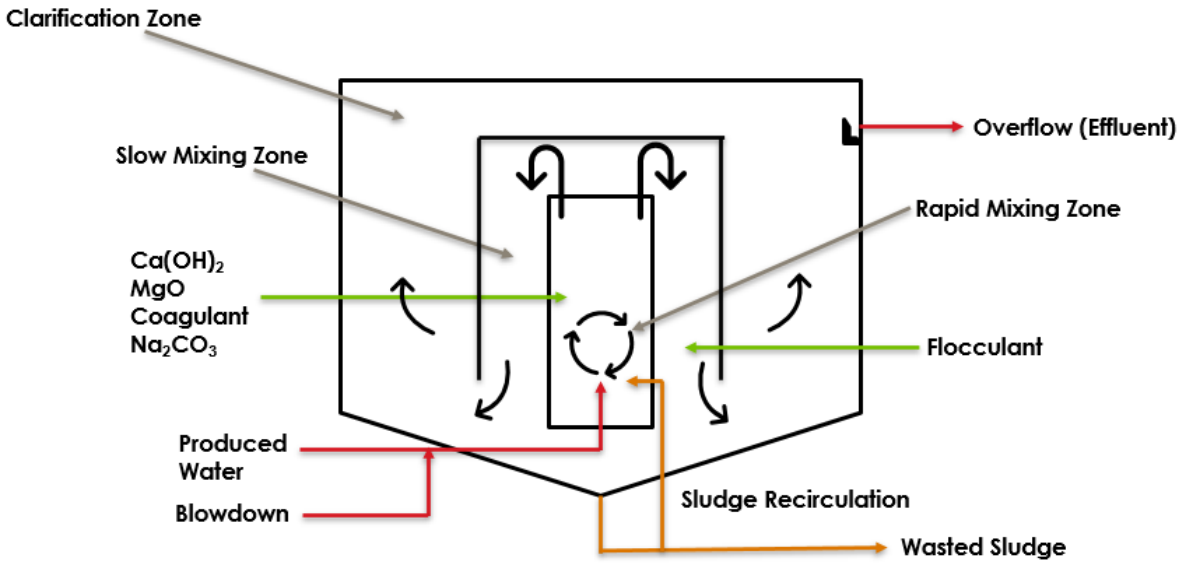

Figure 1.2. Simplified schematic of warm lime softener.

In a WLS operation, it is critical to control M alkalinity (HCO_3^-) and P alkalinity (CO_3^{2-}) for the most effective removal of the soluble hardness. Some of the reactions occurring within the WLS are as follows:

$$Ca(OH)_2 \rightarrow Ca^{2+} + 2OH^-$$

$$HCO_3^- + OH^- \rightarrow CO_3^{2-} + H_2O$$

$$Ca^{2+} + CO_3^{2-} \rightarrow CaCO_3 \downarrow$$

$$Mg^{2+} + 2OH^- \rightarrow Mg(OH)_2 \downarrow$$

$$Mg^{2+} + CO_3^{2-} \rightarrow MgCO_3^- \downarrow$$

Table 1.1 outlines typical WLS feed water characteristics. $Ca(OH)_2$ and MgO slurries are added into the rapid mixing zone where soluble calcium and magnesium hardness precipitate as $CaCO_3$ and $Mg(OH)_2$ and silica precipitates by reacting with MgO through adsorption and coprecipitation. The addition of $Ca(OH)_2$ raises the pH (or provides OH^- alkalinity) and shifts bicarbonate

alkalinity to carbonate (CO_3^{2-}) alkalinity. The target pH is approximately 9.5 – 10.5. The OH^- and carbonate alkalinity promote the removal of Mg^{2+} and Ca^{2+} hardness, respectively. Some PW is rich in ferrous and ferric, which can also be removed at the operating pH of a WLS unit through precipitation reactions. The addition of MgO also helps raise the pH but with the main goal to remove silica by both adsorption and coprecipitation. Na_2CO_3 is typically added on an as-needed basis to provide supplementary alkalinity to the feed water. The coagulant is added to the rapid mixing zone to neutralize the charges on the precipitated particles to promote agglomeration, as well as to help with the removal of dissolved organics. The flocculant is added to the slow mixing zone to enhance settling. Some SAGD operators may add bentonite clay into the WLS to help remove excessive oil carried over from the upstream processes.

Table 1.1: Typical SAGD WLS feed water characteristics

Parameters	**Value**
pH (s.u)	7.5 – 9.0
TDS (mg/L)	3,000
Hardness (mg/L as $CaCO_3$)	10 - 25
Bicarbonate Alkalinity (mg/L as HCO_3^-)	350 - 700
TOC (mg/L)	150 - 800
Silica (mg/L as SiO_2)	150 - 350

1.3 Zeta Potential

In an aqueous system, suspended particle surfaces can develop surface charges in three principal ways: 1. Chemical reactions at the surfaces may cause the formation of surface charges; 2. Lattice imperfections at the solid surface or isomorphous replacements within the lattice at the phase

boundary may lead to surface charge development; 3. The adsorption of a hydrophobic species or surfactant ions may also promote the development of a surface charge (Stumm 1992). One of the most classic models to demonstrate the electric state of a particle surface is the Gouy-Chapman diffuse model shown in **Figure 1.3**. In this model, a particle surface carries charges and is surrounded by a layer of free ions in the liquid phase. The layer is referred to as an electric double layer, which comprises of a stern layer (also known as Helmholtz layer) and a diffuse layer. The Stern layer represents the counterions bounded to the particle surface. The diffuse layer consists of an atmosphere of ions in rapid thermal motion around the particle surface (Israelachvili 1992). The interface of the stern layer and the diffuse layer is often described as the slipping plane or the shear plane. Due to the charges on the particle surfaces, particles tend to repel each other which makes them suspended and difficult to settle. Therefore, coagulants and flocculants are commonly used in water and wastewater sedimentation and clarification processes with the intent to neutralize particle charges and promote settling. The significance of particle surface charges can not be easily overestimated in many water and wastewater treatment processes. However, the surface charge on a particle surface can not be directly measured. Zeta potential (ζ) or electrokinetic potential, which reflects the potential difference between the slipping plane and the diffuse layer, is a commonly used parameter to qualitatively represent the surface charge of particles.

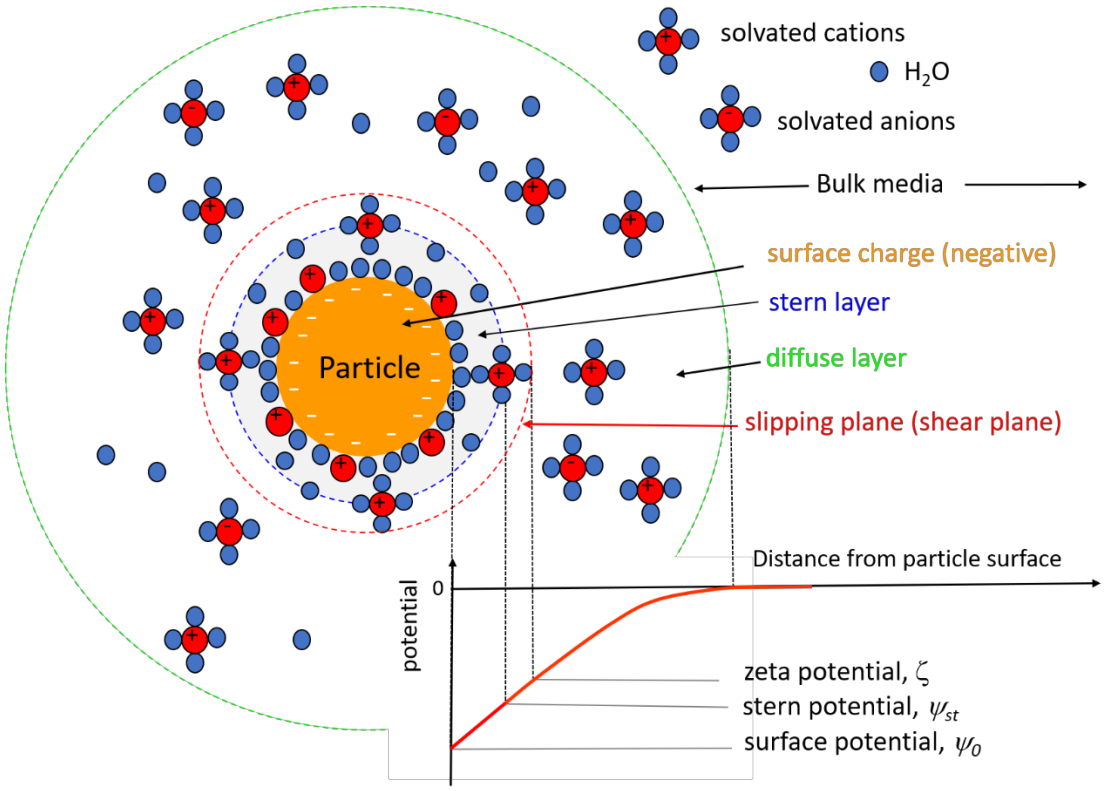

Figure 1.3. Schematic of an electric double layer.

The zeta potential of a suspended particle can be measured by using the technique called electrophoresis, which refers to the movement of the suspended and charged particles relative to a stationary solution in an electric field applied (Bratby 2006). A commonly used method to measure the mobility of the charged particles is dynamic light scattering . **Figure 1.4** shows the principles of a dynamic light scattering-based zeta potential measurement instrument. A water sample containing suspended particles is injected into a measurement cell or vial, which has a pair of electrodes. The measurement cell is then placed in a zeta potential measurement instrument, where a voltage is applied onto the electrodes and create an electrical field at either end of the measurement cell. Due to the electric field applied, the charged particles move to the oppositely charged electrode. At the same time, the laser generates two beams of light – one directly goes through the measurement cell where the light is scattered resulting in a change of frequency, and

the other one is acting as the reference beam. The electrophoretic mobility of particles, which is determined by comparing the frequencies of the two beams of light, is used to calculate the zeta potential using the Henry equation (Skoglund et al. 2017):

$$\mu_e = 2\varepsilon_r\varepsilon_0\zeta f(\kappa a)/3\eta,$$

where μ_e is the electrophoretic mobility, ε_r is the relative permittivity, ε_0 is the permittivity of vacuum, ζ is the zeta potential, η is the viscosity of water, and $f(\kappa a)$ is the Henry function. Henry equation can be simplified by replacing the term $F(\kappa a)$ with a value of 1.5 – the simplified equation is known as the Helmholtz Smoluchowski Equation (Skoglund et al. 2017).

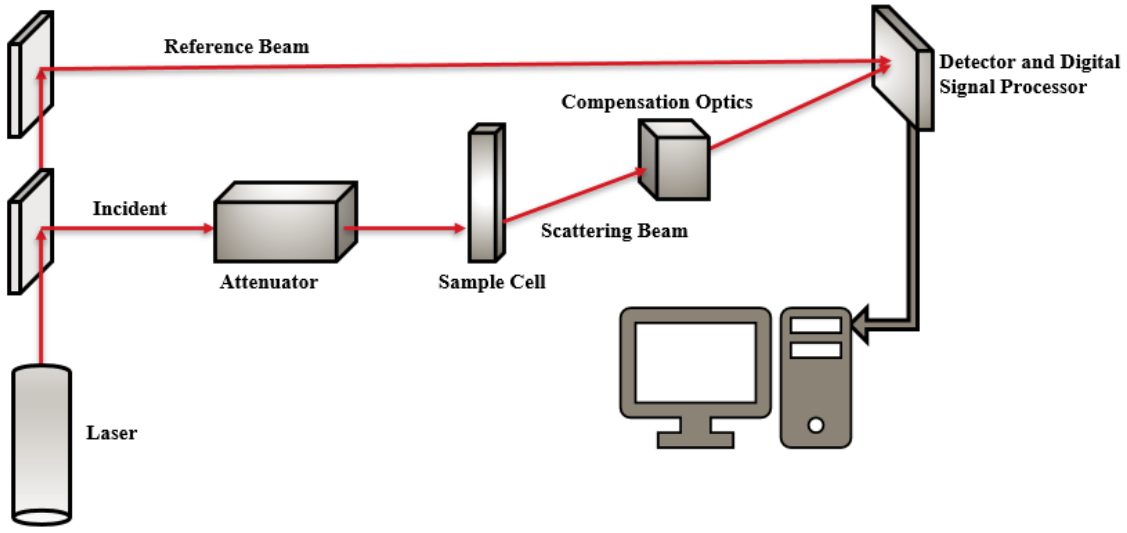

Figure 1.4. Schematic of zeta potential measurement

1.3.1 Electrokinetic Properties of $CaCO_3$

$CaCO_3$ particles are commonly present in many water and wastewater treatment processes. Most of the studies conducted by others focus on the charge characterization of $CaCO_3$ particles under

simulated municipal CLS conditions. Black and Christman (1961) performed CLS experiments and reported that $CaCO_3$ particles (freshly precipitated and filtered sludge) were negatively charged when pH is in the range of 9 to 11, and the presence of $Mg(OH)_2$ particle and the addition of Mg^{2+} ions reversed the surface charge of $CaCO_3$ particles from negative to positive. In another CLS study, it was reported that freshly precipitated $CaCO_3$ particles shown a slight positive zeta potential at lower pH values, negative zeta potential at pH values ranging from 9 to 10.5, and positive zeta potential at pH values ranging from10.5 to 11.6 (Russell et al. 2009). Some of the published studies focused on exploring the potential determine ions (PDIs) of $CaCO_3$ particles. Moulin and Roque suggested that the PDIs of $CaCO_3$ particles are Ca^{2+} and HCO_3^-(Moulin and Roques 2003). Alroudhan et al. found that Ca^{2+} and Mg^{2+} ions have very comparable impact on the zeta potential of natural calcite ($CaCO_3$), which became more negatively charged with the increasing concentrations of Ca^{2+} and Mg^{2+} (Alroudhan, Vinogradov, and Jackson 2016). Foxall et al. indicated in their study that the zeta potential (via electrophoretic mobility) of $CaCO_3$ particles is primarily driven by PDIs and secondarily affected by pH (Foxall et al. 1979; Eriksson, Merta, and Rosenholm 2007; Thompson and Pownall 1989). Based on X-ray photoelectron spectroscopy (XPS) and low energy electron diffraction (LEED) methods, it was shown that $CaCO_3$ particles carry $>CO_3H$ and >CaOH functional groups in an aqueous system (S. L. Stipp and Hochella 1991). These functional groups can interact with PDIs, such as H+, OH-, metal ions, carbonate (CO_3^{2-}), bicarbonate (HCO_3^-) and CO_2 (aq), by adsorption or desorption (Stumm 1992). Stumm also suggested the schematic shown in **Figure 1.5** to describe the shifting of functional groups under various influences.

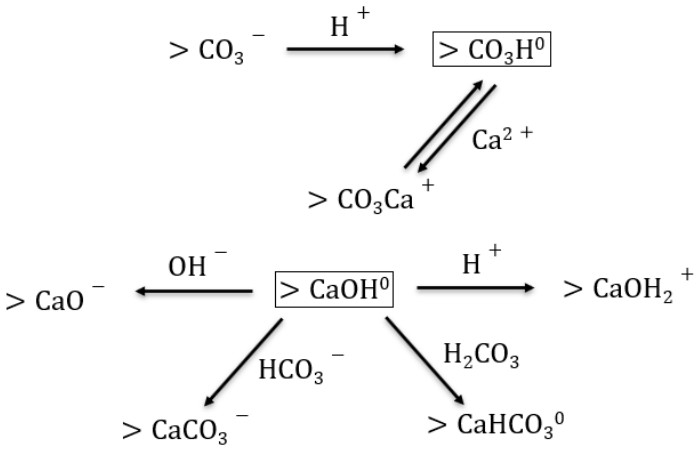

Figure 1.5. $CaCO_3$ particle charge development scheme

These studies have shown a large variety of charges on $CaCO_3$ particles and some results were even contradictory. Additionally, almost all studies reviewed were concentrating on assessing the zeta potential of $CaCO_3$ particles at room temperature and non-SAGD lime softening conditions regarding water chemistry.

1.3.2 Electrokinetic Properties of $Mg(OH)_2$

Compared to $CaCO_3$ particles, there are much fewer studies conducted to investigate the zeta potential of $Mg(OH)_2$ particles. One of the early studies done by Park suggested that point zero charge (PZC) of $Mg(OH)_2$ particles is approximately 12 (Parks 1965). Using electrokinetic measurement, McLaughlin et al indicated that the PZC of brucite (preformed $Mg(OH)_2$ particles) is greater than a pH of 12 (McLaughlin, White, and Hem 1993). In another study, it was found the PZC of freshly precipitated $Mg(OH)_2$ particles is around pH of 10.8 (Schott 1981). These studies indicated that $Mg(OH)_2$ particles are generally positively charged when pH is greater than 12 and negatively charged when pH is less than 10.8, depending on particle origin. Russell et al reported

a similar observation, and found that freshly precipitated $Mg(OH)_2$ particles were amorphous at all tested pH conditions by looking at environmental scanning electron microscopy (ESEM) images; they also suggested that the possible potential functional groups of $Mg(OH)_2$ particles are $>MgO^-$, $>MgOH^0$, and $>MgOH^{2+}$(Russell et al. 2009). Parks suggested in his study that H^+, OH^- and all hydroxo complexes would either adsorb physically (non-dissociatively) or chemically (dissociatively) onto particle surfaces and play important roles in establishing surface charge, and are PDIs for $Mg(OH)_2$ particles (Parks 1965). Similar to the available studies done on $CaCO_3$ particles, most of the studies done on $Mg(OH)_2$ particles were performed at CLS conditions that might not be directly applied to SAGD WLS particles.

1.3.3 Electrokinetic Properties of Humic Acids

Humic acids are typically heterodisperse, acidic, polymeric colored, and chemically complex macromolecules (Bratby 2006). Depending on the origin, HAs may have various chemical structures and are anionic polyelectrolytes, which in general consist of 5-14% carboxyl functional groups (-COOH), 12-19% carbonyl functional groups (>CO), and 50-70% hydroxyl functional groups (-OH) (Kuwatsuka, Tsutsuki, and Kumada 1978). The presence of these functional groups provides HA with the ability to form complexes with a number of different metal ions such as Ca^{2+} and Mg^{2+} (Karim 2018). A typical chemical structure of HA is shown in **Figure 1.6**.

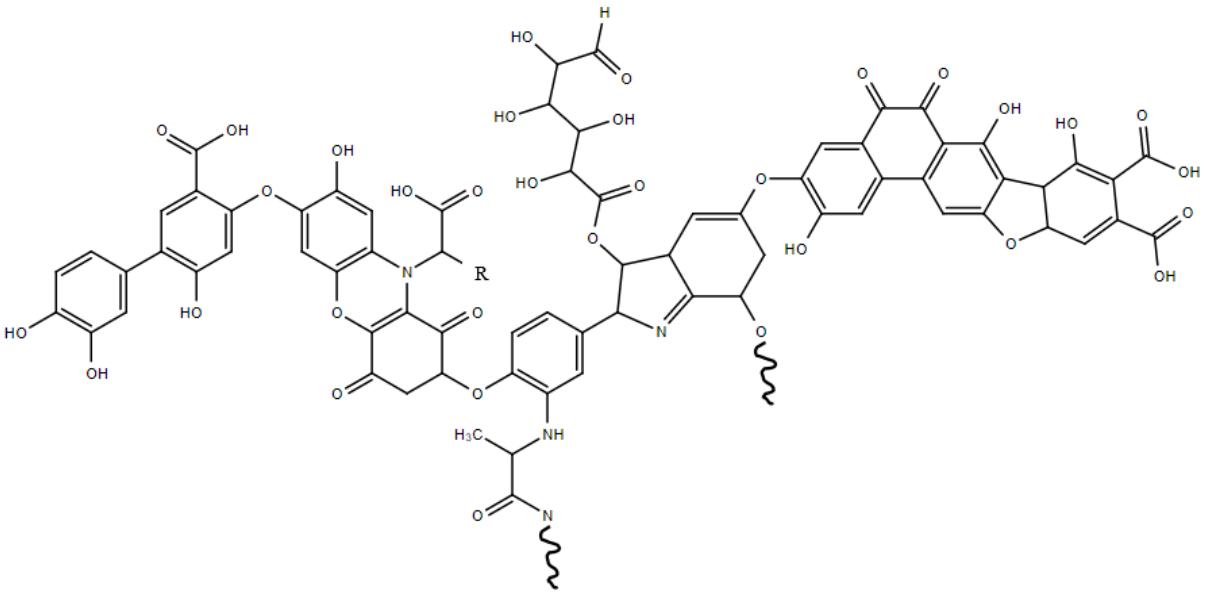

Figure 1.6. Chemical structure of a typical HA molecule

In aquatic systems, HAs were reported to serve as colloidal stabilizing agents (Stumm, 1992) indicating an aquatic system with HAs would present stable colloidal behavior with a zeta potential of around -30 mV (Pate and Safier 2016; D.F. Evans 1999). At high pH values, the -COOH functional groups will dissociate (deprotonated) resulting in strong negative charges on the surface; At a very low pH value, these groups will be protonated diminishing the surface charge and may even become positively charged (Skybova, et al., 2007). Studies also found that the net charge of HAs increases with pH and decreases with Ca^{2+} content (Yoon et al. 1998). Due to the hydrophobicity, HAs tend to accumulate at the solid-water interface. HAs were also reported as naturally present endogenous surface-active components (Razi et al. 2016) and have similar properties to the dissolved organic acids in an SGAD PW (Fatema et al. 2015); therefore, HAs are

commonly used in bench-scale testing to represent the organic matter and total dissolved carbon present in SAGD PW.

1.3.4 Electrokinetic Properties of Silica

Silica is one of the main contaminants in SAGD PW (causing scaling within process equipment) and is mainly removed in the WLS process. In a downstream BBD treatment process (disposal water treatment), silica is typically removed by pH adjustment (neutralization process) – as silica solubility is highly sensitive to pH values and typically increases with increasing pH (Iler 1979) and temperature. When pH is greater than 9.0 and temperature is around room temperature, the chemical and physical properties of silica solution will remain relatively unchanged for a long period; When the pH is reduced to 9.0, fast silica nucleation and aggregation will start; when the temperature is raised to 80°C, silica aggregation occurs when pH is lower than 8 (Fatema 2014). Soluble silicate has three major species: $Si(OH)_4$ at pH < 9.4 (uncharged silica gel), $SiO(OH)_3^-$ at pH > 9.4, and $SiO_2(OH)_2^-$ at pH > 12 (Feng et al. 2012). When in suspended form, silica particles are generally negatively charged by partial ionization of the surface OH^- groups to SiO^- anionic sites (Iler 1979). It was reported the zeta potential of colloidal silica ranged from -20 to -60 mV under various conditions (with and without HA), and became more negative with HA primarily because to the phenolic groups absorbed onto the surface of silica particles and carboxylic groups oriented to outside of the silica particles (Zhou et al. 2017). This agreed with what was typically observed that many organic molecules with polar groups are absorbed and held to the SiOH groups through hydrogen bonding (Iler 1979). The PZC of silicate has been reported to be around pH 2 – 3 (Stumm 1992; Nordström et al. 2011). In SAGD PW studies, sodium silicate is commonly used to represent the dissolved silica content (Fatema 2014).

1.3.5 Electrokinetic Properties of Clay

Clay is a part of the fines content of oil sands (3%) (Natural Resources Canada 2013) and is abundant in tailings water. In the WLS process, bentonite clay can be applied when there is excessive oil in the incoming PW. As water intensity is a significant part of sustainable resource development, tailings water at times is recirculated back to WLS to reduce the make-up water consumption and lower a plant's overall water intensity. However, this operation strategy can add clay loading into the process. Cay is also part of the total suspended solids in the PW. Clay is typically considered to have three layers with one (1) octahedral layer formed by metal oxide and is sandwiched by two (2) tetrahedral layers of silicon oxide $(SiO_4)^{4-}$(Duman and Tunç 2009). The clay particles generally carry negative charges due to the broken bonds in the Si-O-Si (siloxane) group (Ersoy and Çelik 2002), Al^{3+} for Si^{4+} substitution in the tetrahedral sites (isomorphic substitutions), and Mg^{2+} for Al^{3+} substitution in octahedral sites (Duman and Tunç 2009). It was also reported that the zeta potential of bentonite clay (sodium-based) ranged from -33 to -35 mV and was not impacted by the concentration of clay. In another study, the zeta potential of bentonite was reported to be -32.2 mV (Otsuki and Hayagan 2020), which agreed with their data. Ersoy and Çelik conducted electrokinetic studies on clay (clinoptilolite) and didn't observe a PZC point when pH ranged from 2 to 12 (Ersoy and Çelik 2002) – this indicates that clay would be negatively charged throughout the WLS operating pH values. It was also reported that the zeta potential of clay particles can be impacted by the concentrations of di- and tri-valent ions – which can reduce the negative charges on the clay particles by proton exchange and reduction in the double layer thickness (Duman and Tunç 2009).

1.4 Visual MINTEQ Modelling

Visual MINTEQ was first published online in 2000 and was developed based on the MINTEQA2, which was coded by the U.S. Environmental Protection Agency (EPA). It is a commonly used geological equilibrium modelling tool, which is based on an extensive database of reliable thermodynamic data, for computing equilibria among the dissolved, adsorbed, solid, and gas phases in an environmental setting (U.S. Environmental Protection Agency 1991). The input data required to predict the equilibrium speciation consists of characterization of the water sample to be modeled such as dissolved concentrations for the components of interest and any other relevant invariant measurements for the system of interest (e.g. pH or the partial pressures of one or more gases) (U.S. Environmental Protection Agency 1991). When formulating and solving multi-component chemical equilibrium problems, the software uses the approach of equilibrium constant method or simultaneous solution of the nonlinear mass action expressions and linear mass balance relationships (U.S. Environmental Protection Agency 1991).

During the electrokinetic study of softening particles, Visual MINTEQ 3.1 was employed to predict precipitated speciation by calculating the saturation indices (SIs) under a variety of manipulated conditions (pH, temperature, CO_2 exposure, chemical species, etc.) and to ultimately assist with zeta potential results interpretation.

1.5 Coagulation/flocculation and Polyamine Coagulant

Coagulation and flocculation is a commonly applied process in many water and wastewater treatment plants and can be key to the performance of clarification and sedimentation. Coagulation refers to a process where suspended particles and colloids are destabilized and flocculation refers to a process where destabilized particles form larger agglomerates (Bratby 2006). However, the

divisions between coagulation and flocculation are not rigid (Environmental Protection Agency 2002), and often they are used interchangeably in the field. Coagulation and flocculation can be achieved by four primary mechanisms; (i) double layer compression, (ii) charge neutralization, (iii) particle bridging, and (iv) precipitate enmeshment (Ghernaout et al. 2020). Coagulation/flocculation requires the dose of chemicals, which can be either inorganic metal salts or polyelectrolytes (also referred to as polymers in the field). Inorganic coagulants are mainly aluminum and iron based such as aluminum chloride, polyalumium chloride (PAC), ferric sulfate. Common organic polymers can be categorized into three groups: melamineformaldehyde, poly diallydimenthyl ammonium chloride (PolyDADMAC), and epichlorohydrin-dimethylamine (EPI-DMA). The organic coagulants are superior in the sense that they have no effect on the pH of the solution and do not add additional metal ions (i.e. like aluminum and iron) to the solution (Yin 2010).

A high molecular weight polyamine based coagulant tends to be linear and can be produced by the reaction of EPI and DMA with the use of a modifying agent - 1,2-diaminoethane (ethylenediamine) as (Wang et al. 2009). **Figure 1.7** presents a typical chemical structure of a polyamine molecule. The amino nitrogens form reaction sites and lead to positively charge nitrogens in water (**Figure 1.8**). Polyamine based polymers have been reported to be of very high charge density due to the abundance of nitrogens (Zueva et al. 2015; Yue et al. 2008) and used as coagulation/flocculation aid in many industries.

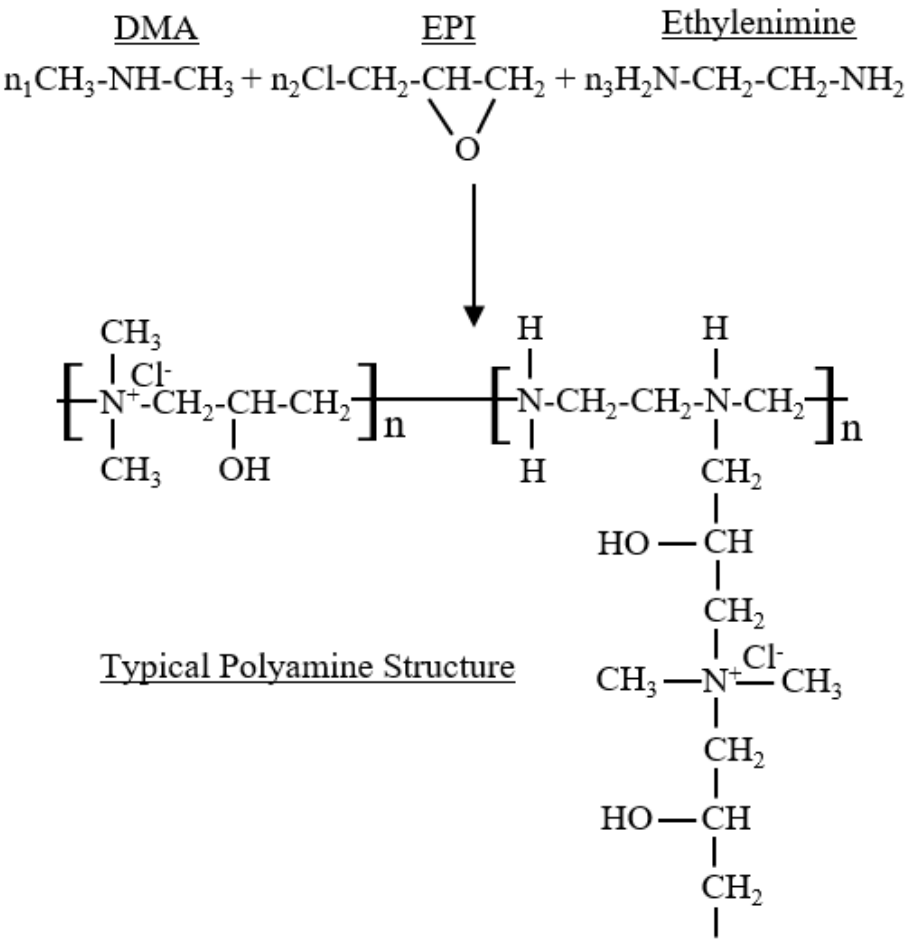

Figure 1.7. Synthesis process and chemical structure of a typical polyamine based coagulant

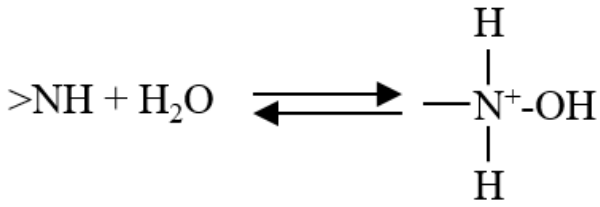

Figure 1.8. Simplified illustration of charge development of an amino nitrogen

1.6 Motivation for Work

The WLS process is based on complex chemical reactions and interactions and has been operating for a few decades in the oil sands industry, but progress on the performance optimization and process control is still lagging. Fundamentally, very little research has been done to understand the electrokinetic properties of the particles generated. The fundamental understanding is of paramount significance as it provides an essential angle to understand issues currently reside within the WLS process and it also directly relates to sedimentation and clarification performance. Although there were some studies done on the particles generated from the traditional cold lime softening (CLS) process. The SAGD WLS is unique when it comes to the influent water characteristics such as high temperature (80 °C), high organic and high silica content. There are very few reported data and methodical studies on the zeta potential of $CaCO_3$ and $Mg(OH)_2$ particles under the WLS conditions. Additionally, there is a lack of systematic coagulation studies performed at high temperatures that investigate the impact of feed water deviations on the coagulant demand for the WLS process. A lot of reported data doesn't account for the changes in water chemistry when varying experimental conditions.

The objectives of this research are to:

1. Assess the zeta potential of $CaCO_3$ and $Mg(OH)_2$ particles under numbers of experimental conditions including pH, presence of other ions, aging, temperature, and the addition of HA, clay, and silica.
2. Incorporate the use of thermodynamic modelling to predict chemical speciation at various manipulated conditions for data interpretation.

3. Evaluate the impact of feed water deviations on the coagulant demand including concentrations of HA, silica, clay, Mg^{2+}, Ca^{2+}, CO_3^{2-}, HCO_3^-, and doses of $Ca(OH)_2$ and MgO.

The findings of this research can provide valuable and possible practical knowledge for the operation of the WLS such as improvements on the onsite chemical optimization, enhanced process monitoring, and possible controls during an influent water off-specification event.

1.7 Thesis Format and Structure

This thesis consists of the following six chapters:

1. Chapter 1 provides background information on the SAGD operation including the WLS process, and literature reviews on the electrokinetic properties and zeta potential of $CaCO_3$, $Mg(OH)_2$, humic acids, silica, and clay, as well as polyamine coagulant aid and the motivation of this research.
2. Chapter 2 presents a published manuscript titled "Electrokinetic Study of Calcium Carbonate and Magnesium Hydroxide Particles in Lime Softening" including research methods, results, and conclusion.
3. Chapter 3 presents a submitted manuscript titled "Impact of Solution Feed Deviations on Polymer Coagulant Dose in Synthetic SAGD Produced Water" including research methods, results, and conclusion.
4. Chapter 4 closes this thesis by summarizing conclusions from the two manuscripts (Chapter 3 and 4) and providing recommendations for future work

The manuscripts included in Chapters 2 and 3 were also formatted accordingly to the Thesis Formatting Guidelines provided by the Faculty of Graduate Studies. The numbering of sections,

tables, figures, and equations in the two manuscripts has been updated to improve the flow and readability of the thesis.

Chapter 2 Electrokinetic Study of Calcium Carbonate and Magnesium Hydroxide Particles in Lime Softening

2.1 Introduction

Chemical precipitative lime softening is a common and established process in water and wastewater treatment, during which the pH of the treated water is raised sufficiently to remove calcium and magnesium hardness by converting Ca^{2+} to $CaCO_3$ and Mg^{2+} to $Mg(OH)_2$, both precipitating from the treated water as solids (AWWA 1990). During lime softening, chemicals normally added are lime (the process is referred to as lime softening) or lime in combination with soda ash (referred to as lime-soda softening). The former is typically used to remove carbonate hardness, and the latter can remove both carbonate and non-carbonate hardness (Ostovar and Amiri 2013). Although there is not a clear distinction, depending on the operating temperature, lime softening can be classified as cold (i.e. 15 to 60°C), warm (i.e. 60 to 85°C) and hot lime softening (i.e. 90 to 105 ^{0}C). Usually, cold lime softening is deployed for softening drinking water in municipal applications, while warm and hot lime softening processes are used for treating industrial water. For example, a warm or hot lime softening process is commonly applied to treat oilfield produced water derived from steam-assisted gravity drainage (SAGD) oil recovery operations (W. F. Heins 2009) as well as industrial cooling (Knight 1981) and boiler feed waters.

The understanding of the electrokinetic properties of $CaCO_3$ and $Mg(OH)_2$ particles relevant to lime softening conditions is of importance and has not been well explored, especially for warm and hot lime softening where the industrial wastewater is composed of multi-components and higher temperature might play an important role as well. The zeta potential is a parameter used to evaluate the electrokinetic behavior of particles which can provide information on their surface

charge, particle stability, and subsequent easiness to coagulate (Black and Christman 1961; Israelachvili 1992). Many laboratory experiments have reported on the zeta potential of $CaCO_3$ particles (Al Mahrouqi, Vinogradov, and Jackson 2017; Wolthers, Charlet, and Van Cappellen 2008), however, very few reported the zeta potential of $CaCO_3$ particles at conditions relevant to lime softening. Most measurements of zeta potential of $CaCO_3$ were conducted using natural samples of calcite or using preformed $CaCO_3$ particles, however, $CaCO_3$ particles generated during lime softening are mostly freshly precipitated (in some cases, preformed $CaCO_3$ particles may be added or lime sludge is recycled back into the precipitation system to facilitate precipitation during lime softening). In comparison to $CaCO_3$ particles, the zeta potential measurements of $Mg(OH)_2$ particles have been even less explored (Black and Christman 1961; Larson and Buswell 1940; Russell et al. 2009). The published results regarding the surface charge of $CaCO_3$ particles are often contradictory, and there has been a lot of debate over the sign of the surface charge and the PDIs (Eriksson, Merta, and Rosenholm 2007). Even among the reported zeta potential of $CaCO_3$ and $Mg(OH)_2$ particles at conditions relevant to water softening, the published results on the surface charge of $CaCO_3$ and $Mg(OH)_2$ particles are not consistent, even the sign of their surface charge being opposite among some reports. For example, Larson and Buswell (1940) found $Mg(OH)_2$ particles to be positively charged, and $CaCO_3$ particles to be negatively charged throughout the pH range of water softening (the lower end of the pH range was not specified but the higher end was specified as pH 12). Black and Christman (1961) reported that throughout the entire pH range of lime-soda softening, the zeta potential of freshly precipitated $Mg(OH)_2$ was positive (pH ranging from 10.2 to 11.2), and the zeta potential of freshly precipitated $CaCO_3$ was negative (pH ranging from 9.0 to 11.0). Russell et al. (2009) reported that the zeta potential of $CaCO_3$ was dependent on $CaCO_3$ source with preformed $CaCO_3$ having a negative zeta potential

at pH of 10.4 while freshly precipitated $CaCO_3$ having a positive zeta potential at the same pH, furthermore, the sign of the zeta potential of both freshly precipitated $CaCO_3$ and freshly precipitated $Mg(OH)_2$ depended on pH: freshly precipitated $CaCO_3$ was negatively charged at pH values lower than 10.5 but positively charged at pH values higher than 10.5; freshly precipitated $Mg(OH)_2$ was negatively charged at pH values lower than 11.5 but positively charged at pH values higher than 11.5.

In this work, a systematic study was carried out to understand the electrokinetic properties of $CaCO_3$ and $Mg(OH)_2$ particles through zeta potential measurements throughout the wide pH range possibly encountered in lime softening. The zeta potential measurements were conducted under controlled conditions including pH, temperature, aging time while exposed to the atmosphere, varied concentration of cations (Mg^{2+} and Ca^{2+} for $CaCO_3$ particles only) and anions (CO_3^{2-} and HCO_3^- for $Mg(OH)_2$ particles only), the presence of possible interacting species in water including humic acid (HA), silicate and clay. Freshly precipitated $CaCO_3$ and $Mg(OH)_2$ particles were obtained from synthetic water samples and their zeta potentials were measured. The rationale for studying these influencing parameters is as follows: 1), pH is an important factor affecting zeta potential and lime softening; 2), exposure to CO_2 can influence zeta potential measurements and its impact needs to be addressed (Wolthers, et al., 2008); 3), the temperature dependence of zeta potential for $CaCO_3$ and $Mg(OH)_2$ remains poorly understood and needs to be addressed, especially at the higher temperatures of warm/hot softening; 4), the effect of CO_3^{2-} and HCO_3^- was studied as alkalinity control is an important lime softening operational parameter; 5), the interaction between $CaCO_3$ and $Mg(OH)_2$ particles was studied because $CaCO_3$ and $Mg(OH)_2$ particles might be formed simultaneously during lime softening and most softening sludges

contain both $CaCO_3$ and $Mg(OH)_2$ particles (Black and Christman, 1961); and 6), the interaction between humic acid (HA, mimicking natural organic matter), silicate (representing silica) as well as clay (mimicking suspended solids) and $CaCO_3$/$Mg(OH)_2$ particles was studied, because these compounds are commonly present in wastewater and can interact with $CaCO_3$/$Mg(OH)_2$ particles during lime softening (Adusei-Gyamfi et al. 2019; Latour, Miranda, and Blanco 2014). For example, natural organic matter (NOM) can be removed through coprecipitation with formed $CaCO_3$ and $Mg(OH)_2$ during lime softening (Mercer, Lin, and Singer 2005; Russell et al. 2009; Russell, Lawler, and Speitel 2009). For comparison with freshly precipitated particles, preformed $CaCO_3$ and $Mg(OH)_2$ were also studied to understand how sample preparation might affect the zeta potentials of $CaCO_3$ and $Mg(OH)_2$ particles.

Thermodynamic modeling using Visual MINTEQ software was used to predict precipitates as a function of solution chemistry and assist with zeta potential data interpretation. The results from this detailed and systematic study will provide a better understanding of the interactions and electrokinetic properties of $CaCO_3$ and $Mg(OH)_2$ particles in these complicated and multicomponent systems, which is important to better understand their coagulation and flocculation mechanisms.

2.2 Experimental

2.2.1 Chemicals

Calcium chloride dihydrate ($CaCl_2 \cdot 2H_2O$, ACS reagent, 99+%), magnesium chloride hexahydrate ($MgCl_2 \cdot 6H_2O$, ACS reagent, 99+%), sodium bicarbonate ($NaHCO_3$, ≥ 99.7%), sodium carbonate (Na_2CO_3, anhydrous, ≥99.5%) and sodium hydroxide (NaOH, ACS reagent, ≥97%) were purchased from Fisher Chemicals. Calcium carbonate ($CaCO_3$, ReagentPlus, ≥99%), magnesium

hydroxide ($Mg(OH)_2$, ≥99%), sodium metasilicate (Na_2SiO_3, granular), HA (technical), bentonite analogue (montmorillonite, $Al_2O_3{\cdot}SiO_2{\cdot}H_2O$) were purchased from Sigma Aldrich. Milli-Q water (Millipore deionized with a resistivity of 18.2 MΩ·cm) was used for the preparation of all water samples.

2.2.2 Sample Preparation and Tests

Fresh stock solutions of $CaCl_2$, Na_2CO_3, $MgCl_2$, NaOH, and $NaHCO_3$ were prepared. $CaCl_2$ and Na_2CO_3 stock solutions were used to produce $CaCO_3$ precipitation; $MgCl_2$ and NaOH stock solutions were used to produce $Mg(OH)_2$ precipitation. Water samples containing preformed $CaCO_3$ and $Mg(OH)_2$ were also prepared. Each water sample (WS) was prepared in a 50 mL plastic centrifugation tube (Fisher Scientific) and mixed at 200 rpm in the Multi-Thermal Shaker (Mandel Scientific, CAN) for 5 min. Detailed sample information is provided in **Table 2.1** and **Table 2.2**. The pH was measured by a Fisher Scientific™ Accumet AE150 pH Benchtop Meter which was calibrated using the standard buffer solutions with known pH values (pH 4.0, 7.0, and 10.0). NaOH (1 M) and HCl (1 M) solutions were used for pH adjustment.

Table 2.1. Preparation of stock solutions

Stock Solution	Molar Concentration
$CaCl_2{\cdot}2H_2O$	100 mM
Na_2CO_3	100 mM
$MgCl_2{\cdot}6H_2O$	100 mM
NaOH	200 mM
$NaHCO_3$	100 mM

Table 2.2. Preparation of water samples (each volume = 25 mL)

Water Sample (WS)	Procedure Using Stock Solution
WS 1.1 - Freshly precipitated $Mg(OH)_2$ (4 mM $MgCl_2$ and 8 mM NaOH)	1 mL $MgCl_2 \cdot 6H_2O$ + 2 mL NaOH
WS 1.2 - Preformed $Mg(OH)_2$ (4 mM $Mg(OH)_2$)	5.83 mg of commercial $Mg(OH)_2$
WS 2.1 - Freshly precipitated $CaCO_3$ (8 mM $CaCl_2$ and 4 mM Na_2CO_3)	2 mL $CaCl_2 \cdot 2H_2O$ + 1 mL Na_2CO_3
WS 2.2 - Freshly precipitated $CaCO_3$ (4 mM $CaCl_2$ and 4 mM Na_2CO_3)	1 mL $CaCl_2 \cdot 2H_2O$ + 1 mL Na_2CO_3
WS 2.3 - Freshly precipitated $CaCO_3$ (4 mM $CaCl_2$ and 8 mM Na_2CO_3)	1 mL $CaCl_2 \cdot 2H_2O$ + 2 mL Na_2CO_3
WS 2.4 - Preformed $CaCO_3$ (4 mM $CaCO_3$)	10.00 mg of commercial $CaCO_3$
WS 3.1 - Preformed $Mg(OH)_2$ and $CaCO_3$ (0 mM $Mg(OH)_2$ and 4 mM $CaCO_3$)	0 mg of $Mg(OH)_2$ and 10.00 mg of $CaCO_3$
WS 3.2 - Preformed $Mg(OH)_2$ and $CaCO_3$ (2 mM $Mg(OH)_2$ and 4 mM $CaCO_3$)	2.92 mg of $Mg(OH)_2$ and 10.00 mg of $CaCO_3$
WS 3.3 - Preformed $Mg(OH)_2$ and $CaCO_3$ (4 mM $Mg(OH)_2$ and 4 mM $CaCO_3$)	5.83 mg of $Mg(OH)_2$ and 10.00 mg of $CaCO_3$
WS 3.4 - Preformed $Mg(OH)_2$ and $CaCO_3$ (8 mM $Mg(OH)_2$ and 4 mM $CaCO_3$)	11.66 mg of $Mg(OH)_2$ and 10.00 mg of $CaCO_3$
WS 4.1 - Preformed $Mg(OH)_2$ and Na_2SiO_3 (0.4 mM Na_2SiO_3 and 4 mM $Mg(OH)_2$)	1.22 mg of Na_2SiO_3 and 5.83 mg of $Mg(OH)_2$
WS 4.2 - Preformed $Mg(OH)_2$ and Na_2SiO_3 (2 mM Na_2SiO_3 and 4 mM $Mg(OH)_2$)	6.10 mg of Na_2SiO_3 and 5.83 mg of $Mg(OH)_2$
WS 4.3 - Preformed $Mg(OH)_2$ and Na_2SiO_3 (4 mM Na_2SiO_3 and 4 mM $Mg(OH)_2$)	12.2 mg of Na_2SiO_3 and 5.83 mg of $Mg(OH)_2$
WS 4.4 - Preformed $Mg(OH)_2$ and Na_2SiO_3 (8 mM Na_2SiO_3 and 4 mM $Mg(OH)_2$)	24.4 mg of Na_2SiO_3 and 5.83 mg of $Mg(OH)_2$
WS 5.1 - Preformed $CaCO_3$ and Na_2SiO_3 (0.4 mM Na_2SiO_3 and 4 mM $CaCO_3$)	1.22 mg of Na_2SiO_3 and 10.00 mg of $CaCO_3$
WS 5.2 - Preformed $CaCO_3$ and Na_2SiO_3 (2 mM Na_2SiO_3 and 4 mM $CaCO_3$)	6.10 mg of Na_2SiO_3 and 10.00 mg of $CaCO_3$
WS 5.3 - Preformed $CaCO_3$ and Na_2SiO_3 (4 mM Na_2SiO_3 and 4 mM $CaCO_3$)	12.2 mg of Na_2SiO_3 and 10.00 mg of $CaCO_3$

WS 5.4 - Preformed $CaCO_3$ and Na_2SiO_3 (8 mM Na_2SiO_3 and 4 mM $CaCO_3$)	24.4 mg of Na_2SiO_3 and 10.00 mg of $CaCO_3$
WS 6.1 - Preformed $Mg(OH)_2$ and HA (0.4 mM HA and 4 mM $Mg(OH)_2$)	2.27 mg of HA and 5.83 mg of $Mg(OH)_2$
WS 6.2 - Preformed $Mg(OH)_2$ and HA (2 mM HA and 4 mM $Mg(OH)_2$)	11.36 mg of HA and 5.83 mg of $Mg(OH)_2$
WS 6.3 - Preformed $Mg(OH)_2$ and HA (4 mM HA and 4 mM $Mg(OH)_2$)	22.72 mg of HA and 5.83 mg of $Mg(OH)_2$
WS 6.4 - Preformed $Mg(OH)_2$ and HA (8 mM HA and 4 mM $Mg(OH)_2$)	45.43 mg of HA and 5.83 mg of $Mg(OH)_2$
WS 7.1 - Preformed $CaCO_3$ and HA (0.4 mM Na_2SiO and 4 mM $CaCO_3$)	2.27 mg of HA and 10.00 mg of $CaCO_3$
WS 7.2 - Preformed $CaCO_3$ and HA (2 mM Na_2SiO and 4 mM $CaCO_3$)	11.36 mg of HA and 10.00 mg of $CaCO_3$
WS 7.3 - Preformed $CaCO_3$ and HA (4 mM HA and 4 mM $CaCO_3$)	22.72 mg of HA and 10.00 mg of $CaCO_3$
WS 7.4 - Preformed $CaCO_3$ and HA (8 mM HA and 4 mM $CaCO_3$)	45.43 mg of HA and 10.00 mg of $CaCO_3$

Zeta potential is an experimentally determined parameter that describes the electrostatic charge of particles in solutions (**Figure 1.3**). The zeta potential of the suspended particles in water samples was analyzed by a Malvern Zetasizer Nano ZS with a high concentration zeta potential cell (Zen1010) which has a temperature limit of 70 °C. The temperature of water samples was controlled at 25, 35, 45, 55, and 65°C to study the temperature effect. The equipment utilizes dynamic light scattering for determining the electrophoretic mobility of particles (**Figure 1.4**). Then the zeta potential of the particles is calculated from the measured electrophoretic mobility (i.e., velocity) using the Smoluchowski Equation:

$$U_E = \varepsilon\zeta/\eta$$

where U_E, ε, ζ and η are the electrophoretic mobility, dielectric constant of water, zeta potential, and viscosity of water, respectively. A single measurement on each sample was repeated 5 times and mean values with standard deviations are reported.

2.2.3 Prediction of Precipitates Using Thermodynamic Modeling

The potential precipitates under different conditions (pH, temperature, CO_2 exposure, chemical species, etc.) were predicted by calculating saturation indices (SIs) using thermodynamic modeling (Visual MINTEQ, version 3.1). The saturation index (SI) is defined as:

$$SI = \log \frac{IAP}{K_{SP}}$$

where IAP and K_{sp} are the ionic activity product in the chemical reaction and thermodynamic solubility product of the precipitate, respectively. The SI indicates the potential of a specific precipitate to be formed. When SI > 0, the solution is supersaturated and the precipitate can form; when SI < 0, the solution is undersaturated and the precipitate cannot form; when SI = 0, the solution is in equilibrium.

2.3 Results and Discussion

2.3.1 The zeta potential of $Mg(OH)_2$ Particles

The zeta potentials of freshly precipitated $Mg(OH)_2$ (precipitated from 4 mM $MgCl_2$ and 8 mM NaOH) and preformed $Mg(OH)_2$ particles (4 mM commercially purchased $Mg(OH)_2$ in water) were measured as a function of pH, temperature, aging, and varying concentration of $NaHCO_3/Na_2CO_3$ (**Figure 2.1**), as described in the following sections.

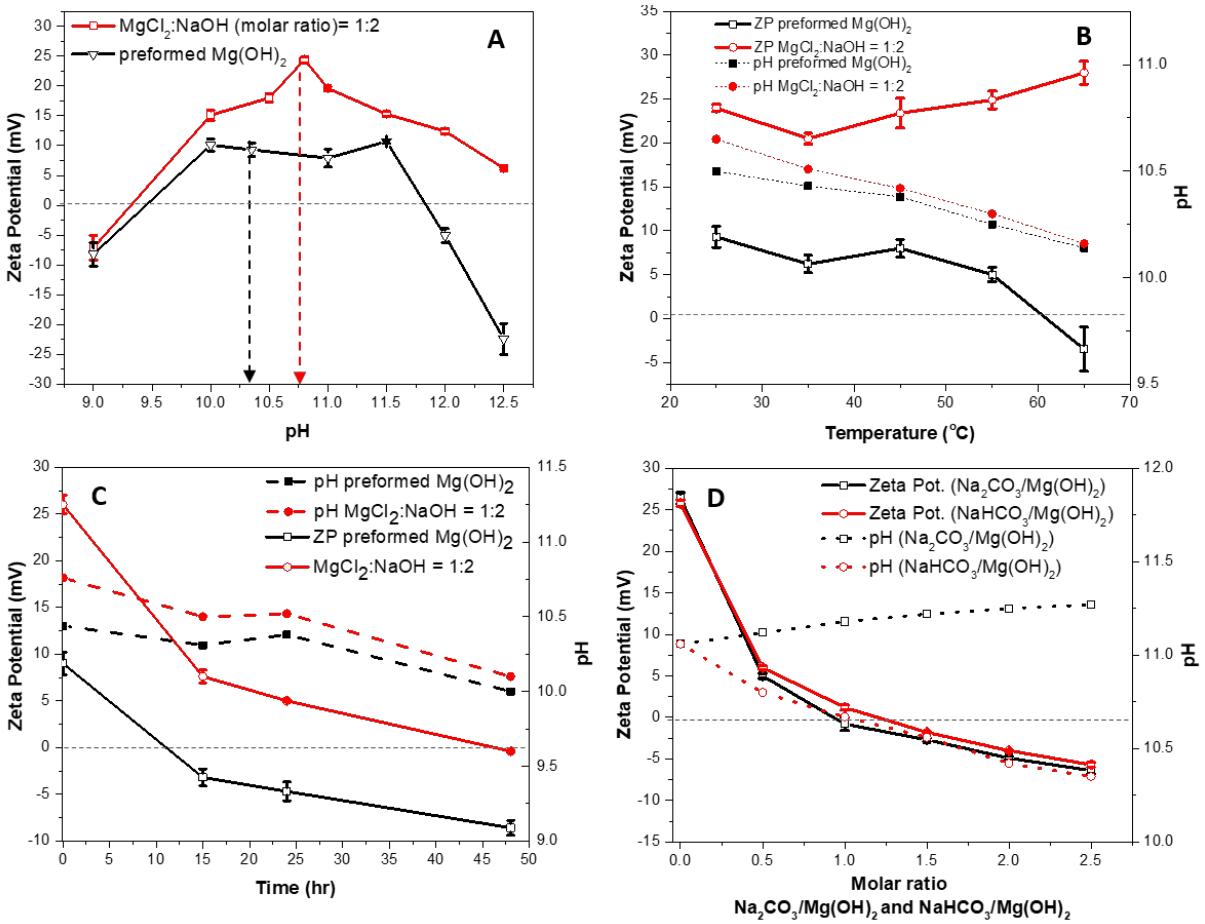

Figure 2.1. The effect of (A) pH on the zeta potential at 25 °C (dashed arrows indicating initial pH of the water samples), (B) temperature on the pH and zeta potential, (c) aging on the pH and zeta potential at 25 °C, and (d) $Na_2CO_3/NaHCO_3$ on the pH and zeta potential at 25 °C of $Mg(OH)_2$ in water. Preformed and freshly precipitated $Mg(OH)_2$ represent 4 mM preformed $Mg(OH)_2$ suspension in water, and 4 mM $Mg(OH)_2$ in-situ precipitated from 4 mM $MgCl_2$ and 8 mM NaOH, respectively.

2.3.1.1 The effect of pH

The zeta potential measurements of freshly precipitated and preformed $Mg(OH)_2$ particles under various pHs at 25 °C showed that both particles exhibited positive charges at their initial solution pH and over a relatively wide pH range (**Figure 2.1A**). For the preformed $Mg(OH)_2$, the point of zero charge (PZC) was observed around pH 11.8 – 11.9. This observation agrees with the findings of Parks (1965), who reported that the PZC of $Mg(OH)_2$ was at a pH of 12. For the freshly precipitated $Mg(OH)_2$, the zeta potential was still slightly positive at a pH of 12.5; however, a

decreasing trend was quite clear. The decrease in zeta potential of both freshly precipitated and preformed $Mg(OH)_2$ particles with the increasing pH can be caused by the absorption of OH^- on the particle surfaces. At the same pH, the zeta potential of the freshly precipitated particles was higher than that of the preformed $Mg(OH)_2$. For the pH range of 10.2 – 11.0, we observed a similar trend to Black and Christman (1961), who found that freshly precipitated $Mg(OH)_2$ exhibited a zeta potential of approximately +7.5 mV throughout this pH range.

Reducing the pH to 10 from the initial pH did not affect the zeta potential of preformed $Mg(OH)_2$ but lowered that of freshly precipitated $Mg(OH)_2$ from ~25 to ~20 mV (**Figure 2.1A**). At a pH of 9.0, negative zeta potential values were recorded. The modeling with atmospheric CO_2 included (**Figure 2.2 A** and **B**) suggested that hydromagnesite [$Mg_5(CO_3)_4(OH)_2 \cdot 4H_2O$], magnesite ($MgCO_3$) and artinite [$Mg_2(OH)_2CO_3 \cdot 3H_2O$] are the dominant species in descending order at pH > 9.5, only $MgCO_3$ precipitates at a pH of 9.0. The observed negative charge at pH values lower than 9.5 can be ascribed to the formation of a mixture of $MgCO_3$ and $Mg(OH)_2$ (in the form of hydromagnesite). This is in good agreement with the previous report that freshly precipitated $MgCO_3$ was best characterized as a hydromagnesite and carried negative zeta potential (Russell et al. 2009).

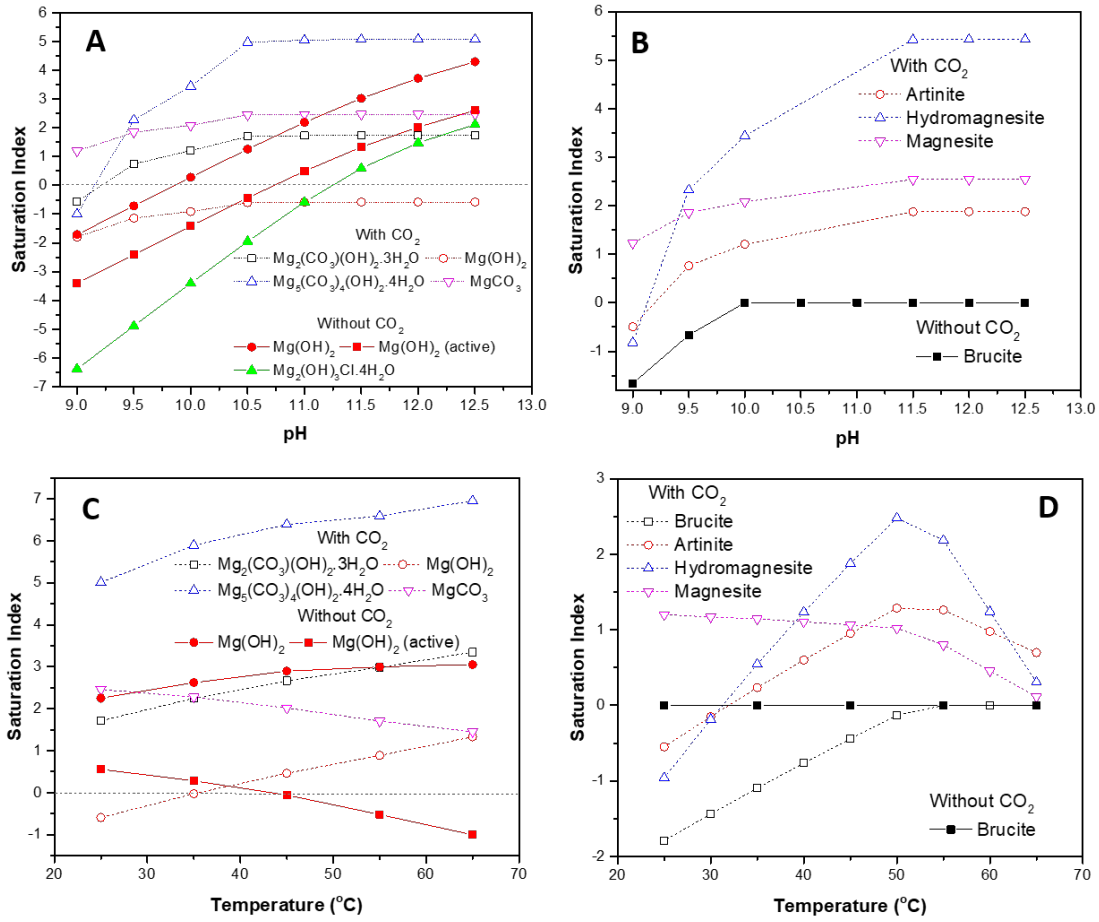

Figure 2.2. Saturation indices (SIs) of magnesium minerals as a function of different pH at 25 ºC (A and B), and as a function of temperature with (P_{CO_2} = 0.00038 atm) and without CO_2 input (P_{CO_2} = 0 atm) (C and D). A and C: freshly precipitated $Mg(OH)_2$ (WS 1.1). B and D preformed $Mg(OH)_2$ (WS 1.2).

2.3.1.2 The effect of temperature

The measured pHs and zeta potentials of suspensions of freshly precipitated and preformed $Mg(OH)_2$ particles as a function of temperature are shown in **Figure 2.1B**. The resulting pH of both suspensions decreased with increasing temperature. The zeta potential of freshly precipitated $Mg(OH)_2$ increased slowly from ~ 22 mV at 25 ºC to ~ 27 mV at 65 ºC. In the case of preformed $Mg(OH)_2$ particles, the zeta potential was positive between 25 to 45 ºC but much lower compared

to the freshly precipitated one (~ 5 mV *vs.* ~ 20 mV at 25 ºC). However, the zeta potential decreased when the temperature was raised to 55 ºC and became negative at 65 ºC (~ -5 mV).

For the freshly precipitated $Mg(OH)_2$ particles, the modelling (**Figure 2.2C**) indicated that the SIs of $Mg(OH)_2$ increased with the increasing temperature regardless of CO_2. The SIs of $Mg_5(CO_3)_4(OH)_2 \cdot 4H_2O$) and $Mg_2(OH)_2CO_3 \cdot 3H_2O$ also increased with the increasing temperature; the SI of $MgCO_3$ decreased with the increasing temperature. The increased zeta potential at higher temperatures could be attributed to the increased precipitation of $Mg(OH)_2$. The freshly precipitated $Mg(OH)_2$ particles are fully hydrated and the formation of other minerals could potentially provide more surface sites for protonation. For the preformed $Mg(OH)_2$, brucite is at equilibrium throughout. The decreased zeta potential of the preformed $Mg(OH)_2$ water sample could be a result of the formation of other minerals (e.g. $Mg_2(OH)_2CO_3 \cdot 3H_2O$, **Figure 2.2D**) which have carbonate functional groups carrying negative charges. Under the initial condition (**Figure 2.2A)**, the zeta potential of the freshly precipitated $Mg(OH)_2$ particles (22 mV) is higher than that of preformed $Mg(OH)_2$ particles (5 mV) indicating potential differences in the structure of lattice, which could be another reason why freshly precipitated and preformed $Mg(OH)_2$ particles behaved differently.

2.3.1.3 The effect of aging

As the concentration of dissolved CO_2 increases due to exposure to the air, the pH and total alkalinity change with time which could result in changes in the charge on the particle surface. As shown in **Figure 2.1C**, the pH of both water samples decreased with increasing exposure time to the ambient CO_2. The zeta potentials of both types of particles followed a decreasing trend with aging time – for the freshly precipitated $Mg(OH)_2$, the zeta potential was reversed to negative. The

SIs predicted (**Figure 2.2 A** and **B** at 25 ºC with CO_2 input) indicated that with aging, $Mg_5(CO_3)_4(OH)_2 \cdot 4H_2O$, $MgCO_3$ and $Mg_2(OH)_2CO_3 \cdot 3H_2O$ in descending order can precipitate. These minerals are expected to dominate the solid phase and all have carbonate functional groups that can acquire negative charges in water.

2.3.1.4 The effect of $NaHCO_3$ and Na_2CO_3

The effect of $NaHCO_3$ and Na_2CO_3 addition on the zeta potential of freshly precipitated $Mg(OH)_2$ was studied (**Figure 2.1D)**. As $NaHCO_3$ solution was added, a steady decrease in the pH from ~11 to 10.3 was observed. This was accompanied by a rapid decrease in the zeta potential initially from 25 to ~ 5 mV and a slow decrease until the zeta potential became negative. In the case of the Na_2CO_3 addition, a similar decreasing trend was observed in the zeta potential, although the pH showed an increase from ~11 to 11.25. The predicted species with SIs greater than zero are $Mg_5(CO_3)_4(OH)_2 \cdot 4H_2O$, $MgCO_3$, and $Mg_2(OH)_2CO_3 \cdot 3H_2O$ in descending order (**Figure 2.3**). HCO_3^- and CO_3^{2-} ions are very likely the PDIs for $Mg(OH)_2$ particles. It was indicated that $>MgOH^0$ could be a potential functional group of $Mg(OH)_2$ particles (Russell et al. 2009). The absorption of HCO_3^- and CO_3^{2-} onto $Mg(OH)_2$ particles can shift the functional groups to negatively charged ones (e.g. $>MgCO_3^-$).

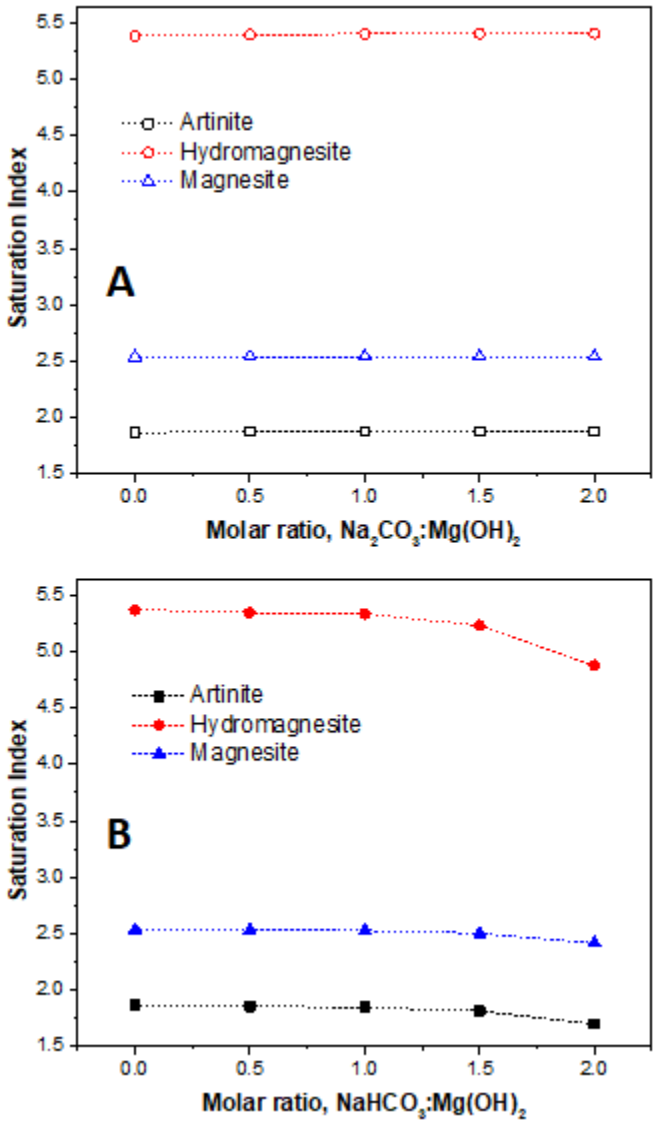

Figure 2.3. Predicted mineral species as a function of molar ratio of (A) Na_2CO_3: $Mg(OH)_2$ and (B) $NaHCO_3$: $Mg(OH)_2$.

2.3.2 The zeta potential of $CaCO_3$ particles

The zeta potentials of the freshly precipitated and preformed $CaCO_3$ particles (4 mM $CaCO_3$ in water) were measured as a function of pH, temperature, aging, and $MgCl_2$ (**Figure 2.4**), as described in the following sections. Three different samples of freshly precipitated $CaCO_3$ were

prepared by varying molar ratios of $CaCl_2$ to Na_2CO_3 from 2:1 to 1:1 and to 1:2, from reactions of 8 mM $CaCl_2$ and 4 mM Na_2CO_3, 4 mM $CaCl_2$ and 4 mM Na_2CO_3, 4 mM $CaCl_2$ and 8 mM Na_2CO_3 in the solutions, respectively.

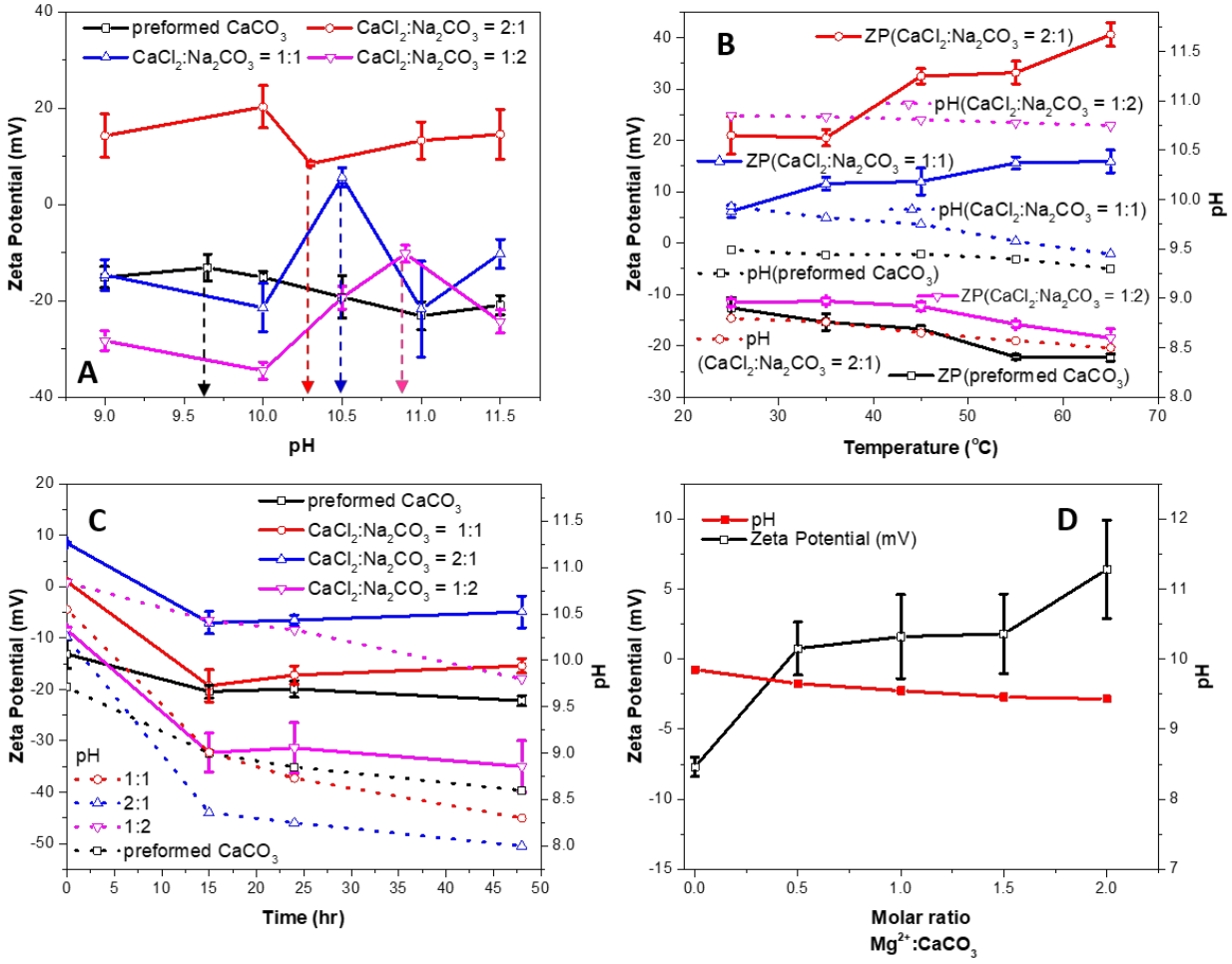

Figure 2.4. The effect of (A) pH on the zeta potential at 25 °C (dashed arrows indicating initial pHs of the water samples), (B) temperature on the pH and zeta potential at 25 °C, (C) aging on the pH and zeta potential, and (D) Mg^{2+} on the zeta potential at 25 °C of $CaCO_3$ in water. Preformed $CaCO_3$ represents 4 mM preformed $CaCO_3$ suspension in water. Three different samples of freshly precipitated $CaCO_3$ were prepared by varying molar ratios of $CaCl_2$ to Na_2CO_3 from 2:1 to 1:1 and to 1:2, from reactions of 8 mM $CaCl_2$ and 4 mM Na_2CO_3, 4 mM $CaCl_2$ and 4 mM Na_2CO_3, 4 mM $CaCl_2$ and 8 mM Na_2CO_3 in the solutions, respectively.

2.3.2.1 The effect of pH

The zeta potential measurements of the preformed and freshly precipitated $CaCO_3$ at 25 °C (**Figure 2.4A**) showed that the zeta potential of the performed $CaCO_3$ was negative throughout the pH range tested (9.0 – 11.5), which is consistent with other reported studies. For example, Bob and Walker (2001) reported a negative zeta potential for $CaCO_3$ throughout the studied pH range of 8.4 – 11.6 in the presence of 0.001 M KCl. Black and Christman (1961) found that both freshly precipitated and resuspended $CaCO_3$ particles were negatively charged throughout the pH range of 9.0 – 11.0. The zeta potential of the performed $CaCO_3$ decreased with increasing pH. (Foxall et al. 1979), Thompson and Pownall (1989), and Stipp (1999) have shown that the electrophoretic mobility of calcite particles is only secondarily affected by the pH and that the bulk concentration of Ca^{2+} and CO_3^{2-} (and other carbonate species) are the PDIs. They found that the zeta potential of preformed $CaCO_3$ was -24.36 mV at pH of 10.4. Somasundaran and Agar (1967) concluded that the principal PDIs of $CaCO_3$ were identified as Ca^{2+}, HCO_3^-, H^+ and OH^-. CO_3^{2-} ions also were found to play a major role above a pH of 9.0. They proposed that the principal mechanism of charge development at the surface was preferential hydrolysis of surface calcium and carbonate ions, or the hydrolysis of the bulk solution ions, followed by the adsorption of the resulting complexes at the surface. Russell et al. (2009) conducted jar tests on softening a water sample composed of $NaHCO_3$, $CaCl_2$, and KNO_3 with $Ca(OH)_2$, and found that the freshly precipitated $CaCO_3$ exhibited a slightly positive zeta potential at lower pH values, negative zeta potential at pH values ranging from 9.0 to 10.5, and positive zeta potential at pH values ranging from 10.5 to 11.6.

In this study, freshly precipitated $CaCO_3$ with molar ratios of $CaCl_2$: Na_2CO_3 of 2:1 and 1:1 showed positive zeta potential, while the freshly precipitated $CaCO_3$ with molar ratio of $CaCl_2$: Na_2CO_3 of

1:2 showed negative zeta potential (**Figure 2.4A**). For freshly precipitated $CaCO_3$ ($CaCl_2$: Na_2CO_3 = 2:1), its zeta potential was positive throughout the pH range tested. The positive zeta potential can be attributed to the presence of excess Ca^{2+} ions. A similar effect was observed in the presence of Mg^{2+} ions which will be discussed later. This is further supported by the fact that reducing the molar ratio of $CaCl_2$ to Na_2CO_3 also lowered the zeta potential. For freshly precipitated $CaCO_3$ ($CaCl_2$: Na_2CO_3 = 1:1), its zeta potential at initial pH was slightly positive but dropped to negative at other tested pHs. For freshly precipitated $CaCO_3$ ($CaCl_2$: Na_2CO_3 = 1:2), its zeta potential was negative throughout the pH range tested, which is accounted for by the excess of carbonate ions in the solution. The trend of zeta potential change was very similar to that of freshly precipitated $CaCO_3$ ($CaCl_2$: Na_2CO_3 = 1:1). There has been debate on the PDIs for $CaCO_3$ and it is more generally accepted that Ca^{2+} and CO_3^{2-} (and other carbonate species) are the PDIs. In our results, comparing the three situations (Ca^{2+} in excess, CO_3^{2-} in excess or equal ratio), it can be clearly seen that in the presence of Ca^{2+} or CO_3^{2-} in the solution, pH plays a less important role in the charge modification of the $CaCO_3$ surfaces, which is in good agreement with previous reports (Derkani et al. 2019; Mahani et al. 2015), supporting that Ca^{2+} and CO_3^{2-} are the PDIs for both preformed and freshly precipitated $CaCO_3$.

The predicted mineral species with SIs greater than zero for in situ formed $CaCO_3$ cases were calcite > aragonite > vaterite > $CaCO_3 \cdot xH_2O$ in descending order, with slightly higher SIs with CO_2 input than that of without (**Figure 2.5 A/B/C**). The SIs predicted for calcite (preformed $CaCO_3$) was zero for the entire pH range, implying an equilibrium between dissolved and precipitated $CaCO_3$ (**Figure 2.5 D**).

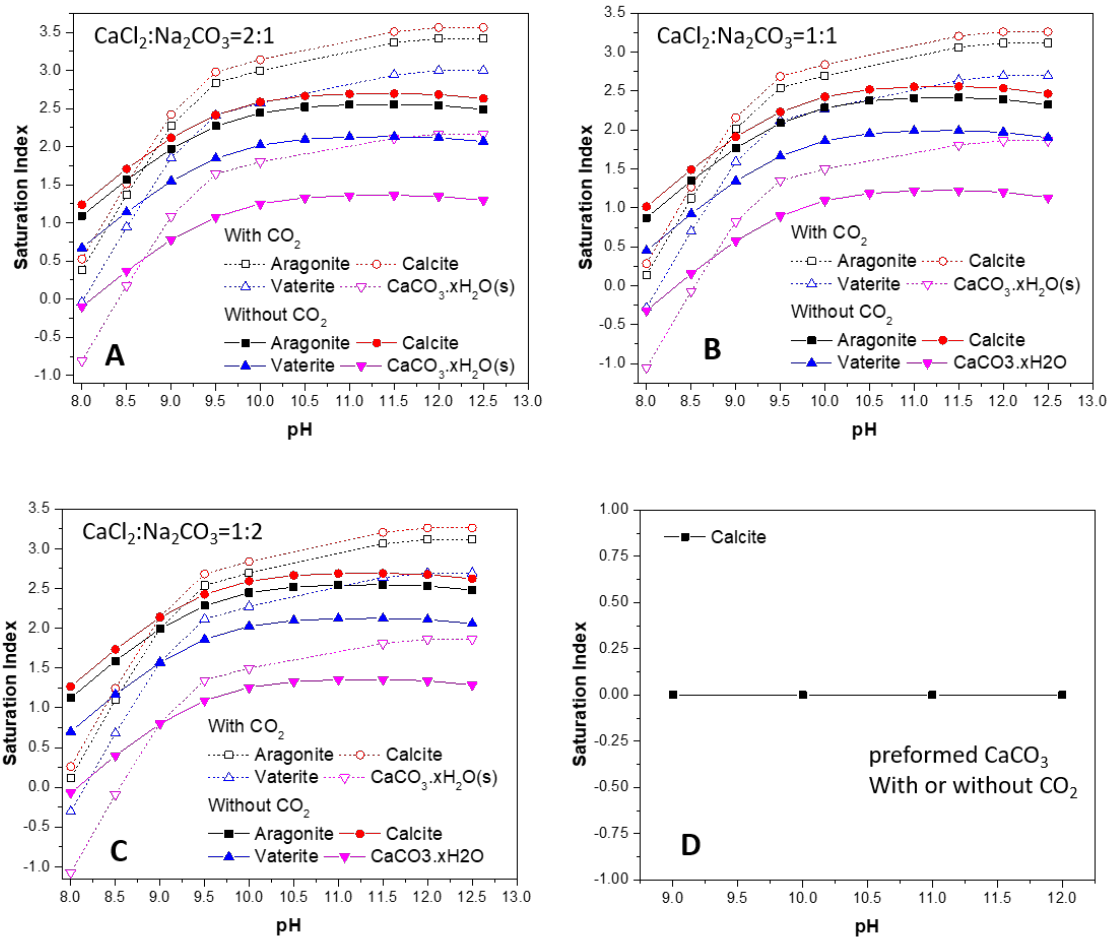

Figure 2.5. SIs of mineral species as a function of pH for in situ formed $CaCO_3$ with a ratio of $CaCl_2$:Na_2CO_3 of (A) 2:1, (B) 1:1, (C) 1:2, and (D) preformed $CaCO_3$ with (P_{CO_2} = 0.00038 atm) and without CO_2 input (P_{CO_2} = 0 atm).

2.3.2.2 The effect of temperature

With increasing in temperature from 25 to 65 ºC, the pH of preformed $CaCO_3$ remained fairly stable, whereas the zeta potential decreased from -12 mV to -22 mV (**Figure 2.4 B**). For freshly precipitated $CaCO_3$, temperature change showed effects depending on the initial molar ratios of precursor materials ($CaCl_2$: Na_2CO_3). Both $CaCl_2$:Na_2CO_3 = 1:1 and $CaCl_2$:Na_2CO_3 = 2:1 showed similar trends of pH and zeta potential. For $CaCl_2$: Na_2CO_3 = 1:1, the pH of the particles started

around 10.0 and decreased with increasing temperature (9.5 at 65 ºC). The zeta potential became more positive (5 to 15 mV) as the temperature increased. For $CaCl_2$:Na_2CO_3 = 2:1 (excess Ca^{2+} ions), the pH was 9.7 and decreased with increasing temperature (8.3 at 65 ºC). The zeta potential was around 20 mV initially and increased further with increasing temperature. For the case of $CaCl_2$: Na_2CO_3 = 1:2 where the water sample has excessive CO_3^{2-} ions, the pH remained fairly close to 11.0 and the zeta potential became more negative as the temperature increased, following the trend of preformed $CaCO_3$.

The predicted mineral species in descending order of SI for in situ formed samples were calcite, aragonite, vaterite, and $CaCO_3.xH_2O$, respectively (**Figure 2.6**). With increasing temperature, the solubility of $CaCO_3$ increases in the absence of atmospheric CO_2, while decreases with atmospheric CO_2 present (Coto et al. 2012; Wells 1915). Thus without CO_2, SI of calcite decreased with increasing temperature; with CO_2, SI of calcite increased with increasing temperature (**Figure 2.6**).

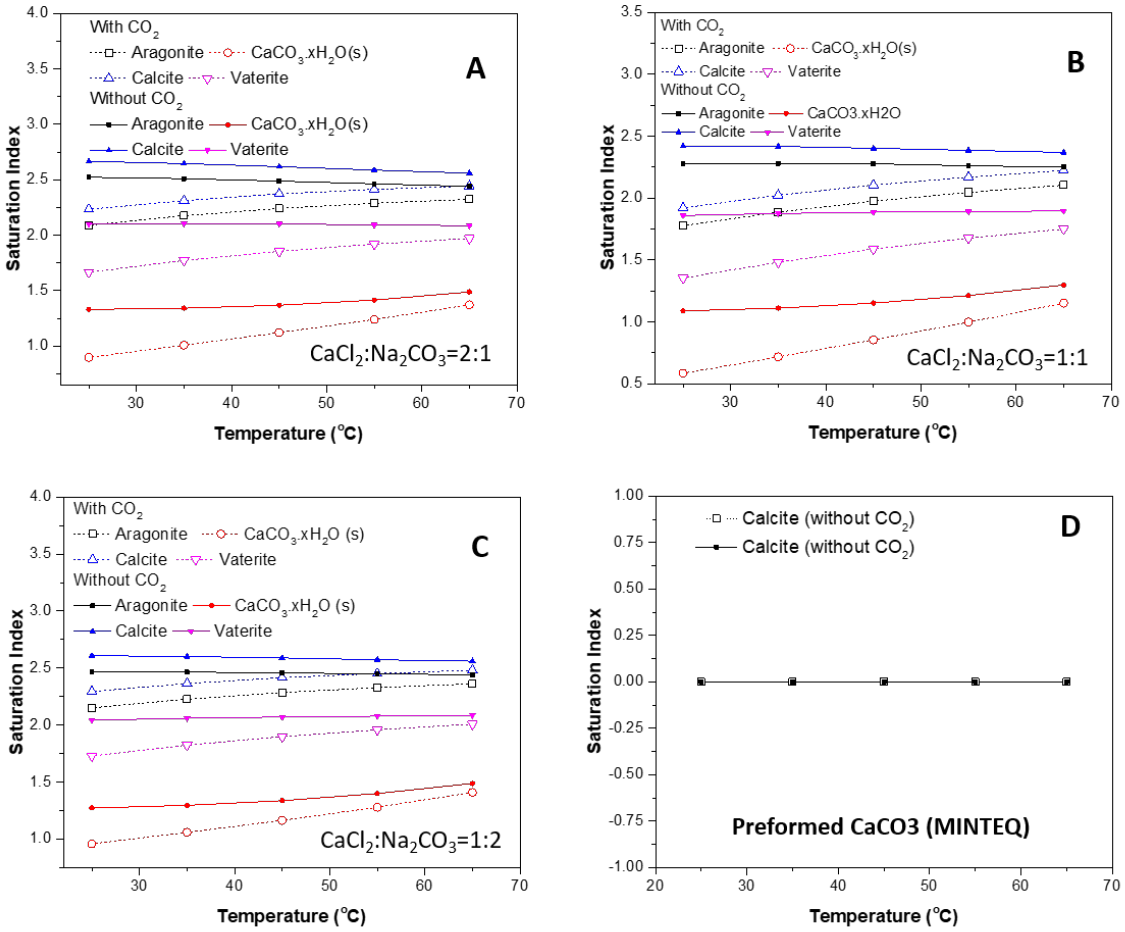

Figure 2.6. Calcium minerals for in situ formed $CaCO_3$ cases at different temperatures with (P_{CO_2} = 0.00038 atm) and without CO_2 input (P_{CO_2} = 0 atm).

Al Mahrouqi et al. (2016, 2017) reported that the zeta potential of natural calcium carbonate became less negative with increasing temperature, which was explained by increased Ca^{2+} concentration resulting from increased calcite dissolution with increasing temperature. Our observation of a different trend for the zeta potential of preformed $CaCO_3$ with respect to temperature could be due to the impact caused by exposure to atmospheric CO_2 in our system, where the solubility of $CaCO_3$ decreases with increasing temperature. Corresponding to the modeling in **Figure 2.6**, the plots of the activity of soluble species (**Figure 2.7**) showed that with

CO_2, for $CaCl_2$: Na_2CO_3 of 1:1 and 2:1, the activity of Ca^{2+} and CO_3^{2-} kept almost the same while that of HCO_3^- obviously decreased with increasing temperature, leading to the observed increased zeta potential with increasing temperature. For $CaCl_2$: Na_2CO_3 of 1:2 and preformed $CaCO_3$, the activity of CO_3^{2-} kept almost the same while that of Ca^{2+} obviously decreased with increasing temperature, leading to the observed decreased zeta potential with increasing temperature.

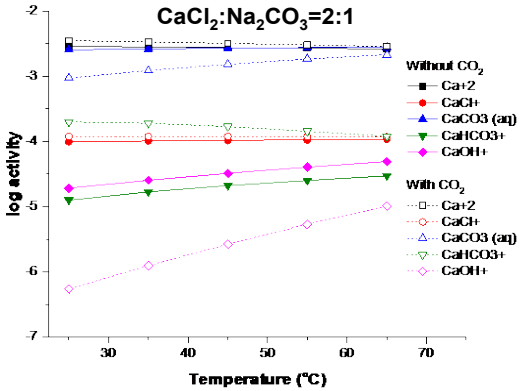
CaCl2:Na2CO3=2:1
log activity
Temperature (°C)
Without CO2
Ca+2
CaCl+
CaCO3 (aq)
CaHCO3+
CaOH+
With CO2
Ca+2
CaCl+
CaCO3 (aq)
CaHCO3+
CaOH+

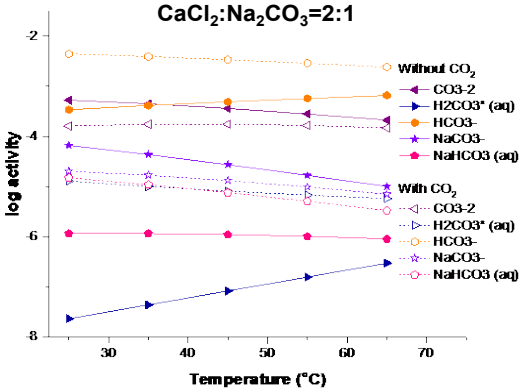
CaCl2:Na2CO3=2:1
log activity
Temperature (°C)
Without CO2
CO3-2
H2CO3* (aq)
HCO3-
NaCO3-
NaHCO3 (aq)
With CO2
CO3-2
H2CO3* (aq)
HCO3-
NaCO3-
NaHCO3 (aq)

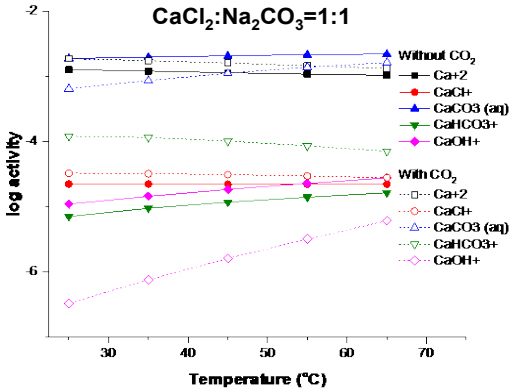
CaCl2:Na2CO3=1:1
log activity
Temperature (°C)
Without CO2
Ca+2
CaCl+
CaCO3 (aq)
CaHCO3+
CaOH+
With CO2
Ca+2
CaCl+
CaCO3 (aq)
CaHCO3+
CaOH+

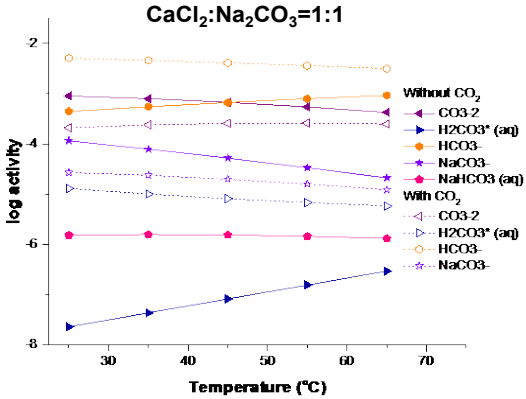
CaCl2:Na2CO3=1:1
log activity
Temperature (°C)
Without CO2
CO3-2
H2CO3* (aq)
HCO3-
NaCO3-
NaHCO3 (aq)
With CO2
CO3-2
H2CO3* (aq)
HCO3-
NaCO3-

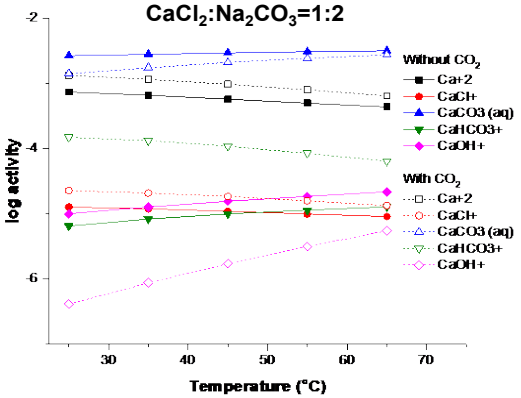
CaCl2:Na2CO3=1:2
log activity
Temperature (°C)
Without CO2
Ca+2
CaCl+
CaCO3 (aq)
CaHCO3+
CaOH+
With CO2
Ca+2
CaCl+
CaCO3 (aq)
CaHCO3+
CaOH+

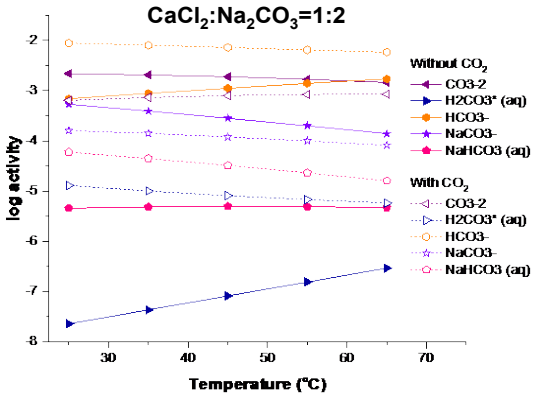
CaCl2:Na2CO3=1:2
log activity
Temperature (°C)
Without CO2
CO3-2
H2CO3* (aq)
HCO3-
NaCO3-
NaHCO3 (aq)
With CO2
CO3-2
H2CO3* (aq)
HCO3-
NaCO3-
NaHCO3 (aq)

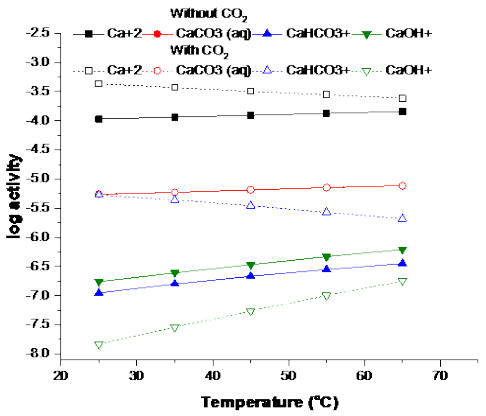
Without CO2
Ca+2
CaCO3 (aq)
CaHCO3+
CaOH+
With CO2
Ca+2
CaCO3 (aq)
CaHCO3+
CaOH+
log activity
Temperature (°C)

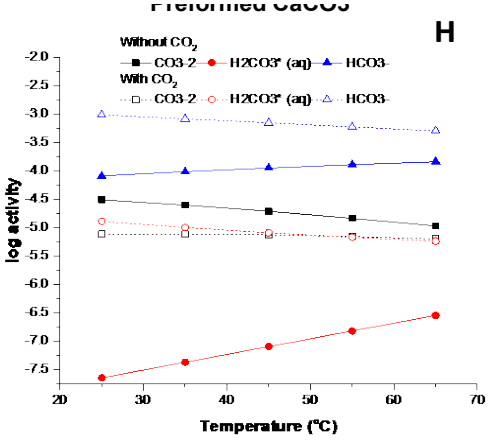
Without CO2
CO3-2
H2CO3* (aq)
HCO3-
With CO2
CO3-2
H2CO3* (aq)
HCO3-
log activity
Temperature (°C)

Figure 2.7. Activity of various ions existing for $CaCO_3$ cases at different temperatures with (P_{CO_2} = 0.00038 atm) and without CO_2 input (P_{CO_2} = 0 atm).

2.3.2.3 The effect of aging

It has been reported that timing and exposure to atmospheric CO_2 can possibly influence the zeta potential measurements of $CaCO_3$ particles (Russell et al. 2009; Wolthers, Charlet, and Van Cappellen 2008). To study the effect of aging, freshly precipitated and preformed $CaCO_3$ were exposed to the atmospheric condition for 48 h, and their zeta potentials and pHs were measured periodically. The observed trend in pH and zeta potential is shown in **Figure 2.4C**, respectively. During the aging test, the pH of all water samples decreased over time due to the increased amount of dissolved CO_2. The zeta potential of all particles decreased over time. For freshly precipitated $CaCO_3$ particles ($CaCl_2$: Na_2CO_3 = 2:1 or 1:1), their zeta potentials started being positive and were eventually reversed to negative. At the end of the aging experiment, the pH of all water samples ranged from 8 – 10 within which HCO_3^- is the dominating species.

2.3.2.4 The effect of $MgCl_2$

$MgCl_2$ stock solution was gradually added to preformed $CaCO_3$ to assess the impact of Mg^{2+} ion on the charge of $CaCO_3$ particles at 25 °C. The Mg^{2+} ions had the same effect on the zeta potential as excess Ca^{2+} ions, as discussed in the sections above. The zeta potential of the $CaCO_3$ was negative but was eventually reversed to positive with the addition of $MgCl_2$ (**Figure 2.4D**). Upon addition of 0.5 mL of $MgCl_2$ (molar ratio of $MgCl_2$ to $CaCO_3$ ~0.5), the average zeta potential was close to zero and the addition of 2 mL of $MgCl_2$ (molar ratio of $MgCl_2$ to $CaCO_3$ >2) reversed the zeta potential of $CaCO_3$ particles to positive. A study done by Black and Christman (1961) showed a similar result – the mobility of $CaCO_3$ (2 mM) became zero when 80 ppm of $MgCl_2$ was added. Also, it was reported that magnesium can be incorporated into the $CaCO_3$ crystal lattice which

results in the formation of a mixed Mg-$CaCO_3$ solid during softening and to more positively charged surfaces (Russell, Lawler, and Speitel 2009). The modeling indicates the potential formation of dolomite ($CaMg(CO_3)_2$) (**Figure 2.8**).

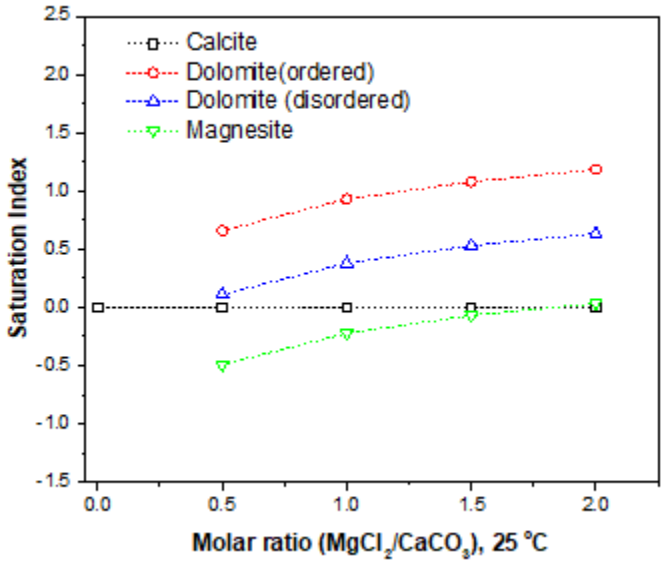

Figure 2.8. Predicted minerals as a function of molar ratio of $MgCl_2/CaCO_3$.

2.3.3 Interactions of Binary Particles

The following sections describe the zeta potential as a function of molar ratio of $CaCO_3$ to $Mg(OH)_2$ at different temperatures (**Figure 2.9A**), impacts of HA (mimicking natural organic matter), silicate (representing silica), clay (mimicking suspended solids) on the zeta potential of $CaCO_3/Mg(OH)_2$ particles systems at 25ºC with different dosage (**Figure 2.9 B-D**) and at different temperatures with the fixed dosage (**Figure 2.9 E** and **F**).

2.3.3.1 $Mg(OH)_2$ and $CaCO_3$ Particles

$CaCO_3$ and $Mg(OH)_2$ particles might be formed simultaneously during lime softening. To study the interaction between $CaCO_3$ and $Mg(OH)_2$ particles under lime softening conditions, the molar ratio of $Mg(OH)_2$ and $CaCO_3$ was varied from 0 to 2, with 0, 2, 4, 8 mM $Mg(OH)_2$ in 4 mM $CaCO_3$ suspensions, respectively, and the zeta potentials were measured at different temperatures (**Figure 2.9A**).

The zeta potential of the binary system was negative at the beginning and became positive when the molar ratio of $Mg(OH)_2$ to $CaCO_3$ was increased to 0.5. Further increasing the ratio to 1 and 2 led to a slow but steady increase in zeta potential at 25 ^oC and 45 ^oC. The trend was slightly different at 65 ^oC, where the zeta potential increased rapidly from molar ratio 0 to 1 and then became stable after that. Since $Mg(OH)_2$ carries positive charges and $CaCO_3$ carries negative charges, the observed change in zeta potential from negative to positive with an increasing ratio of $Mg(OH)_2$ is reasonable. In an early study, Black and Christman (1961)found that both positively and negatively charged particles were present in a softening sludge consisting of both $CaCO_3$ and $Mg(OH)_2$. The relative number of negatively charged particles decreased with increasing pH. Interaction between the two types of particles could also lead to the formation of new minerals with various compositions. The possible species in decreasing order of SIs (**Figure 2.10**) are huntite ($CaMg_3(CO_3)_4$) > hydromagnesite ($Mg_5(OH)_2(CO_3)_4 \cdot 4H_2O$) > dolomite ($CaMg(CO_3)_2$) > magnesite ($MgCO_3$) > artinite ($Mg_2(OH)_2CO_3 \cdot 3H_2O$).

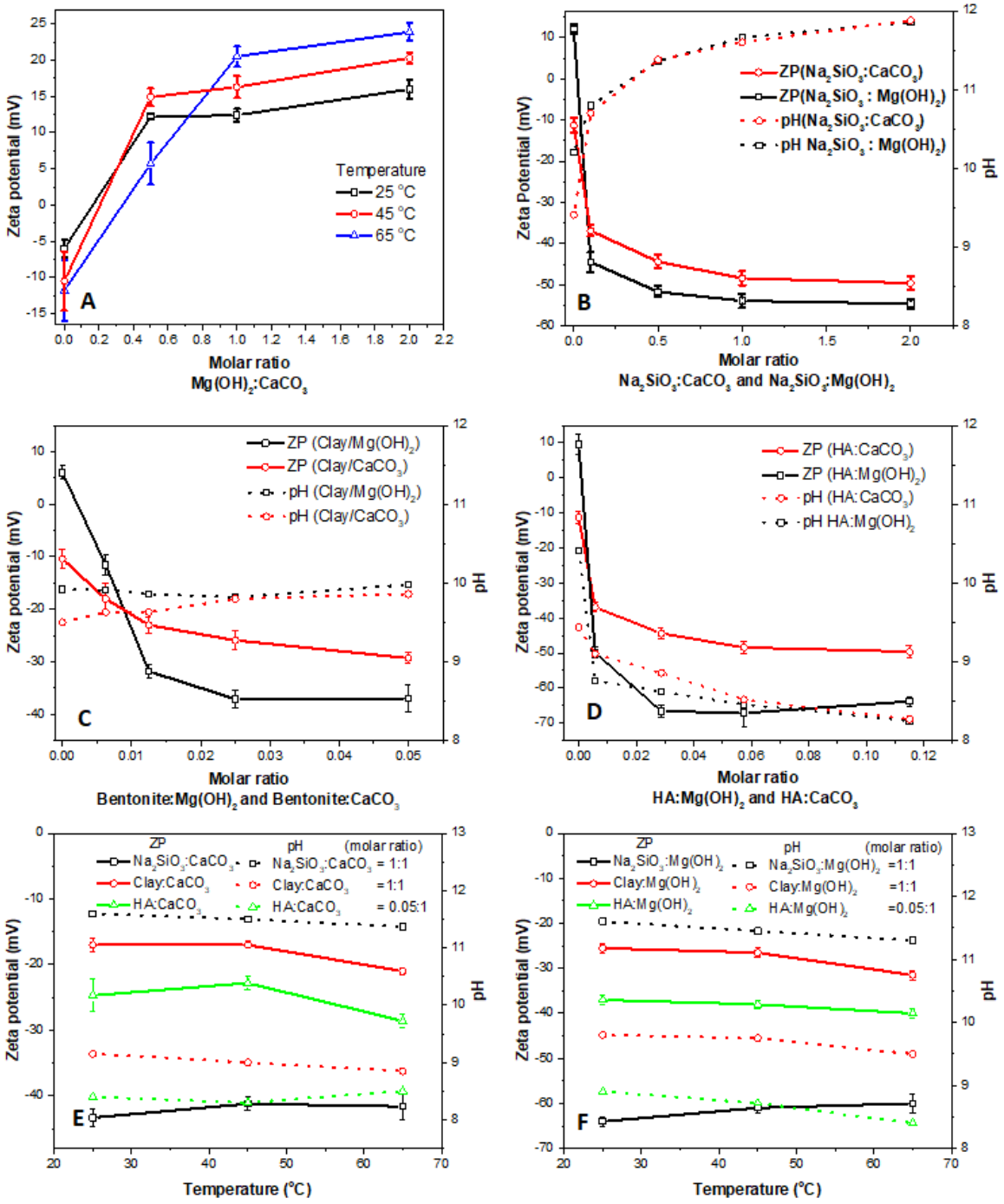

Figure 2.9. (A) The zeta potential as a function of molar ratio of preformed $Mg(OH)_2$ to $CaCO_3$ at different temperature, the effect of (B) sodium silicate, (C) humic acid (HA), and (D) clay on the pH and zeta potential of preformed $CaCO_3$ and $Mg(OH)_2$ particles at 25 °C, and the effect of

temperature on the pH and zeta potential of (E) preformed $CaCO_3$ and (F) $Mg(OH)_2$ particles with fixed dosage of silicate/HA/clay.

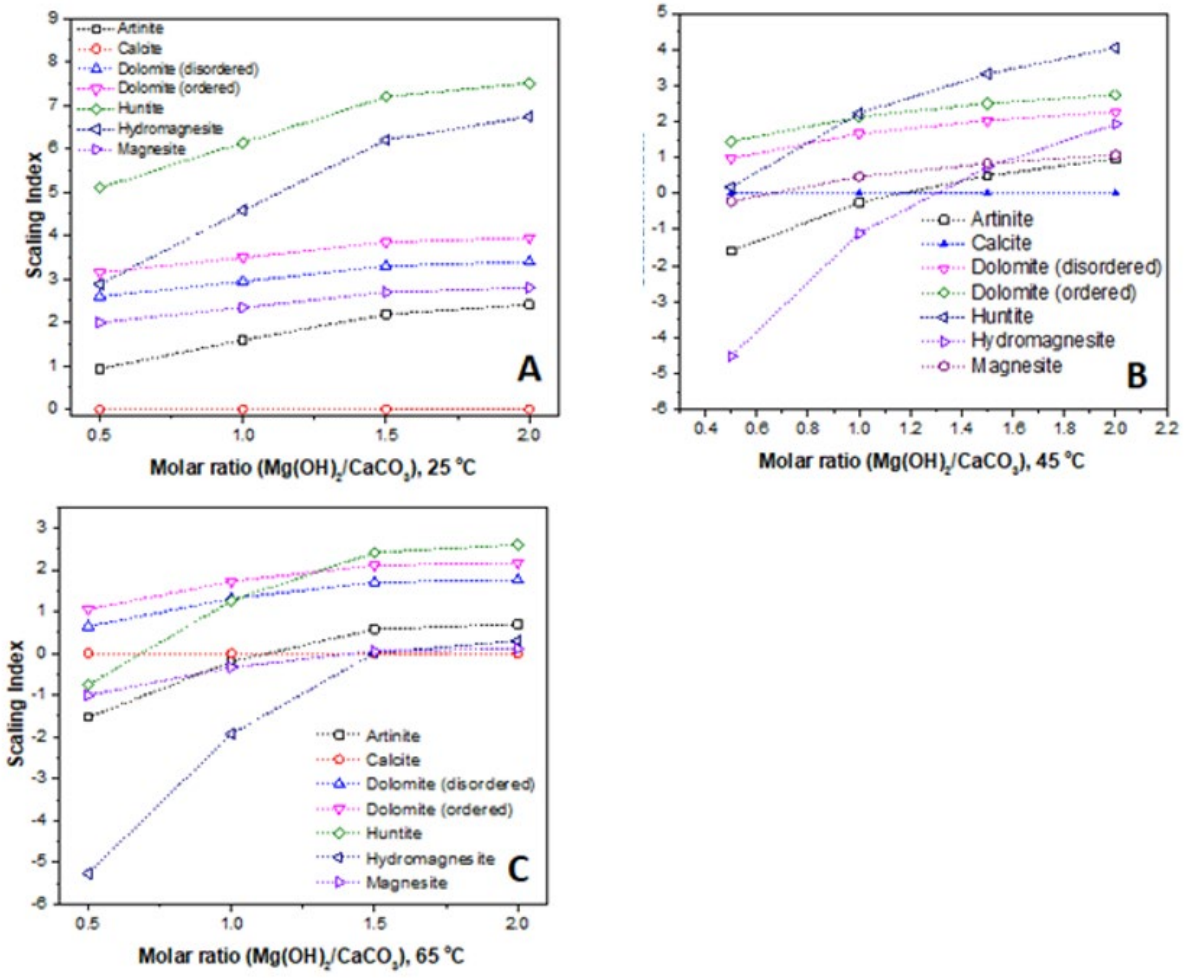

Figure 2.10. Predicted minerals as a function of molar ratio of $Mg(OH)_2/CaCO_3$

2.3.3.2 The effect of silicate on the zeta potential of $CaCO_3$ and $Mg(OH)_2$ particles

Silicate is the ubiquitous constituent of industrial produced water. The pH and zeta potential of $CaCO_3$ and $Mg(OH)_2$ in the presence of various amounts of Na_2SiO_3 (to represent SiO_2) were measured, with 0.4, 2, 4, 8 mM Na_2SiO_3 in 4 mM preformed $Mg(OH)_2$ or $CaCO_3$ suspensions, respectively. The PZC of suspended silicate is around pH 2 – 3 (Stumm, 1992) implying that silicate would be negatively charged throughout the pH range tested in our study.

Figure 2.9B shows the pH and zeta potentials as a function of molar ratios of Na_2SiO_3 and $CaCO_3$ or $Mg(OH)_2$. There was a sharp increase in pH at the molar ratio of 0.1 followed by a slow increase at ratios 0.5 and higher. In the case of $CaCO_3$, zeta potentials showed a sharp decrease from -10 to -37 mV at molar ratio 0.1, followed by a slow decrease to -45 mV between molar ratios 0.5 to 2. $Mg(OH)_2$ and Na_2SiO_3 system also followed the same trend with an increasing ratio of Na_2SiO_3, although the final zeta potential was -55 mV. The negative zeta potential is expected to be dominated by the presence of the charged surface species of $>Si\text{-}O^-$ (Brady and Walther 1989) and a direct result of the increase in pH that shifts functional groups from >Si-OH to $>Si\text{-}O^-$. The modeling indicates that there are no calcium silicate minerals formed for the silicate/$CaCO_3$ system (**Figure 2.11**), while magnesium silicates such as chrysotile ($Mg_3(Si_2O_5)(OH)_4$) may form (**Figure 2.12**) for the silicate/$Mg(OH)_2$ system.

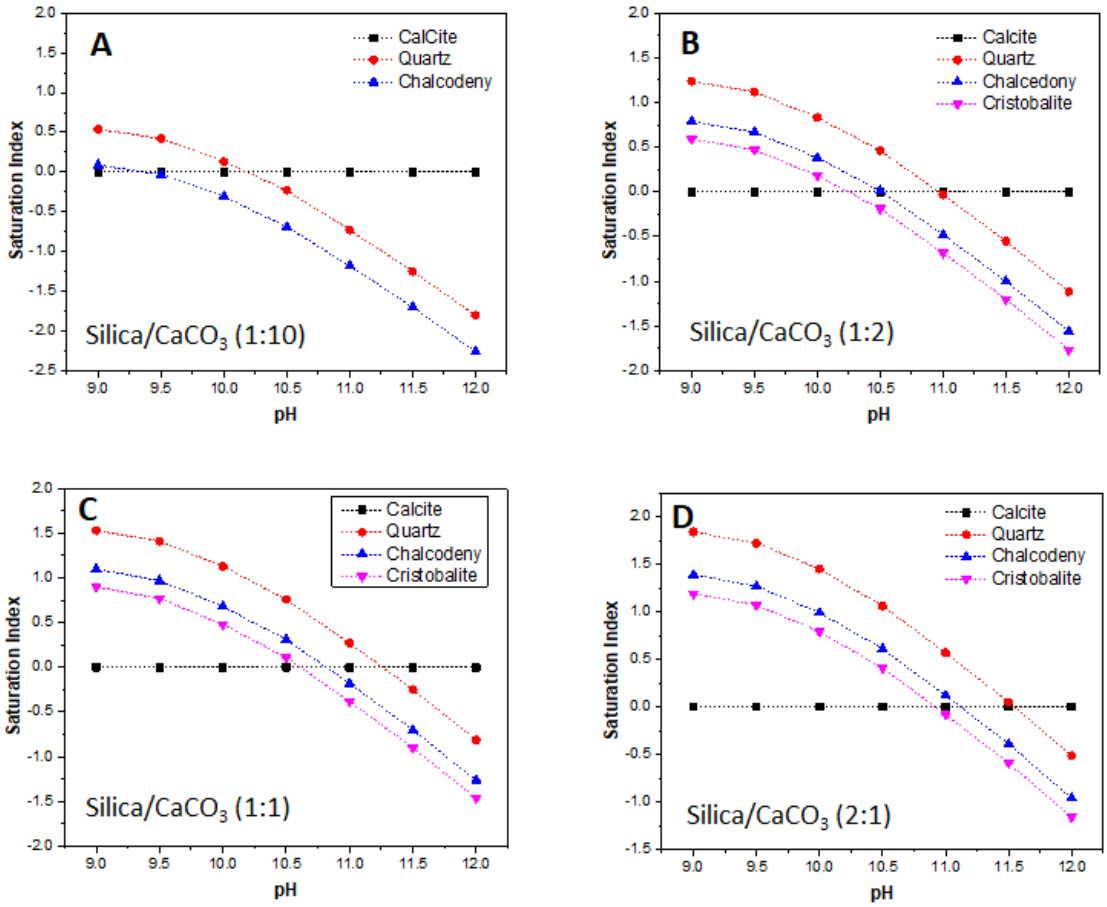

Figure 2.11. Predicted minerals as a function of molar ratio of Silica/$CaCO_3$

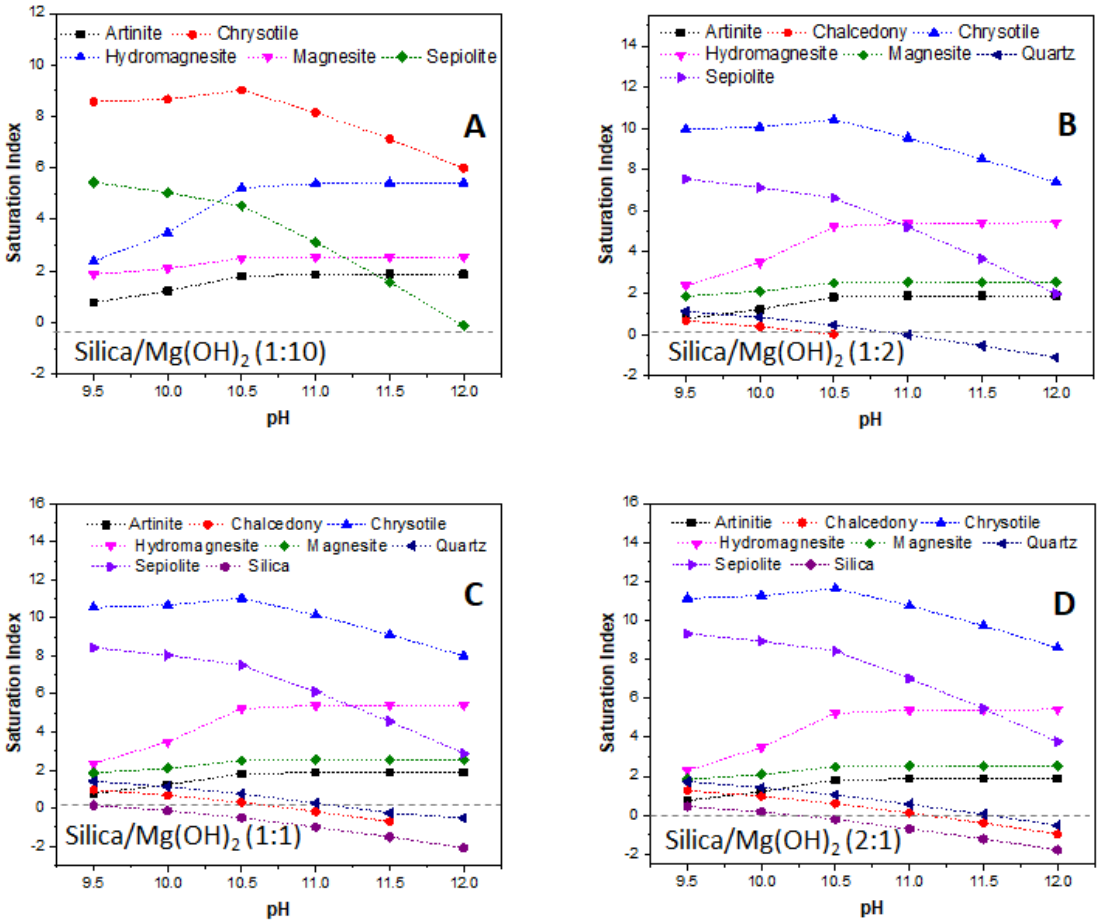

Figure 2.12. Predicted minerals as a function of molar ratio of Silica/$Mg(OH)_2$

As shown in **Figure 2.9 E and F**, with increasing temperature in the range of 25 to 65 ºC, the zeta potential of silicate-$CaCO_3$ (molar ratio 1:1) system remained almost unchanged, for silicate-$Mg(OH)_2$ (molar ratio 1:1) system, the zeta potential remained negative and the magnitude decreased slightly (-64 mV at 25 ºC to -60 mV at 65 ºC), while the pH of both systems slightly decreased.

2.3.3.3 The effect of humic acid (HA) on the zeta potential of $CaCO_3$ and $Mg(OH)_2$ particles

Studies have shown that NOM can be removed during the lime softening process through coprecipitating with $CaCO_3$ and $Mg(OH)_2$ solids (Russell et al. 2009; Russell, Lawler, and Speitel 2009). Oil field produced water and many other industrial wastewaters contain dissolved organic substances that have similar chemical characteristics to HA, most importantly, in the presence of a large number of negatively charged functional groups (Pillai et al. 2017). Hence HA is used in this study to mimic organic matter in produced water. Similar to the silica experiments, the pH and zeta potential of $CaCO_3$ and $Mg(OH)_2$ in the presence of various amounts of HA (to represent NOM) were measured (**Figure 2.9C**), with 0.4, 2, 4, 8 mM HA in 4 mM preformed $Mg(OH)_2$ or $CaCO_3$ suspensions, respectively.

With the increasing concentration of HA, the pH of the $CaCO_3$ solution decreased from 9.45 to 8.3 and the pH of the $Mg(OH)_2$ solution decreased from 10.45 to 8.3 (**Figure 2.9C**). The zeta potential decreased with increasing molar ratios for both $CaCO_3$ and $Mg(OH)_2$ solutions. Stumm (1992) suspected that molecules of dissolved HAs can be considered as flexible polyelectrolytes with anionic functional groups that also have hydrophobic components. Adsorption of HAs on inorganic surfaces could happen from the ligand exchange of functional groups on the humic substances (carboxylic, phenolic) with surface hydroxyl groups on the metal oxides, supplemented by a hydrophobic interaction involving nonpolar components of the humic molecules. In addition, the binding of metal ions to the carboxyl and hydroxyl groups on HA can occur in a monodentate and bidentate form. The Stockholm humic model (SHM) predicts that the dissolution of $CaCO_3$ and $Mg(OH)_2$ increases with the concentration of HA (**Figure 2.13**). Based on modeling data, the dissolved Ca^{2+} ions can form mono- and bidentate complexes, i.e., $HACa^{+}(aq)$ and HA_2Ca and

Mg^{2+} ions form a monodentate complex, $HAMg^{+}(aq)$. In a modeling study reported by Gustafsson (2001), it was suggested that a monodentate calcium complex is the dominant form in acidic pH and the bidentate complex becomes significant only above pH 10. Although electrostatic repulsion arising from the high negative charge density of HA and $CaCO_3$ surfaces at high pH leads to low levels of HA adsorption, as speculated by Bob and Walker (2001), HA does not adsorb to calcite by a simple charge neutralization mechanism, rather, HA adsorbs to calcite through specific or non-specific chemical interactions between HA and the $CaCO_3$ surface.

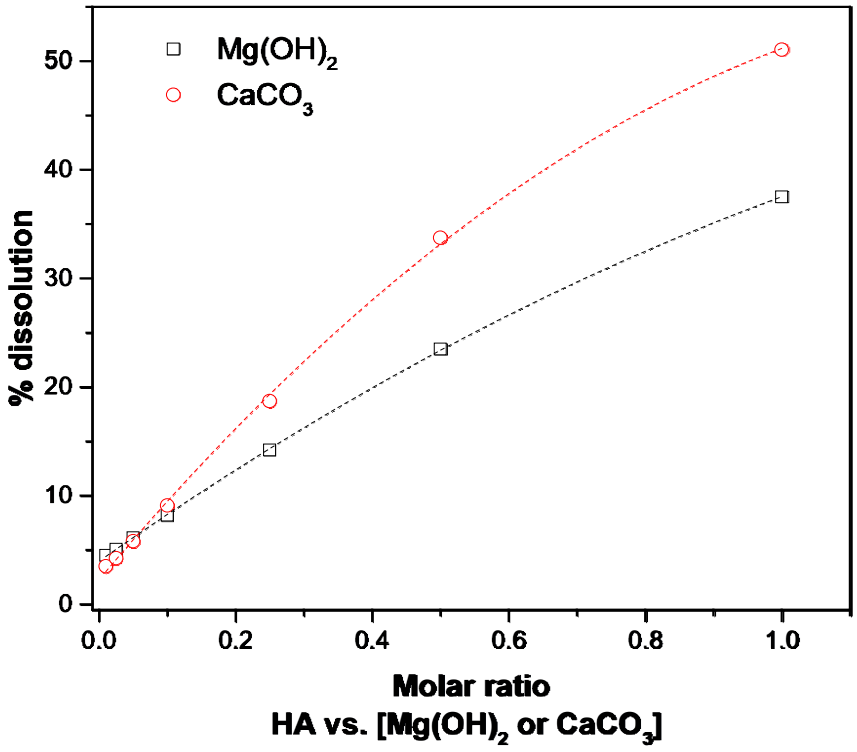

Figure 2.13. Thermodynamic modeling of dissolution of $CaCO_3$ and $Mg(OH)_2$ increasing with the concentration of HA based on the Stockholm Humic Model (SHM).

The pH and zeta potential of HA-$CaCO_3$ and HA-$Mg(OH)_2$ at a fixed molar ratio of 0.05:1 are shown in **Figure 2.9 E** and **F**. Increasing the temperature from 25 to 65 ºC increased slightly the

magnitude of the zeta potential of HA-$CaCO_3$ (-25 mV at 25 ºC to -29 mV at 65 ºC) and HA-$Mg(OH)_2$ system with molar ratio of 0.05:1 (-37 mV at 25 ºC to -40 mV at 65 ºC), while the pH slightly increased for the former and decreased for the latter system.

2.3.3.4 The effect of clay on the zeta potential of $CaCO_3$ and $Mg(OH)_2$ particle systems

Suspended solids can be removed from waters during lime softening. In this study, bentonite was used to represent suspended solids. The PZC of bentonite (montmorillonite, $Al_2O_3{\cdot}4SiO_2{\cdot}H_2O$) is around a pH of 2.5 (Stumm 1992) implying that bentonite would be negatively charged throughout the pH range tested in our study. The effect of increasing clay content on the zeta potential of the clay/$CaCO_3$ and clay/$Mg(OH)_2$ systems was studied. For both experiments, there was no obvious change of pH with the increasing clay concentration. It was observed (**Figure 2.9D**) that when introducing clay to $CaCO_3$ particles, the zeta potential of the system became more negative as more clay was added. At clay: $CaCO_3$ molar ratio of 0.05, the zeta potential was around -28 mV. Similar results were observed for the clay and $Mg(OH)_2$ interaction. Although the zeta potential of $Mg(OH)_2$ started around +10 mV, at the clay: $Mg(OH)_2$ molar ratio of 0.05, the zeta potential was around -37 mV. The modeling (**Figure 2.14**) indicated no formation of new calcium minerals in the clay/$CaCO_3$ system, while there was the potential formation of magnesium silicate precipitates such as chrysotile and sepiolite in clay/$Mg(OH)_2$ systems.

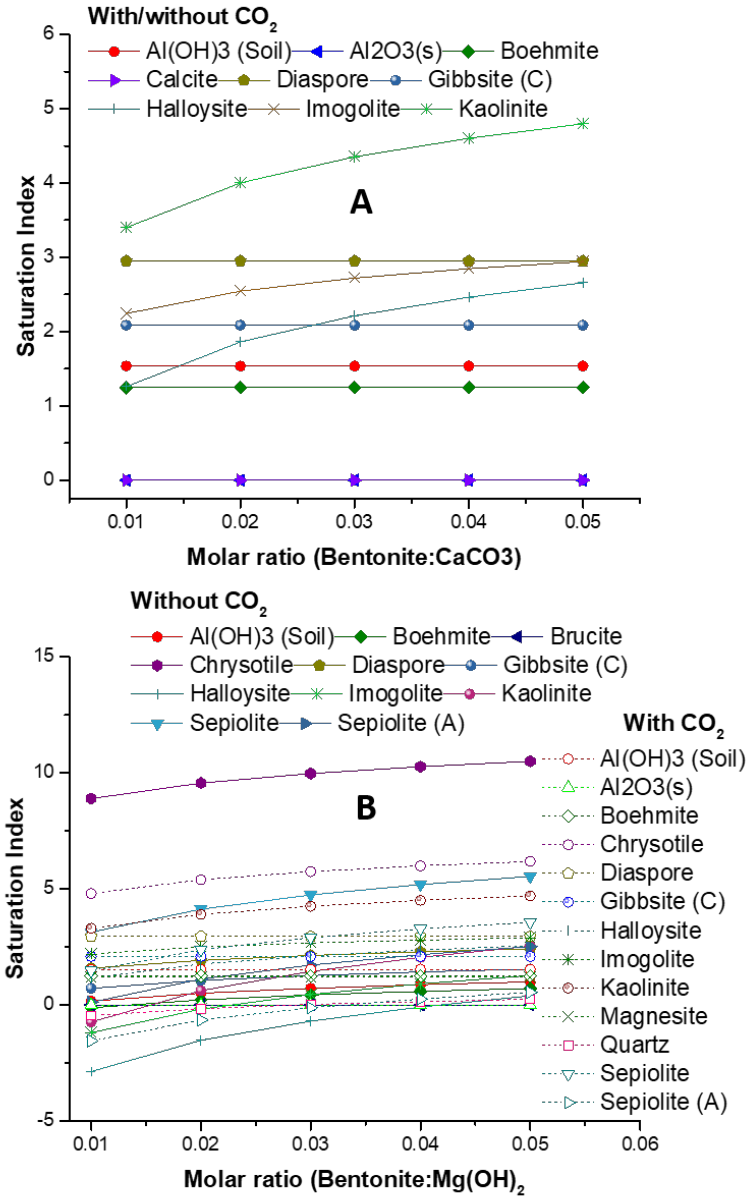

Figure 2.14. Predicted minerals as a function of molar ratio of (A) Bentonite/$CaCO_3$ and (B) Bentonite/$Mg(OH)_2$

The effect of temperature on the pH and zeta potential of clay-$CaCO_3$ and clay-$Mg(OH)_2$ at a fixed molar ratio of 1:1 are shown in **Figure 2.9 E** and **F**. Increasing the temperature from 25 to 65 ºC increased slightly the magnitude of the zeta potential of clay-$CaCO_3$ (-17 mV at 25 ºC to -21 mV

at 65 ºC) and clay-$Mg(OH)_2$ system with molar ratio of 1:1 (-25 mV at 25 ºC to -31 mV at 65 ºC), and the pH decreased slightly for both systems.

2.3.4 Interpretation of the scenarios

2.3.4.1 Surface charge development and zeta potential

The surface charge of $CaCO_3$ and $Mg(OH)_2$ particles in a lime softener depends on the chemical species on their surfaces, the equilibrium reactions between those species and the chemical species present in solution. Stipp and Hochella (1991), on the basis of X-ray photoelectron spectroscopy (XPS) and low energy electron diffraction (LEED) analysis, have shown that $CaCO_3$ contains $>CO_3H^0$ and $>CaOH^0$ as functional groups on the surface in water. These functional groups can interact with potential determining ions (PDI), such as Ca^{2+} and CO_3^{2-} (or HCO_3^- or H_2CO_3) (S. L. S. Stipp 1999; Thompson and Pownall 1989), which could change the surface charge of $CaCO_3$. There are no specific studies available in the literature that investigate the functional groups on the surface of $Mg(OH)_2$ particles. Russell, Lawler, & Speitel (2009) suspected that $>MgOH^0$ could be the functional group dictating the surface charge of $Mg(OH)_2$. Based on the functional group charge development theory, surface equilibrium reactions and potential surface species can be illustrated in **Figure 2.15 A** and **B** for $Mg(OH)_2$ and $CaCO_3$ particles, respectively. Particle surfaces carry charges and are surrounded by a layer of free ions in the liquid phase that is referred to as an electric double layer which consists of a stern layer (or Helmholtz layer) and a diffuse layer. The Stern layer represents the counterions bounded to the particle surface. The diffuse layer is comprised of an atmosphere of ions in rapid thermal motion close to the particle surface (Israelachvili 1992). The particle with the Stern layer acts as a single entity and zeta potential (ζ) is the potential experimentally measured at the shear plane. The Stern potential (ψ_{st}) is determined

by the surface potential and Stern layer structure, and the potential decreases exponentially with distance from the Stern potential through the diffuse layer (Israelachvili 1992).

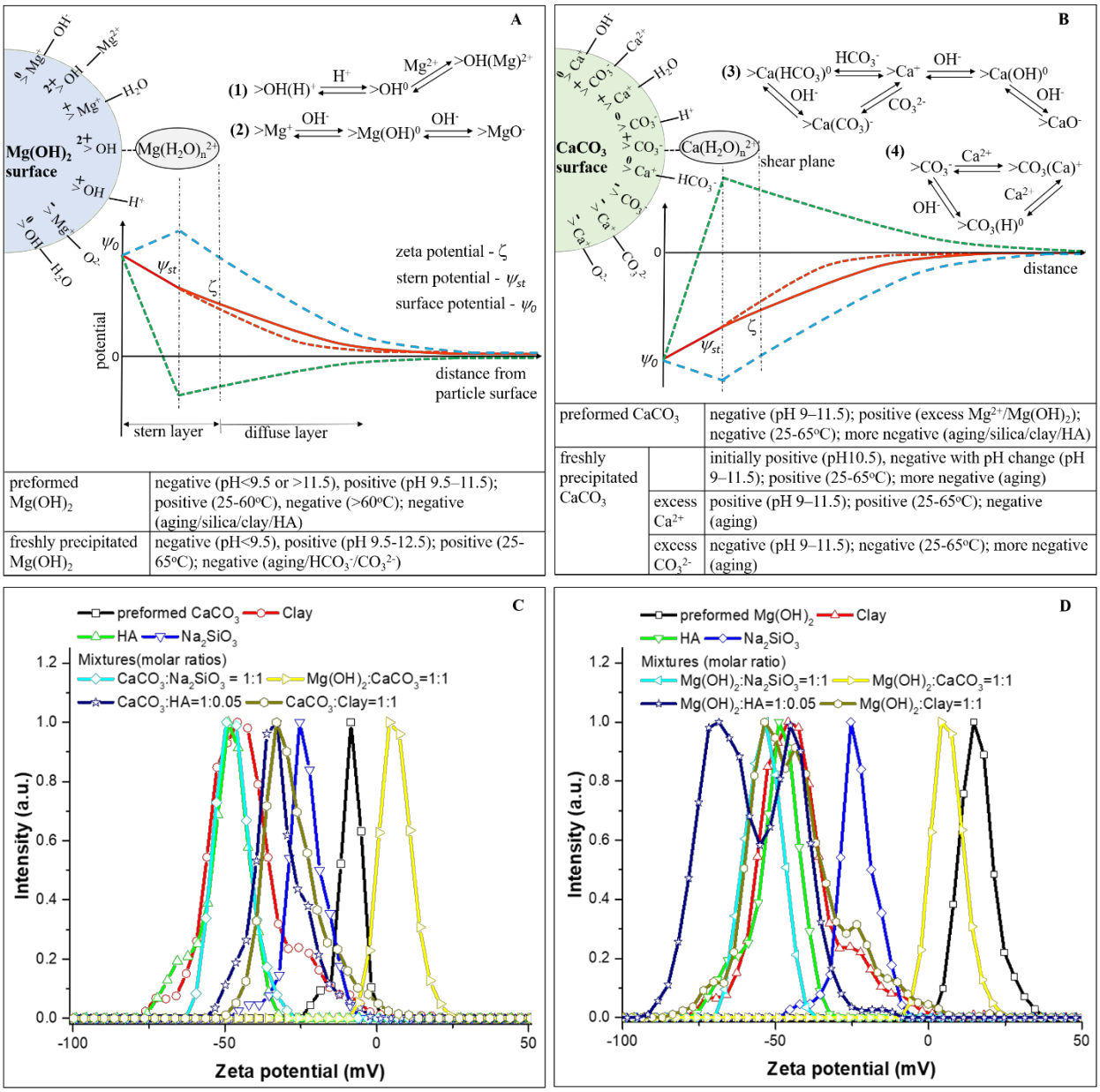

preformed $Mg(OH)_2$	negative (pH<9.5 or >11.5), positive (pH 9.5–11.5); positive (25-60°C), negative (>60°C); negative (aging/silica/clay/HA)
freshly precipitated $Mg(OH)_2$	negative (pH<9.5), positive (pH 9.5-12.5); positive (25-65°C); negative (aging/HCO_3^-/CO_3^{2-})

preformed $CaCO_3$		negative (pH 9–11.5); positive (excess Mg^{2+}/$Mg(OH)_2$); negative (25-65°C); more negative (aging/silica/clay/HA)
freshly precipitated $CaCO_3$		initially positive (pH10.5), negative with pH change (pH 9–11.5); positive (25-65°C); more negative (aging)
	excess Ca^{2+}	positive (pH 9–11.5); positive (25-65°C); negative (aging)
	excess CO_3^{2-}	negative (pH 9–11.5); negative (25-65°C); more negative (aging)

Figure 2.15. Potential species and charge development on the surface of (A) $Mg(OH)_2$ and (B) $CaCO_3$ in water (> represents surface site) with the schematic of zeta potential changes corresponding to changes of Stern potential due to changes of the Stern layer structure (red solid – reference position, green dotted – reversed Stern potential from reference, blue dotted – increased magnitude of Stern potential from reference, red dotted – suppressed diffuse layer from reference

due to increased ionic strength) and data summary of sign of zeta potential under different scenarios. The zeta potential distribution of the binary particles systems for (C) $CaCO_3$ and (D) $Mg(OH)_2$ based systems with the peaks for individual, and binary components.

In this work, positive zeta potential values were observed for $Mg(OH)_2$ particles in water due to the presence of $>OH(Mg)^{2+}$, $>Mg(H_2O)^{+}$, $>OH(H)^{+}$, and $>OH(Mg(H_2O))^{2+}$ functional groups in the Stern layer **(Figure 2.15A**, red solid line, equations (1) and (2). At high pH values, a reduction in the zeta potential was observed, which is due to the increase of $>MgO^{-}$ functional groups. The presence of carbonate alkalinity (CO_3^{2-}/HCO_3^{-}) or exposure to CO_2 from the atmosphere (aging) changed the zeta potential of $Mg(OH)_2$ to less positive or being reversed to negative. This indicates a change of the Stern layer structure due to the strong adsorption of CO_3^{2-}/HCO_3^{-}, leading to less positive or even negative Stern potential (**Figure 2.15A**, green dotted line) and the possible formation of $>MgCO_3^{-}$ functional groups.

Preformed $CaCO_3$ particles exhibit negative zeta potential due to the presence of $>Ca(CO_3)^{-}$ and $>CO_3^{-}$ in the Stern layer (**Figure 2.15B**, red solid line). The pH will shift the equilibrium (**Figure 2.15B,** equations (3) and (4) and causes the variations of zeta potential as a function of pH. The zeta potential of $CaCO_3$ particles changes from negative to positive in excess divalent metal cations (Ca^{2+}, Mg^{2+}) due to the formation of $>CO_3(Ca)^{+}$ and $>CO_3(Mg)^{+}$ functional groups in the Stern layer (**Figure 2.15B**, green dotted line). Excess CO_3^{2-} or aging increases the magnitude of the zeta potential of $CaCO_3$ to more negative due to the adsorption of CO_3^{2-}, HCO_3^{-} and OH^{-} ions shifting the surface equilibrium reactions (**Figure 2.15B**, blue dotted line).

It can be concluded that strong interactions exist among the binary particles systems as new zeta potential distribution peaks were observed in the binary systems compared to those of the individual components (**Figure 2.15 C** and **D**). There were either a zeta potential peak position in

between two peaks from the individual components ($CaCO_3$-$Mg(OH)_2$ of molar ratio 1:1, $CaCO_3$-HA of molar ratio 1:0.05, $CaCO_3$-clay of molar ratio 1:1), a peak at a much more negative position than the two peaks of the individual components ($CaCO_3$-Na_2SiO_3 of 1:1, $Mg(OH)_2$-Na_2SiO_3 of 1:1), or multiple peaks ($Mg(OH)_2$-HA of 1:0.05, $Mg(OH)_2$-clay of 1:1), which are not due to the overlapping of peaks from individual components.

2.3.4.2 Implications to lime softening operation

The understanding of the electrophoretic properties of $CaCO_3$ and $Mg(OH)_2$ particles obtained in this study has important implications for lime softening processes. For example, warm lime softening (WLS) is commonly used in many industrial water treatment applications, including treating oilfield produced water for hardness, alkalinity, and silica removal (Heins, 2009), and softening of cooling water and boiler feed water streams. In spite of the fact that WLS has been commonly used for a few decades now, very little is known about the fundamental interactions and electrokinetic properties (particle charge) of the resulting $CaCO_3$ and $Mg(OH)_2$ particles in the softener. The results of this study will be relevant to WLS onsite chemical dosage evaluation and operational controls, especially during a WLS effluent off-specification event. For example, the zeta potential of $CaCO_3$ and $Mg(OH)_2$ particles decreases in the presence of elevated concentrations of NOM, clay, and silica. For waters subject to significant variability in silica or NOM concentrations (e.g. cyclic steam stimulation enhanced oil recovery operations or river sources after storm events), these changes in raw water quality may influence the dose of the coagulant needed and the efficiency of the softening process for particle removal. As observed in this study, a wide range of other parameters including pH and the concentrations of Ca^{2+} and Mg^{2+} ions, alkalinity and clay have been shown to affect the surface charges of $CaCO_3$ and $Mg(OH)_2$

particles. This research has also found that the particles present in softeners and their surface charge can depend on the presence of atmospheric CO_2. This must be taken into consideration, as some industrial softeners are operated in covered vessels with a nitrogen atmosphere to exclude oxygen and CO_2.

Additionally, temperature affects the surface charge of $CaCO_3$ and $Mg(OH)_2$ particles and the interactions between them, and the zeta potential of precipitated particles may therefore be different for cold, warm and hot softening processes. The bench-scale jar testing for selecting and optimizing coagulant and flocculant needs to be conducted at the same temperature as the real lime softening process, bench-scale jar testing conducted at room temperature will probably provide misleading results for higher temperature lime softening processes. Analytical instruments such as a zeta potential analyzer can provide useful information on particle charge that may augment the information provided by traditional tests.

2.4 Conclusion

The surface charge characteristics of $CaCO_3$ and $Mg(OH)_2$ particles, either preformed or freshly precipitated from synthetic waters, were examined using experimental zeta potential measurements. The influences of various experimental conditions such as pH, temperature, aging time, the presence of various dissolved ions, silicate, organic carbon (HA) and clay on the electrokinetic properties of $CaCO_3$ and $Mg(OH)_2$ particles were studied systematically. This fundamental understanding will provide important insights into the optimization and on-site control of softening processes. The major findings of this study are summarized as follows:

- The zeta potential of both preformed and freshly precipitated $CaCO_3$ and $Mg(OH)_2$ particles varies with solution pH.

- Both preformed and freshly precipitated $Mg(OH)_2$ particles exhibit positive zeta potential between pH 9.5-11.5.

- The zeta potential of preformed $CaCO_3$ particles can vary significantly from that of freshly precipitated particles. Preformed $CaCO_3$ particles exhibit negative zeta potential in the pH range of 9.0-11.5. Freshly precipitated $CaCO_3$ particles can be either negatively or positively charged, depending on the concentrations of other potential determining ions present in the solution.

- The zeta potential of preformed $Mg(OH)_2$ particles can vary significantly from that of freshly precipitated particles. The zeta potential of preformed $Mg(OH)_2$ is ~ +10 mV at room temperature and slowly decreases as the temperature increases over the range of 25 to 65 ^oC and is reversed to ~ -5 mV at 65 ^oC. But the zeta potential of in-situ precipitated $Mg(OH)_2$ is higher (~+25 mV) at room temperature and is not affected much by temperature rise.

- Similarly, the zeta potential of preformed $CaCO_3$ is between -10 and -15 mV at room temperature and becomes more negative as the temperature is increased. The zeta potential of in-situ formed $CaCO_3$ is ~+5 mV and increases with increasing temperature.

- The zeta potential of $CaCO_3$ particles can change from negative to positive resulting from the existence of divalent metal cations (Ca^{2+}, Mg^{2+}) or $Mg(OH)_2$. The divalent metal cations (Ca^{2+},

Mg^{2+}) can adsorb on $CaCO_3$ particles and change its zeta potential from negative to positive. $Mg(OH)_2$ can interact with $CaCO_3$ and gradually decrease the magnitude of its negative charge.

- The presence of carbonate alkalinity (CO_3^{2-}/HCO_3^-) or exposure to CO_2 from the atmosphere (aging) changes the zeta potential of $CaCO_3$ to more negative and $Mg(OH)_2$ to less positive or being reversed to negative.

- The additions of silica, clay or humic acid can easily shift $Mg(OH)_2$ particles from being positively charged to negatively charged and easily increases the magnitude of negatively charged $CaCO_3$ particles.

Chapter 3 Impact of Solution Feed Deviations on Polymer Coagulant Dose in Synthetic SAGD Produced Water

3.1 Introduction

SAGD operation in oil sands industry utilizes high temperature and pressure steam to extract bitumen that is too deep to be mined (Butler 1994). The oily water released after bitumen separation, known as PW, is further treated to reduce the bitumen content to 0.5 ppm (Fatema et al. 2015; Mohammadtabar et al. 2019). PW is typically blended with one or more of the following streams before the combined stream enters the softening process (i) recycled BBD, make-up water (MUW), and pond water. The combined feed is then introduced in the WLS unit for hardness and silica removal which involves the addition of lime, soda ash, MgO, coagulant, and flocculant (Behrman and Gustafson 1940; Bridle 2005; W. F. Heins 2009) as shown in **Figure 1.2** The influent PW stream is at pH of 7.5 – 9.0 with silica of 150-350 ppm, and TOC of 150-800 ppm, total dissolved solids of 1000-2000 ppm, and hardness values that can vary significantly based on make-up water stream composition. The process typically operates at around 80 - 85°C and removes hardness in the produced water through a series of chemical precipitation reactions. Silica is removed through the addition of MgO through not yet fully established adsorption and/or co-precipitation mechanisms (Perdicakis et al. 2019). Dissolved organic matter and silica are removed through adsorption and co-precipitation. During the operation, hydrated lime ($Ca(OH)_2$), magnesium oxide (MgO), soda ash (Na_2CO_3, as needed) are added. Soluble calcium and magnesium hardness precipitate mainly as $CaCO_3$ and $Mg(OH)_2$, and silica precipitates by reacting with MgO. Coagulant and flocculant are then used to destabilize and promote suspended particle aggregation and settling. The doses of $Ca(OH)_2$ and MgO are typically dictated by the WLS overflow pH (e.g. 10.5) and silica (50 ppm), respectively. Silica in the softener overflow is

typically be reduced to less than 50 ppm to maintain the integrity of the downstream steam boilers (Pedenaud et al. 2006), although some debate on the maximum allowable silica concentration in the WLS exists (Bridle 2005). Total inorganic carbon (TIC) in the WLS overflow also needs to be controlled at a desired range (e.g. 15 to 30 ppm as Carbon) to ensure optimum performance and WLS overflow TIC values can be monitored as an additional key performance indicator. Total dissolved hardness in the overflow is typically controlled under 20 ppmmg/L as CaCO3. WLS overflow hardness values that are too low indicate an overdose of soda ash which is expensive and also potentially damage the downstream steam generation assets. WLS overflow hardness values that are too high will place a higher demand on downstream ion exchange units. WLS overflow TIC values can also be monitored (e.g. 15 to 30 ppm as Carbon) as an additional key performance indicator. Total dissolved hardness in the overflow is typically controlled under 20 mg/L as CaCO3. Alkalinity should not be used as a key performance indicator in SAGD WLS's due to the significant impacts of dissolved organics, silica, and sulphides on the alkalinity of the water which interfere with traditional M and P alkalinity measurements.

Coagulation-flocculation has been widely implemented to agglomerate fine suspended particles and colloids into larger ones to reduce turbidity, organic and inorganic pollutants in municipal and industrial effluents. It can be achieved by four primary mechanisms: (i) double layer compression (i.e. 'salting out'), (ii) charge neutralization, (iii) particle bridging, and (iv) colloid entrapment (i.e. 'sweep floc') (Teh et al., 2016). Nearly all colloidal impurities in SAGD operations are negatively charged and remain suspended due to the strong repulsive forces which prevent them from coalescing. Cationic Coagulants can interact with suspended particles and neutralize the surface charge on the particles. As the surface charge diminishes, there is less repulsion between particles

resulting in aggregation due to attractive van der Waals forces (Stumm 1992), thereby converting them into solid-phase aggregates that can be removed in clarification and filtration processes (Pernitsky et al. 2018; Matilainen, Vepsäläinen, and Sillanpää 2010).

Coagulants can be either inorganic (e.g. aluminum sulfate, aluminum chloride, polyalumium chloride, ferric sulfate, ferric chloride) or organic (e.g. polydiallyldimethylammonium chloride (PolyDADMAC), epichlorohydrin-dimethylamine (EPI-DMA)). There is a range of cationic organic coagulants whose molecular weight and charge densities vary significantly, and most of them contain positive charge-bearing quaternary ammonium groups. Quaternary ammonium cationic polymers such as PolyDADMAC and EPI-DMA are widely used in many water utilities and industrial wastewater plants to enhance the coagulation and flocculation of particles (Pernitsky et al. 2018; Zeng, Li, and Mitch 2016). EPI-DMA polymers have high charge density and can function as both coagulants and flocculants . (Yin 2010; Szyguła et al. 2008). The coagulation-flocculation of colloids by polyelectrolytes is governed by two of the four mechanisms indicated above: the electrostatic patch mechanism, where polyelectrolytes bearing charge opposite to the suspended particles adsorb and reduce the potential energy of repulsion between adjacent colloids, and the bridging model, where polyelectrolytes bound on the colloid surfaces bind together two adjacent colloids (Bratby 2006; Ji et al. 2013).

It is known that the coagulant and flocculant doses are impacted by pH, temperature, dissolved organic matter (DOM) (typically measured as total organic carbon (TOC)), solution salinity, particle concentration and particle surface charge (Ji et al. 2013; Bratby 2006; Parsons and Jefferson 2009). However, the effect of these multiple physicochemical parameters in a complex environment such as industrial WLS units remains relatively unexplored. In our recent work, we

showed that the surface charges of $CaCO_3$ and $Mg(OH)_2$ particles relevant to lime softening were affected by solution chemistry such as inorganic carbon (CO_3^{2-}/HCO_3^-), divalent cations (Ca^{2+}/Mg^{2+}), humic acid, silicate, and clay in the system (Zhang et al. 2020). The ability of various solution components to influence the zeta potentials of $CaCO_3$ and $Mg(OH)_2$ particles varied from one component to another. Humic acid (HA) and silica, in particular, can easily shift the zeta potentials of the softener particles to large negative values even at low concentrations due to their high negative charge density. While this provides the understanding of the binary interactions, the interactions among various particles in a multicomponent system such as a WLS unit is far more complicated and not easily determined. Therefore, a quantitative understanding of the impact of solution chemistry deviations on the coagulant and flocculant demand is of great significance for industrial water treatment process. Of particular interest is assessing how dominant on coagulant demand the properties of the inlet water (e.g., TOC, TSS content) are in comparison to the dry chemicals used in the process (e.g., lime, soda ash, MgO). In this study, we reported a systematic study of the influence of various constituents in synthetic SAGD produced water on the dose of an EPI-DMA coagulant required to achieve charge neutralization for particle settling. The concentration of dissolved calcium, dissolved magnesium, Na_2SiO_3 (representing silica), HA (mimicking natural organic matter), clay (mimicking suspended solids), and bicarbonate ($NaHCO_3$) was varied and zeta potential measurement was employed to determine the optimum coagulant dose for each water sample. The impact of the addition of (Na_2CO_3), lime ($Ca(OH)_2$) and MgO on coagulant dose was also studied

3.2 Experiment and Methods

3.2.1 Chemicals

Calcium chloride dihydrate ($CaCl_2$. $2H_2O$, ACS reagent, 99+%,), magnesium chloride hexahydrate ($MgCl_2$.$6H_2O$, ACS reagent, 99+%), sodium bicarbonate ($NaHCO_3$, ≥ 99.7%), sodium chloride (NaCl, ACS regent, 99+%) and sodium hydroxide (NaOH, ACS regent, ≥97%) were purchased from Fisher Chemicals. Calcium hydroxide ($Ca(OH)_2$, puriss, p.a., ≥96%) sodium silicate (Na_2SiO_3, 99.5% trace metal basis), humic acid (HA, technical grade), and bentonite clay (montmorillonite, Al2O3·SiO2·H2O) were purchased from Sigma Aldrich, Canada. Magnesium Oxide was provided by received from Baymag Inc. High molecular weight of polyamine based cationic coagulant EPI-DMA (SUPERFLOC C-581) , (density: 1.1-1.2 g/cm3, viscosity: ca. 5000 mPa·.s) was obtained from obtained from Kemira chemicals. The actual formulation of the coagulant is not disclosed. Milli-Q water (Millipore deionized with a resistivity of 18.2 MΩ·cm) was has been used for preparation of synthetic water samples.

3.2.2 Instruments

A PB-900™ Series Programmable Jar Testers was used to perform jar tests. The jar tester was operated along with a temperature-controlled water bath. During the jar test, a heater and temperature switch was used to heat up water samples and maintain the temperature at 65 °C. A VWR® general purpose water bath with built-in temperature control was used to heat up the water samples and maintain the temperature at 65 °C after the jar test was complete. An Inkbird temperature switch was used to maintain water sample temperature (working temperature range

from -40 to 100°C). A portable heater was used along with the Inkbird temperature switch to heat up water samples to 65°C.

The zeta potential of the suspended particles in water samples was analyzed by a Malvern Zetasizer Nano ZS with a high concentration zeta potential cell (Zen1010). Samples of the raw and treated water suspensions were collected from the center of the test jar and transferred to the zeta potential cell using a 1 mL syringe The temperature of the water sample in the cell was controlled by the instrument. An electric field is applied across the electrodes of the cell and the resulting electrophoretic mobility is measured by dynamic light scattering. The electrophoretic mobility of particles, which is determined by comparing the frequencies of the two beams of light, is used to calculate the zeta potential using the Henry equation (Skoglund et al. 2017)

$$U_E=2\varepsilon\zeta F(\kappa a)/3\eta$$

where μ_e is the electrophoretic mobility, ε_r is the relative permittivity, ε_0 is the permittivity of vacuum, ζ is the zeta potential, η is the viscosity of water, and f(κa) is the Henry function. Henry equation can be simplified by replacing the term $F(\kappa a)$ with a value of 1.5 – the simplified equation is known as the Helmholtz Smoluchowski Equation (Skoglund et al. 2017).

A Thermo Scientific™ iCAP™ 7200 inductively coupled plasma optical emission spectrometer (ICP-OES) was used to determine the concentration of Si in the water samples. The pH was measured by a Fisher Scientific™ Accumet AE150 pH Benchtop Meter which was calibrated using standard buffer solutions with known pH values at room temperature (pH 4.0, 7.0, and 10.0).

An ultraviolet-visible (UV-vis) spectrophotometer (Shimadzu UV-2600) was used to analyze the concentration of HA in the water samples (Maan et al. 2019). A UV visible absorbance spectrum

of 25 ppm humic acid is shown in the supporting information (**Figure 3.1A**). Humic acid has a broad featureless absorbance spectrum due to its complex composition and thus the absorbances at three wavelengths were compared. A set of humic acid standard solutions (1 to 100 ppm) were prepared by serial dilution to generate Beer-lambert plots. The calibration curves generated at 350, 400, and 500 nm are shown in the supporting information (**Figure 3.1B**). The standard plots were then used to determine the concentration of humic acid after coagulation.

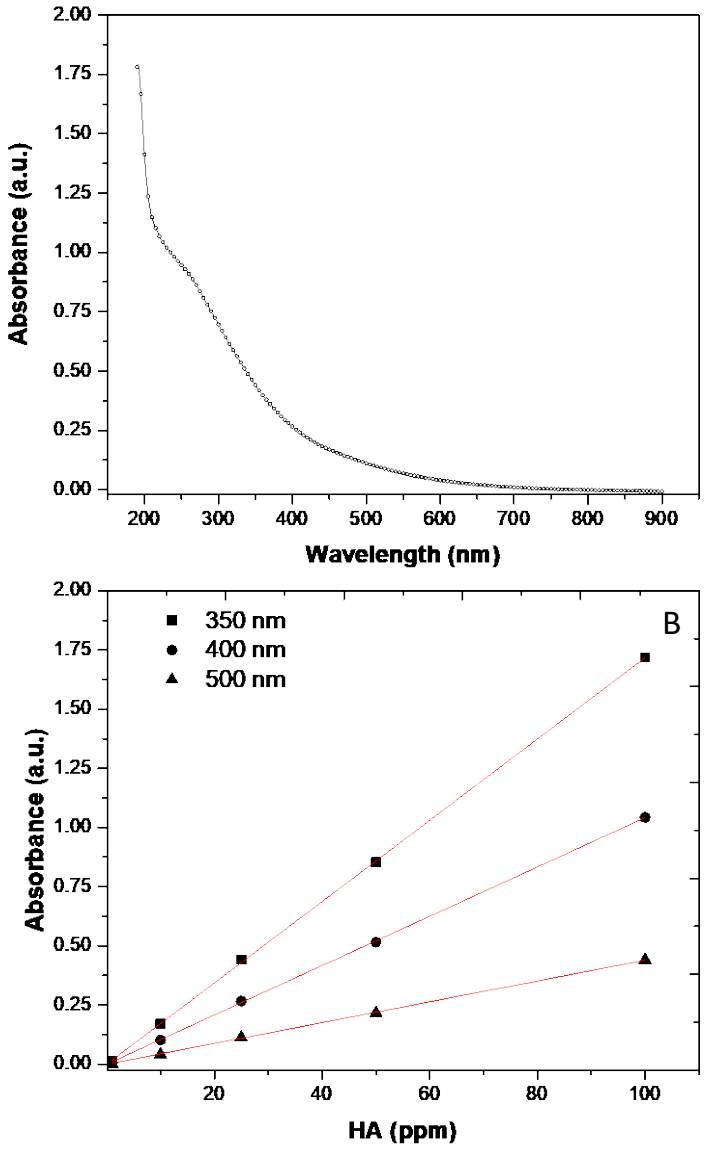

Figure 3.1. (A) UV visible spectrum of 25 ppm humic acid solution and (B) calibration curves at 350, 400, and 500 nm ($R^2 > 0.99$)

3.2.3 $Ca(OH)_2$ and MgO dose estimation

During industrial operation, hydrated lime is added into the rapid mixing zone of a WLS to raise the pH of the influent water and shift alkalinity speciation to carbonate (CO_3^{2-}) which reacts with

calcium hardness (Ca^{2+}) to form $CaCO_3$ precipitate. The increased pH also leads to increased OH^- alkalinity which reacts with magnesium hardness (Mg^{2+}) to form $Mg(OH)_2$ precipitate. If there is no sufficient CO_3^{2-} present in the produced water, Na_2CO_3 is added to promote the precipitation of calcium hardness. The ideal pH to form $CaCO_3$ and $Mg(OH)_2$ precipitation in a typical WLS operating condition (85 ºC) ranges from 9.5 to 10.5. Due to the temperature limit of the zeta potential instrument (70 ºC), the temperature of the experiment was controlled at 65 ºC. Typical lime softening reactions are summarized as follows (Sawyer and McCarty 1978; AWWA 1999):

(1) carbon dioxide removal: $CO_2(g) + Ca(OH)_2(s) \rightleftharpoons CaCO_3(s) + 2H_2O\ (l)$

(2) calcium carbonate hardness removal: $Ca(HCO_3)_2\ (aq) + Ca(OH)_2\ (s) \rightleftharpoons 2CaCO_3(s) + 2H_2O\ (l)$

(3) calcium non-carbonate hardness removal: $Ca^{2+}(aq) + Na_2CO_3\ (aq) \rightarrow CaCO_3\ (s) + 2Na^+(aq)$

(4) magnesium carbonate hardness removal: $Mg(HCO_3)_2\ (aq) + 2Ca(OH)_2\ (s) \rightarrow 2CaCO_3\ (s) + Mg(OH)_2\ (s) + 2H_2O\ (l)$

(5) magnesium non-carbonate hardness removal: $Mg^{2+}\ (aq) + Ca(OH)_2\ (s) + Na_2CO_3\ (aq) \rightarrow CaCO_3\ (s) + Mg(OH)_2\ (s) + 2Na^+(aq)$

(6) reduction of excess alkalinity: $2HCO_3^-\ (aq) + Ca(OH)_2\ (s) \rightarrow CaCO_3\ (s) + CO_3^{2-}\ (aq) + 2H_2O\ (l)$

MgO is added to remove dissolved silica present in the produced water. An excess of MgO (MgO to SiO_2 mass ratio of ≈1.54) was used to reduce SiO_2 to 50 mg/L aligning with the target in the WLS overflow.

3.2.4 Water sample preparation and testing procedure

Fresh stock solutions of $CaCl_2.2H_2O$ (10,000 ppm as Ca), NaCl (181,600 ppm), $MgCl_2.6H_2O$ (6,000 ppm as Mg), and $NaHCO_3$ (56,000 ppm as HCO_3^-) were prepared. A typical SAGD PW composition was used for the preparation of the synthetic water sample (benchmark water sample), as shown in **Table 3.1**. Based on the benchmark water sample, 154 mg/L MgO dose (MgO/SiO_2 molar ratio of 1.54) was used for silica reduction and 259 mg/L $Ca(OH)_2$ dose was used to increase the pH of the solution to the target value of approximately 10.2.

Table 3.1: Typical SAGD PW Composition (Benchmark Water Sample)

Parameters	**Value**	**Comments**
NaCl (mg/L)	2000	Sodium chloride (NaCl) was used to represent total dissolved solids (TDS)
Magnesium hardness (mg/L as Mg^{2+})	15	$MgCl_2.6H_2O$ stock solution was used
Calcium hardness (mg/L as Ca^{2+})	25	$CaCl_2.2H_2O$ stock solution was used
Bicarbonate Alkalinity (mg/L as HCO_3^-)	700	$NaHCO_3$ stock solution was used
Humic Acid (mg/L as HA)	150	weighed amount of HA was added to represent TOC (Based on the average molecular formula of HA ($C_{187}H_{186}O_{89}N_9S_1$) the TOC content is ~84 mg/L.)

Silica (mg/L as SiO_2)	150	Weighted amount of Na_2SiO_3 was added

To study the factors driving coagulant dose, the concentrations of Mg^{2+}, Ca^{2+}, HCO_3^-, HA, silica, and clay were systematically varied in the water samples while the concentrations of all the other components were kept the same as that of the benchmark water sample. The water bath was used to maintain the temperature of the synthetic water samples at 65 ºC. Then the water samples were dosed with 259 mg/L $Ca(OH)_2$ and 154 mg/L MgO while agitated at 200 rpm in the jar tester to simulate the lime softening process. After lime softening, the coagulant was added, and the sample was mixed for 2 min at 200 rpm to simulate the rapid mixing zone of the WLS. The zeta potential was measured both before and after coagulant addition and was used to determine coagulant dose. Zeta potential is related to the magnitude of the charge and a direct indicator of the stability of colloidal dispersion. Colloids with high zeta potential are electrically stabilized whereas colloids with low zeta potential tend to coagulate. Thus, the optimum coagulant dose was deemed to be obtained when the zeta potential of water samples ranged from -5 to +5 mV (ASTM 2012). Similar procedure was followed to study the impact of $NaCO_3$, $Ca(OH)_2$ and MgO addition to the benchmark water sample.

The sample for ICP measurement was prepared as follows: a10 mL water sample taken after lime softening and coagulation was transferred to a centrifuge tube and any aggregates were removed by centrifugation at 4000 rpm for 5 min. Then 2 mL of the supernatant was diluted with 2% HNO_3 solution to a final volume of 10 mL and passed through a 0.45 μm syringe filter prior to ICP measurement. For all the measurements, each experiment was repeated at least 3 times and mean values with standard deviations were reported.

3.3 Results and Discussion

The study of coagulation and flocculation processes in industrial wastewater is challenging because there are numerous components including soluble and insoluble inorganic compounds and organic matter. To understand the phenomenon, it is necessary to study the impact of each individual component and their interdependence. Influent into a SAGD WLS commonly contains Mg^{2+}, Ca^{2+}, HCO_3^-, silica and organic matter and its treatment typically involves the formation of $CaCO_3$ and $Mg(OH)_2$ precipitates through lime and soda ash treatment, silica reduction with the addition of MgO particles, and enhanced settling of particles with the addition of coagulants/flocculants. The electrokinetic properties of $CaCO_3$ and $Mg(OH)_2$ particles relevant to SAGD WLS have been reported in our previous study (Zhang et al. 2020). Following the warm lime softening process, the suspended particles are treated with coagulant and flocculant to induce aggregation for better separation. In the sections below, we systematically describe the role of the solution chemistry on the dose of a high charge density EPI-DMA coagulant in coagulation-flocculation process using synthetic SAGD produced water (benchmark water sample in **Table 3.1**) with varied concentrations of individual inlet components (HA, silica, clay, $MgCl_2$, $CaCl_2$, HCO_3^-) and dry chemicals (soda ash, lime, MgO). The observations were correlated to the understanding of the electrokinetic properties of $CaCO_3$ and $Mg(OH)_2$ particles in lime softening reported in our previous study (Zhang et al. 2020).

3.3.1 Coagulant dose as a function of the concentration of humic acid (HA)

Dissolved organic matter is far more significant in determining the coagulant dose than other suspended solids in industrial wastewater. The carboxyl content of HA was around 10 μeq/mg of organic carbon, independently of HA sources (Oliver, Thurman, and Malcolm 1983). The dissolved organic matters commonly found in surface, ground, and wastewaters, have been shown

to have structural properties that are similar to humic acid and most importantly the presence of large number of negatively charged functional groups (Pillai et al. 2017; Maan et al. 2018; Zhang et al. 2020). Therefore, HA was chosen as a model compound to represent dissolved organic matter in SAGD produced water to study its impact on coagulant dose. **Figure 3.2A** shows the change of the zeta potential of water samples with HA concentration ranging from 0 to 300 ppm and the other constituents kept the same as that of the benchmark water sample (**Table 3.1)**. Lime (259 mg/L) and MgO (154 mg/L) were added before the addition of coagulant. The initial zeta potential for all samples before the addition of coagulant was around -30 mV. HA itself carries significant negative charges in the alkaline system (Zhang et al. 2020; Oliver, Thurman, and Malcolm 1983). Angelico et al. (2014) reported that the zeta potential of humic acid in 0.015 M NaCl varied from –16 mV at pH of 2 to −36 mV at pH of 10. Dissolved natural organic substances similar to HAs, have been reported as colloidal stabilizing agents in aquatic systems (Stumm 1992) indicating an aquatic system with humic acid would present stable colloidal behavior with a zeta potential of around -30 mV (Pate and Safier 2016) due to the presence of a large number of carboxyl (COOH) and hydroxyl (OH) groups. At high pH, the surface carboxylic groups will dissociate, and the surface acquires strong negative charges. At a very low pH, these groups will be protonated with diminishing surface charge and may even become positively charged (Skybová et al. 2007). With the addition of coagulant, the negative charge was neutralized and the zeta potential of all samples gradually became less negative. Once the optimum dose of coagulant was added, the zeta potential was between -5 to +5 mV, indicating that the surface charge became nearly neutral

Figure 3.2B summarizes the optimum coagulant dose vs. HA concentration. The optimum coagulant dose increased linearly with increasing HA concentration (*slope* = 0.70, R^2 = 0.998).

The pH of the water samples at different concentrations of HA was also measured before the addition of coagulant, which ranged between 10 and 10.2 at all tested HA concentrations as shown in **Figure 3.2B**. The effect of humic acid concentration on the coagulant dose was also studied separately in the absence of silica. The plot of optimal coagulant doses at various concentrations of humic acid is shown in **Figure 3.3**. A linear increase in coagulant demand was also observed with the increasing humic acid concentration.

In our previous study (Zhang et al. 2020), the pH and zeta potential of HA-$CaCO_3$ and HA-$Mg(OH)_2$ systems at different molar ratios were examined. Because $CaCO_3$ and $Mg(OH)_2$ surfaces are sensitive to changes in the ionic composition of the solution, the addition of HA in small quantities (molar ratio of HA to $CaCO_3$ and HA to $Mg(OH)_2$ = 0.01 to 0.1) can significantly influence the zeta potential of the system.Strong interactions were observed between the binary particles ($CaCO_3$-HA and $Mg(OH)_2$-HA) (Zhang et al. 2020). Humic acid can alter the properties of $CaCO_3$ and $Mg(OH)_2$ particles in various possible ways: (1) high negative charge density of humic acid easily dominating the net charge of the colloidal suspension, (2) dissolved Ca and Mg forming monodentate and bidentate complexes with humic acid, and (3) increased dissolution (Zhang et al. 2020). It is expected that the addition of highly negatively charged HA to the suspension will require more coagluant to neutralize particle surfaces surfaces, and is supported by the data shown in **Figure 3.2 A** and **B**.

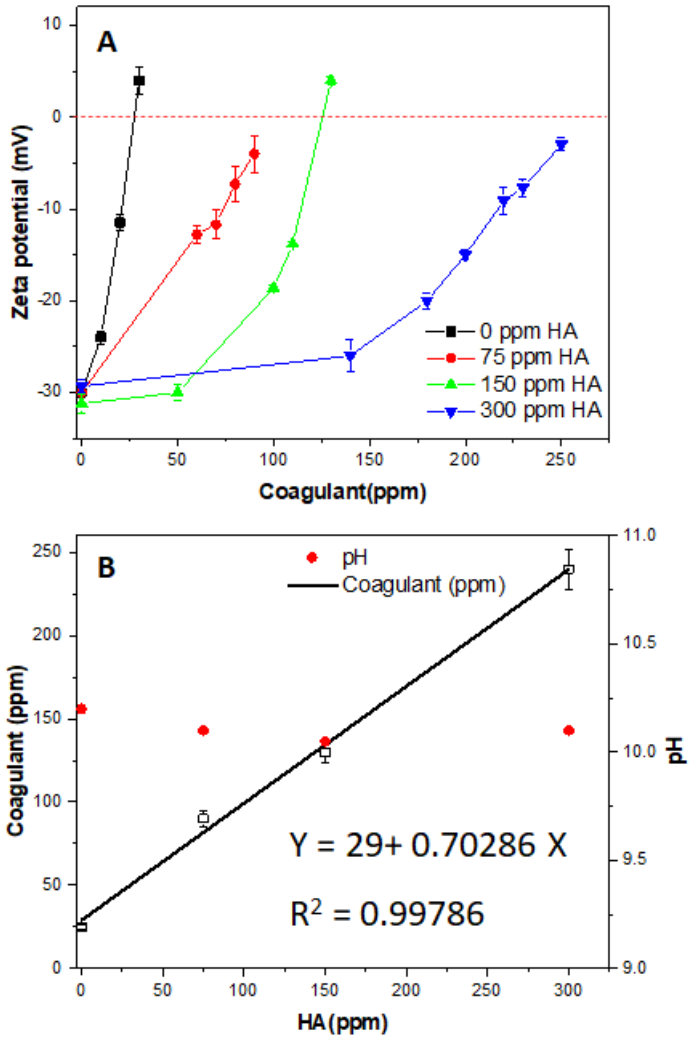

Figure 3.2. (A) the zeta potential of water samples with various humic acid (humic acid) concentrations as a function of coagulant dosage at 65 ºC, and (B) corresponding coagulant dose required to achieve zero charge as a function of the concentration of humic acid determined from the zeta potential measurements.

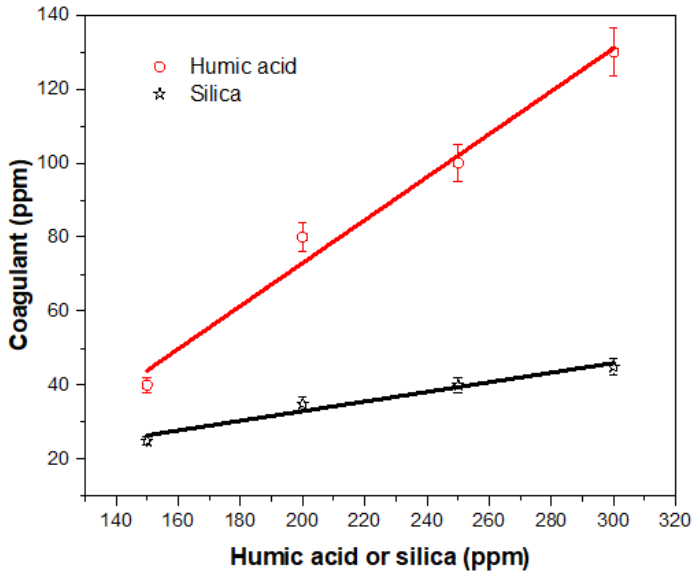

Figure 3.3. Optimum coagulant dosage as a function of the concentration of humic acid (without silica, Y = -43 + 0.58 X, R^2 = 0.98271) and silica (without humic acid, Y = 7 + 0.13 X, R^2 = 0.99178) determined from the zeta potential measurements.

3.3.2 Coagulant dose as a function of the concentration of silica

To study the impact of silica concentration on the coagulant demand, water samples were prepared with silica ranging from 0 to 300 ppm, while all the other constituents stayed the same as that of the benchmark water sample (**Table 3.1)**. Lime (259 mg/L) and MgO (154 mg/L) were added before the coagulant addition. In aqueous solution at room temperature, sodium metasilicate exists as three major species: $Si(OH)_4$ (uncharged silica gel) at pH < 9.4, $SiO(OH)_3^-$ at pH > 9.4, and $SiO_2(OH)_2^{2-}$ at pH > 12.6 (Feng et al. 2012). Therefore, in the experimental conditions, silica particles are expected to present negative charges. As shown in **Figure 3.4A**, the zeta potential of all samples before the coagulant addition ranged from -30 to -35 mV and coagulant was added stepwise until the zeta potential increased to a value ranging from -5 to +5 mV.

Similar to the case of HA, a linear relationship was observed between the optimum coagulant dose and silica concentration (*slope* = 0.54, R^2 = 0.984, **Figure 3.4B**). The slope was smaller than that calculated for humic acid (i.e. 0.54 vs. 0.70) which indicated that silica exerted a smaller coagulant demand than HA. **Figure 3.4B** also shows that the pH increased slightly with the increasing concentration of silica, which can be explained by the use of sodium metasilicate to represent soluble silica. We investigated the effect of silica concentration on the coagulant demand in the absence of dissolved organic matter, i.e. humic acid. The plot of optimum coagulant doses at various concentrations of silica without dissolved organic matter is shown in **Figure 3.3**. A linear increase in coagulant demand was also observed with the increasing silica concentration.

We also studied the effect of silica on $CaCO_3$ and $Mg(OH)_2$ particles during WLS (Zhang et al. 2020). The zeta potential of silica-$CaCO_3$ and silica-$Mg(OH)_2$ binary systems (molar ratio between 0.1 to 2) was negative and strong interactions of binary particles were observed (Zhang et al. 2020). It is reasonable that the addition of highly negatively charged silica to the suspension will require more coagulant to neutralize particle surfaces, and is supported by the data shown in **Figure 3.4 A** and **B**.

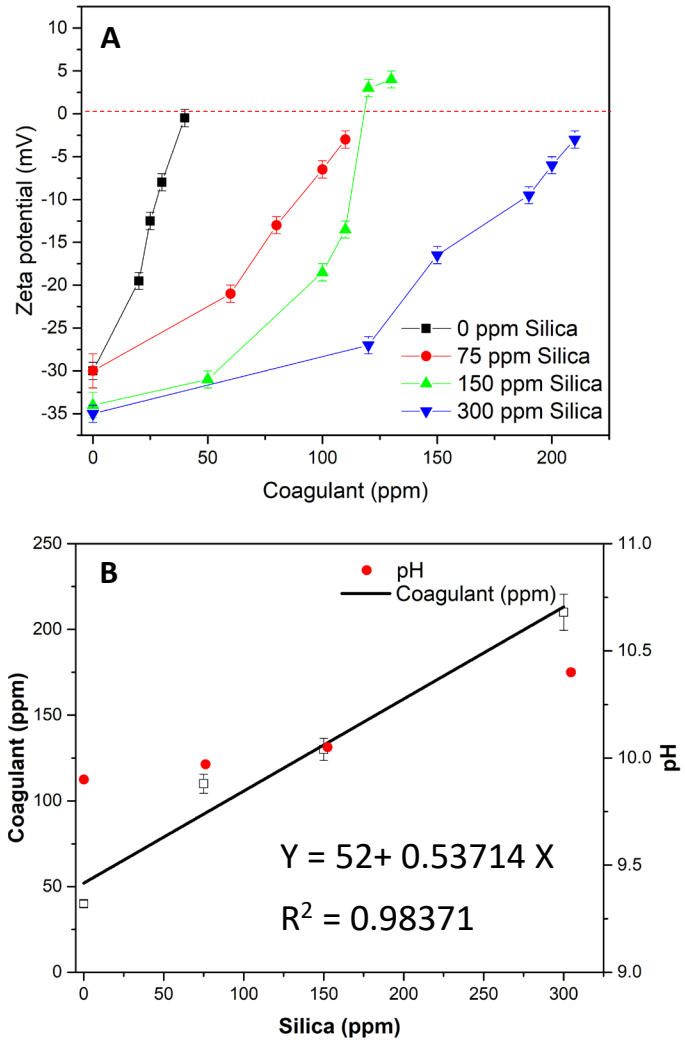

Figure 3.4. (A) the zeta potential of water samples with various concentrations of silica as a function of coagulant dose at 65 ºC, and (B) corresponding optimum coagulant dose required to achieve zero charge as a function of the concentration of silica determined from the zeta potential measurements.

3.3.5 Coagulant dose as a function of the concentration of clay

In this study, clay is used to mimic the TSS and turbidity in the WLS feed water. To improve water reuse, it is possible to recycle tailing water into the WLS process. Tailing water has extremely high clay content - although the volume added in is typically minor comparing to PW, the clay concentration in WLS could be elevated up to 25 ppm. To study the effect of clay on the coagulant,

bentonite clay ($Al_2O_3.SiO_2.H_2O$) was added to the water samples at concentrations 0, 5, 10, and 20 ppm. Bentonite has been reported to be negative charged (-30 to -35 mV) from pH 2 to 12 and behaves slightly more negative with increasing pH (Au and Leong 2013). **Figure 3.5A** shows that the initial zeta potential of the solution was approximately -35 mV and the coagulant was added until the charge neutralization was achieved (–5 to +5 mV zeta potential range). From **Figure 3.5B**, it is clear that up to 5 ppm of clay concentration, there was nearly no change in coagulant dose; at 10 and 20 ppm of clay concentrations, the coagulant dose increased by 30 ppm. The pH decreased with increasing concentration of clay, which is due to the amphoteric nature of Al_2O_3 found in clay.

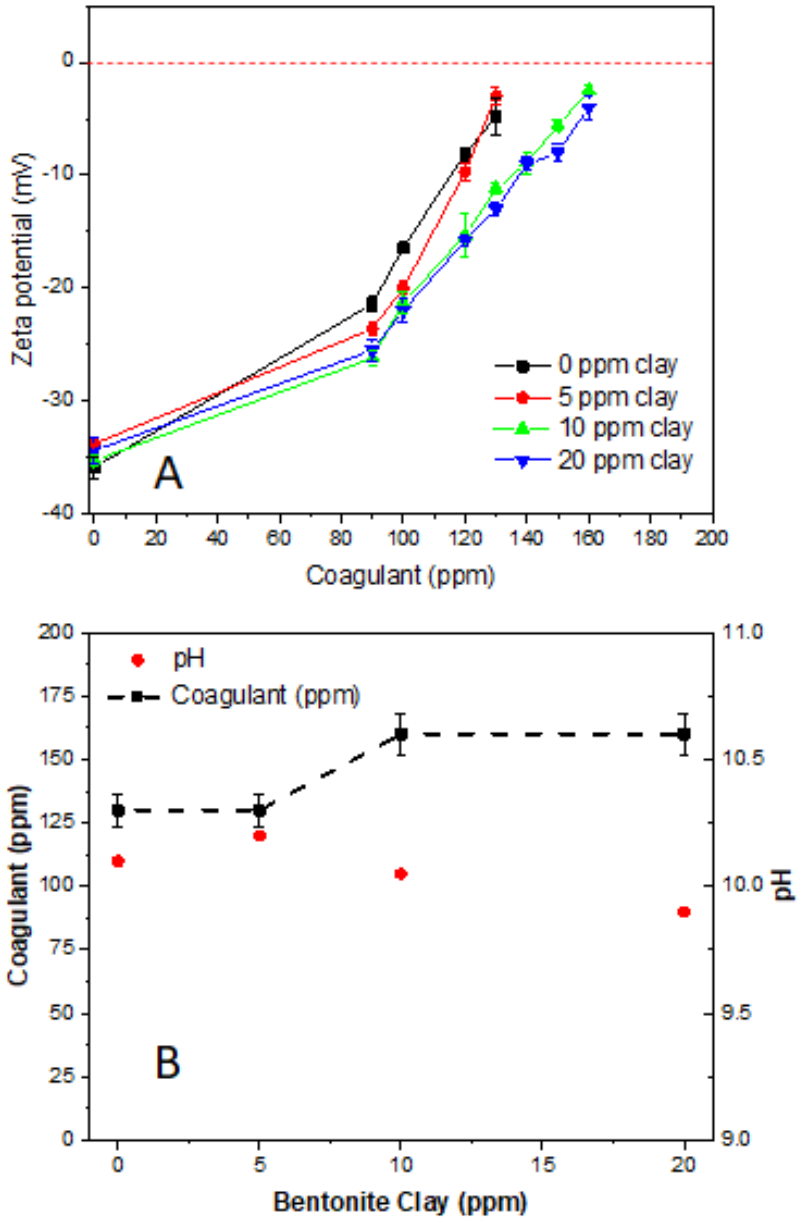

Figure 3.5. (A) the zeta potential of water samples with various concentrations of clay as a function of coagulant dosage at 65 °C, and (B) corresponding optimum coagulant dosage as a function of the concentration of clay determined by the zeta potential measurements.

The zeta potential of clay-$CaCO_3$ and clay-$Mg(OH)_2$ binary systems was negative and strong interactions of binary particles were observed (Zhang et al. 2020). When the molar ratio of clay to $CaCO_3$ ranged from 0.01 to 0.05, the zeta potential decreased from -20 to -30 mV; the zeta potential of clay-$Mg(OH)_2$ system in the same ratio decreased from -10 to -40 mV (Zhang et al. 2020). It is

reasonable that the addition of negatively charged clay to the suspension will require more coagulant to neutralize particle surfaces, however, the SAGD produced water was dominated by high concentrations of HA and silica. It is known that the charge demand of DOM could be 10 to 100 times greater than that of clay. Due to the higher charge demand of DOM (i.e. HA) and low concentration of clay in the system relative to HA, no obvious impact on coagulant dose was observed with such low concentration of clay.

3.3.3 Coagulant dose as a function of $MgCl_2$

Magnesium and calcium metal ions are categorized as dissolved hardness in the WLS process. The influence of each metal ion was systematically studied. First, the impact of $MgCl_2$ on the coagulant dose was studied by changing the concentration of Mg^{2+} from 0 to 30 ppm while all the other constituents stayed the same as that of the benchmark water sample (**Table 3.1)**. Lime (259 mg/L) and MgO (154 mg/L) were added before the addition of coagulant. As shown in **Figure 3.6A**, the zeta potential was approximately -35 mV when no $MgCl_2$ was added and gradually became less negative with increasing $MgCl_2$ concentration (-30 mV at 30 ppm Mg^{2+}), which agrees well with what we previously reported (Zhang et al. 2020). It was found that with the increasing concentration of Mg^{2+} ions, the negative charge of the $CaCO_3$ suspension becomes less negative and eventually becomes positive once the concentration exceeds the overall negative charge of the $CaCO_3$ particles (Zhang et al. 2020). The proposed rationale is that divalent metal cations can adsorb onto the negatively charged particle surfaces to make the surfaces less negatively charged and finally reverse their charge (Zhang et al. 2020).

For the given concentration range, the coagulant dose was not strongly influenced by the concentration of dissolved Mg ions, which suggested that the total negative charge of the system

still dominates even after the addition of $MgCl_2$. **Figure 3.6B** shows that at 0 and 7.5 ppm Mg^{2+}, the coagulant dose was marginally greater than that of 15 and 30 ppm Mg^{2+}. Based on t-test analysis, there was no significant difference between the optimum coagulant dose as a function of $MgCl_2$ [$t = 3.46$, $df = 2$, $p = 0.05$, $t_{critical} = 4.3$]. The pH of the system remained near 10 at 0, 7.5 and 15 ppm Mg^{2+} but dropped to 9.5 at 30 ppm Mg^{2+}, which is due to the weak acidic nature of $MgCl_2$.

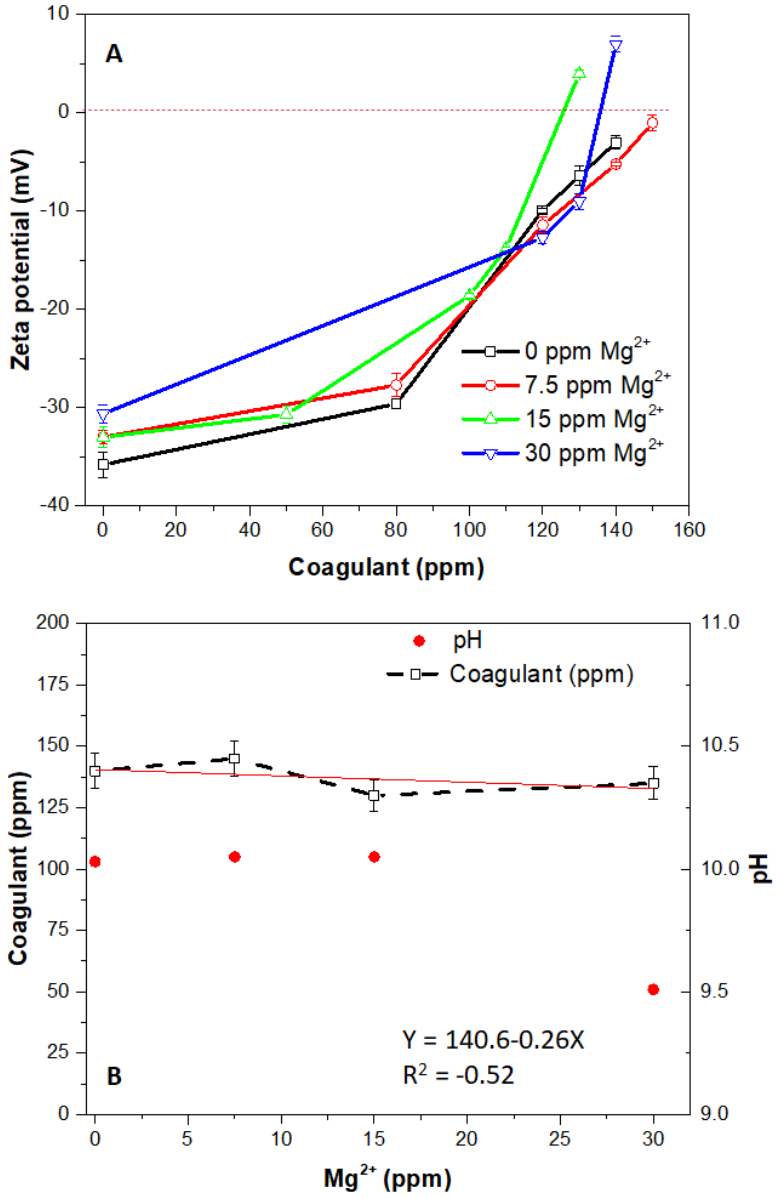

Figure 3.6. (A) the zeta potential of water samples with various concentrations of Mg^{2+} as a function of coagulant dosage at 65 ºC, and (B) corresponding optimum coagulant dosage as a function of the concentration of Mg^{2+} determined from the zeta potential measurements.

3.3.4 Coagulant dose as a function of $CaCl_2$

The effect of dissolved calcium hardness on coagulant dose was studied at different concentrations of $CaCl_2$ (0 to 50 ppm) while the concentrations of all the other constituents stayed the same as that of the benchmark water sample (**Table 3.1)**. Lime (259 mg/L) and MgO (154 mg/L) were added before the addition of coagulant. As in the case of $MgCl_2$, the initial zeta potential of the water sample was dependent on the concentration of $CaCl_2$ added in the solution. At 0 ppm calcium ion concentration, the zeta potential was approximately -35 mV and it became less negative as the calcium ion concentration was increased, which is consistent with our previous study (Zhang et al. 2020). Several studies have reported the effect of calcium ions on the $CaCO_3$ and $Mg(OH)_2$ particle surface charges (Derkani et al. 2019; Black and Christman 1961; Foxall et al. 1979; Al Mahrouqi, Vinogradov, and Jackson 2017; Russell et al. 2009). An excess of calcium ion on $CaCO_3$ particle shifts the zeta potential of negatively charged particles to positive (Zhang et al. 2020). Excess calcium ions can also bind to the humic acid surface to form molecular complexes as well as exchange with other metal cations in the precipitated salts through ionic reactions (Gustafsson 2001).

The optimum coagulant dose did not show any significant difference at 0, 25, and 50 ppm except a small decrease was observed at 12.5 ppm. Based on the t-test analysis, the measured coagulant doses are not statistically different at calcium ion concentration range studied [t = -1, df = 2, p = 0.05, $t_{critical}$ = 4.3] The plot of optimum coagulant doses at different calcium ion concentrations is shown in **Figure 3.7B**. The pH of the system was close to 10 for all the tested Ca^{2+} concentrations (slightly greater than 10 at 0, 12.5, and 25 ppm and slightly lower than 10 at 50 ppm).

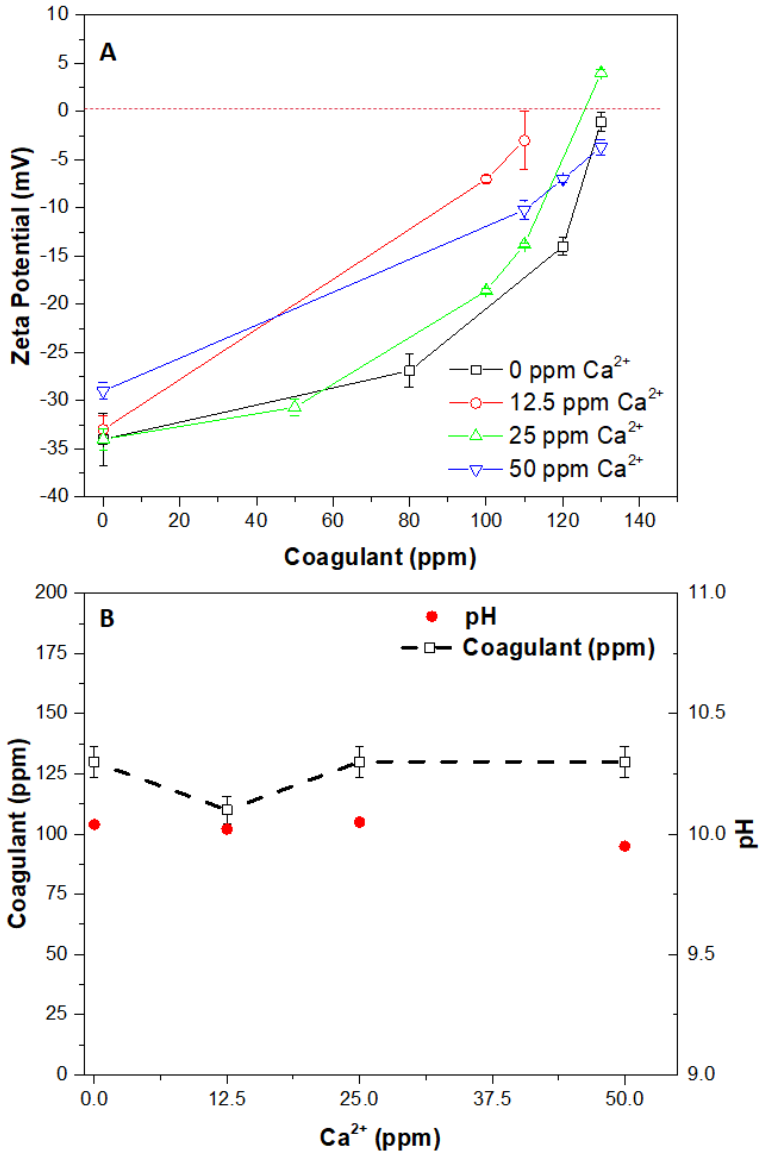

Figure 3.7. (A) the zeta potential of water samples with various concentrations of Ca^{2+} as a function of coagulant dosage at 65 ºC, and (B) corresponding optimum coagulant dosage as a function of the concentration of Ca^{2+} determined from the zeta potential measurements.

3.3.6 Coagulant dose as a function of the addition of $NaHCO_3$

Coagulant dose was determined after different concentrations of HCO_3^- ranging from 0 to 1400 ppm were added into the benchmark water sample (**Table 3.1**). In the previous study (Zhang et al. 2020), where the effect of HCO_3^- on $CaCO_3$ and $Mg(OH)_2$ particles was studied, we found that the

dissolved HCO_3^- ions would introduce negative charges on particles and zeta potential became more negative. Here a similar effect of HCO_3^- on the initial zeta potentials of the system was observed. The initial zeta potentials were approximately -20, -30, -35 and -30 mV at 0, 350, 700 and 1400 ppm HCO_3^- concentration, respectively (**Figure 3.8A**). The coagulant dose was also influenced by the initial zeta potential of the system. As shown in **Figure 3.8B**, the coagulant dose was the lowest in the absence of HCO_3^-. However, once HCO_3^- was added further (addition ranging from 350 to 1400 ppm), the optimum coagulant dose was more or less independent of the HCO_3^- concentration. The t-test analysis also indicated that there was no statistically significant difference between the coagulant doses at these concentrations [$t = 3$, $df = 1$, $p = 0.05$, $t_{critical} = 12.71$]. The pH decreased from 10.75 to 9.7 when the concentration of HCO_3^- increased from 0 to 1400 ppm (**Figure 3.8B**).

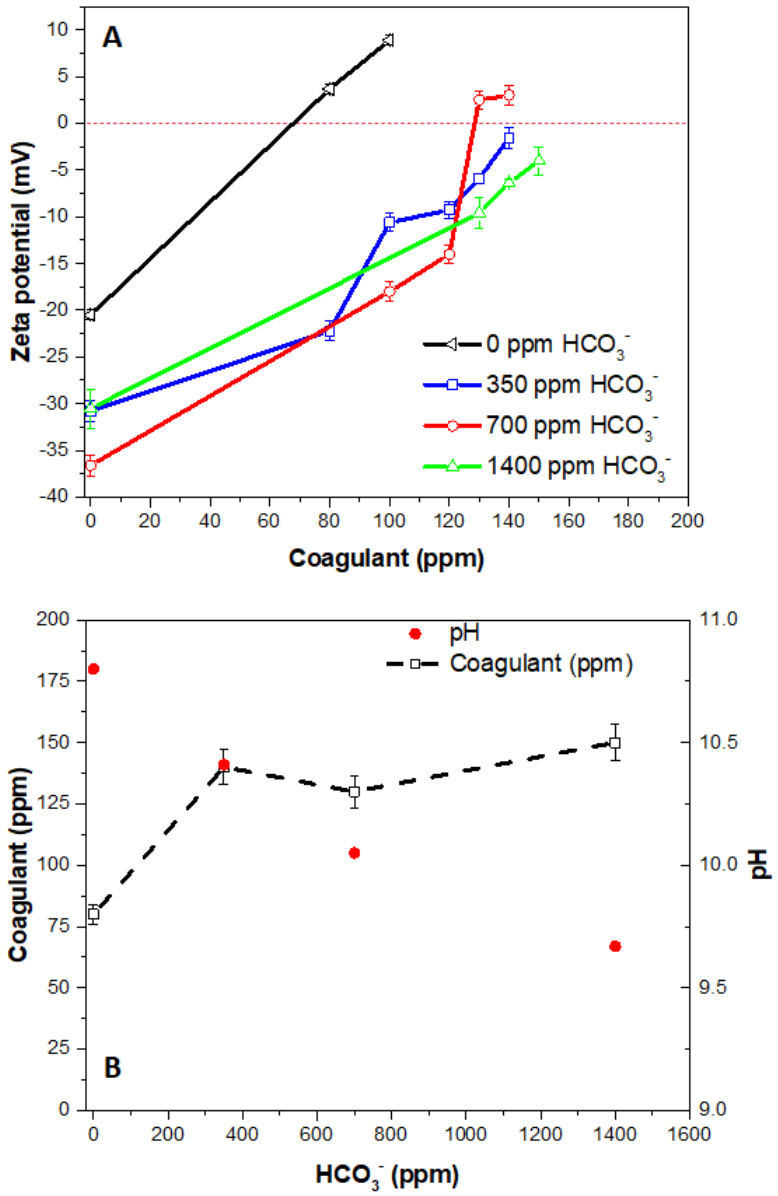

Figure 3.8. (A) the zeta potential of water samples with various concentrations of HCO_3^- as a function of coagulant dose at 65 ºC, and (B) corresponding optimum coagulant dose as a function of the concentration of HCO_3^- determined from the zeta potential measurements.

3.3.7 Coagulant dose as a function of the addition of Na_2CO_3

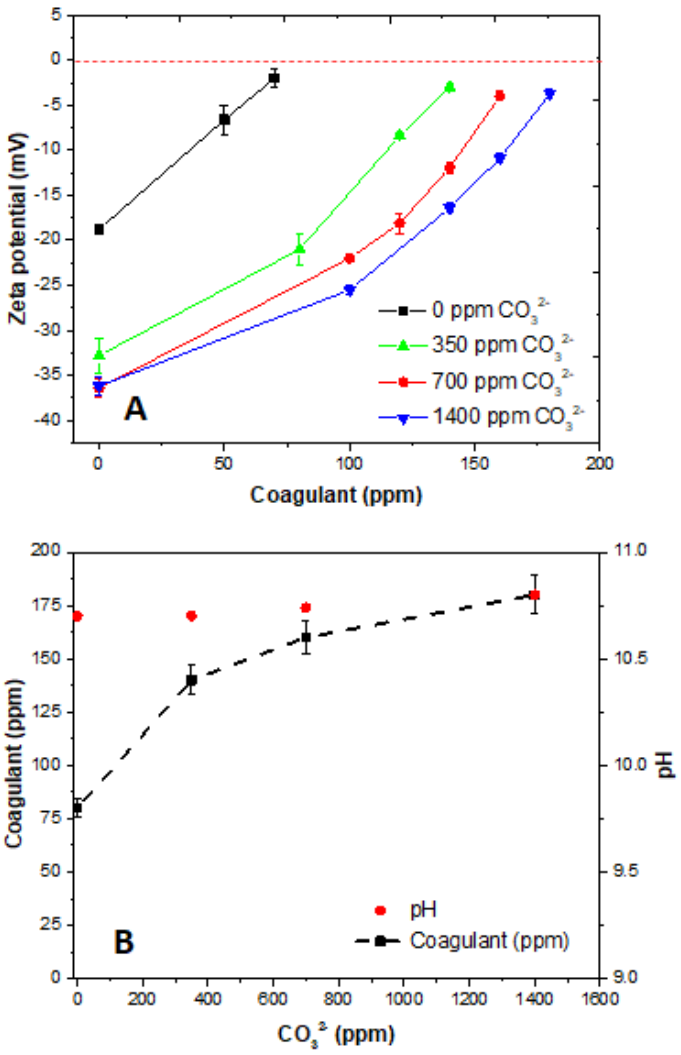

Figure 3.9. (A) the zeta potential of water samples with various concentrations of CO_3^{2-} as a function of coagulant dosage at 65 ºC, and (B) corresponding optimum coagulant dosage as a function of the concentration of CO_3^{2-} determined by the zeta potential measurements**.**

The effect of CO_3^{2-} addition (0, 350, 700 and 1400 ppm) on the coagulant dose was studied. It is known that the presence of CO_3^{2-} can add negative charges on particle surfaces. Our prior study on the effect of CO_3^{2-} on the $CaCO_3$ and $Mg(OH)_2$ particles showed that CO_3^{2-} ions adsorbed on the particle surfaces can impart negative charge to the particles (Zhang et al. 2020). As shown in

Figure 3.9A, the initial zeta potential of the solution was dependent on the concentration of CO_3^{2-} ions. In the absence of CO_3^{2-} ions, the initial zeta potential was less negative (~ -20 mV) and became more negative with the increasing concentration of CO_3^{2-} ions.

The pH of the solution did not change significantly with the addition of variable amounts of CO_3^{2-}, but the pH was higher compared to the pH of the solution prepared using HCO_3^- alkalinity (**Figure 3.9B**). The coagulant dose required to neutralize the particles was plotted against the initial CO_3^{2-} ion concentration which is shown in **Figure 3.9B**. At 0 ppm, the required coagulant dose was 80 ppm. As CO_3^{2-} concentration increased, the coagulant dose also increased. The dose was higher than in the case of HCO_3^- ion shown in **Figure 3.8B**. The increase in coagulant demand in the case of CO_3^{2-} can be attributed to the increase in the pH with increasing CO_3^{2-} concentration. The higher negative charge of CO_3^{2-} ions compared to HCO_3^- ions (-2 vs -1) introduces more negative charge on the particles suspended in solution, and additional carbonate precipitation with increasing concentration. For industrial applications, these results suggest that MUW with high carbonate values may require higher coagulant demands

3.3.8 Coagulant dose as a function of the addition of $Ca(OH)_2$

Lime is added to increase the pH in a WLS and to subsequently result in the precipitation of $CaCO_3$, $Mg(OH)_2$, and Mg-Si complex particles. The zeta potential of benchmark water samples with $Ca(OH)_2$ concentrations from 0 to 516 ppm was measured as a function of coagulant dose. Before coagulant addition, the zeta potential ranged between -30 and -40 mV as shown in **Figure 3.10A**. The initial zeta potential with 0 ppm $Ca(OH)_2$ was close to -30 mV and became more negative with the increasing $Ca(OH)_2$ addition. As shown in **Figure 3.10A**. At 516 ppm of $Ca(OH)_2$ addition, the zeta potential was close to -40 mV. The increased negative charge of the

water sample with the dose of $Ca(OH)_2$ is a result of increasing pH at higher doses of $Ca(OH)_2$ which is demonstrated in **Figure 3.10B**. The increased pH resulted in the formation of more precipitated particles and also increased the negative charge of the dissolved organic and inorganic particles, thus the required dose of coagulant to achieve charge neutralization increased. Clearly, a steady increase in coagulant dose was observed with increasing addition of $Ca(OH)_2$, as shown in **Figure 3.10B**. The R^2 value also indicated a fairly linear relationship between the coagulant demand and $Ca(OH)_2$ added. Based on modeling (Zhang et al. 2020), possible products were calcite ($CaCO_3$), dolomite ($CaMg(CO_3)_2$) and huntite ($Mg_3Ca(CO_3)_4$). For industrial applications, these results suggest that WLS's operating at high pH's or lime feed rates may require higher coagulant demands

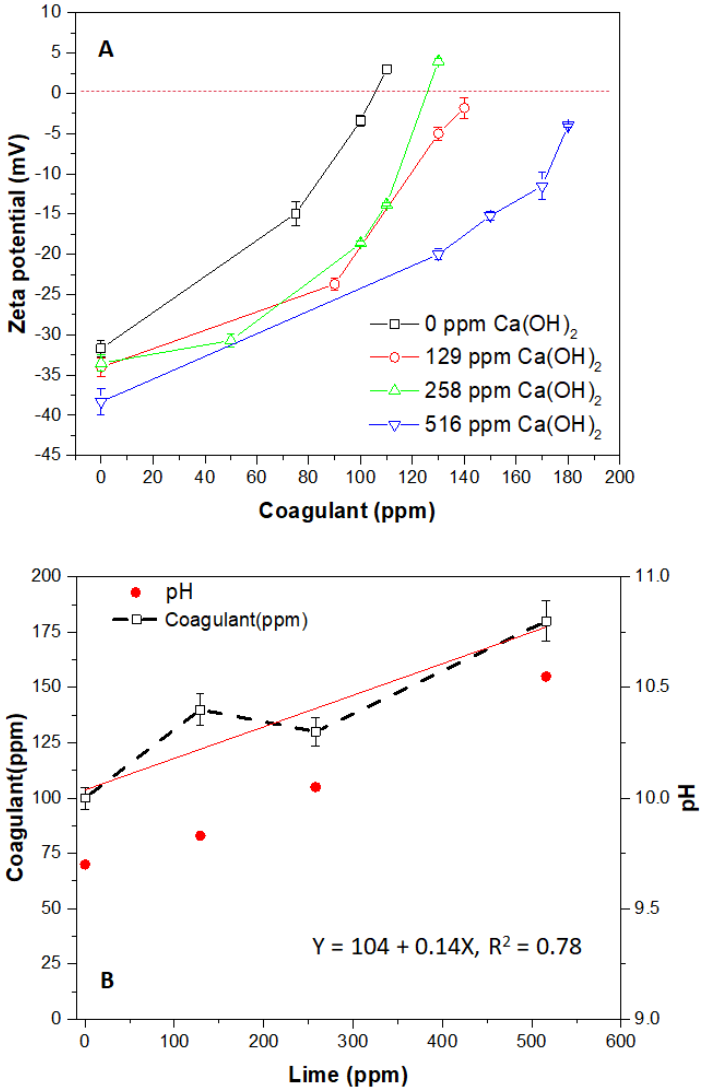

Figure 3.10. (A) the zeta potential of water samples with various concentrations of $Ca(OH)_2$ as a function of coagulant dose at 65 ºC, and (B) corresponding optimum coagulant dose as a function of the concentration of $Ca(OH)_2$ determined from the zeta potential measurements.

3.3.9 Coagulant dose as a function of MgO

MgO is used in the WLS process to reduce silica levels. Using the benchmark water sample, the effect of MgO on the coagulant dosage was studied at four concentrations of MgO: 0, 75, 150, and 300 ppm. The initial zeta potential of the water sample was approximately -43 mV in the absence

of MgO; after MgO addition, the zeta potential of the system became less negative, approaching -30 mV at 150 ppm and 300 ppm of MgO (**Figure 3.11A**). The shift in zeta potential toward less negative with the addition of MgO is due to the positively charged surface of MgO in water at high temperature and interactions of MgO with silica (Zhang et al. 2020). The coagulant dose did not show significant deviation as the MgO amount was increased in the system, as shown in **Figure 3.11B**. The pH of the system was approximately 9.8 at 0 ppm MgO and increased to around 10.1 at 75 ppm MgO. At 150 and 300 ppm MgO, the pH was close to 10.

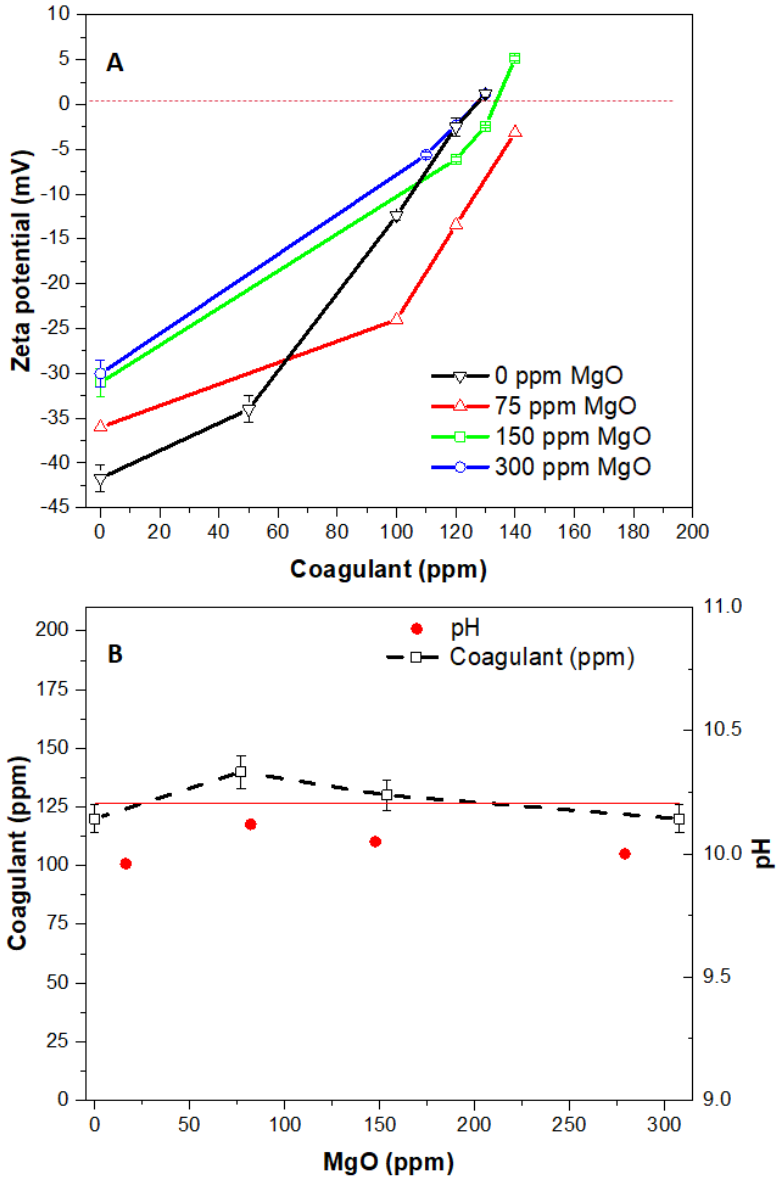

Figure 3.11. (A) the zeta potential of water samples with various concentrations of MgO as a function of coagulant dose at 65 °C, and (B) corresponding optimum coagulant dose as a function of the concentration of MgO determined from the zeta potential measurements.

3.3.10 Determination of silica and humic acid removal

Ca, Mg, silica and humic acid reduction after lime softening was studied using the benchmark water samples. **Figure 3.12 A** and **B** show the concentrations of silica, Ca, and Mg measured by

ICP-OES as a function of the concentration of silica and humic acid, respectively. Based on our prior study, precipitation of silica by MgO most likely led to the formation of chrysotile ($Mg_3(Si_2O_5)(OH)_4$) followed by sepiolite ($Mg_4Si_6O_{15}(OH)_2 \cdot 6H_2O$) based on the saturation indexes from modelling. For the range of initial silica concentrations tested (i.e. 75, 150, 300 ppm), about 55 to 60% silica reduction was achieved. The MgO concentration was fixed (150 ppm) in all the cases and thus, MgO: silica ratio decreased with increasing silica concentration. Meanwhile, Ca^{2+} concentration ranged between 0 and 10 ppm at all silica concentrations. The benchmark concentration of Ca^{2+} and dose of $Ca(OH)_2$ dose were 25 ppm and 259 ppm, respectively. Mg^{2+} concentration was approximately 25 ppm at 0 ppm silica concentration and decreased gradually with the increasing silica concentration. Note that the measured value was higher than the added $MgCl_2$ solution (benchmark - 15 ppm Mg^{2+}) which indicated that some of the added MgO (benchmark - 154 mg/L) was dissolved to release extra Mg^{2+} ions into the solution.

In another experiment, silica concentration was kept constant (150 ppm) and the humic acid concentration was varied as shown in **Figure 3.12B**. A silica reduction between 30 to 60% was observed. For 0 to 150 ppm humic acid, the concentration of $Ca^{2+}$was between 0 and 5 ppm; the concentration of Ca^{2+}increased slightly at 300 ppm HA. Mg concentration was approximately 10 ppm for 0 to 150 ppm humic acid and increased to about 20 ppm at 300 ppm humic acid. The benchmark concentrations of Ca^{2+} and $Ca(OH)_2$ dose were 25 ppm and 259 ppm, respectively; while the benchmark concentrations of Mg^{2+} and MgO dose are 15 ppm and 154 ppm, respectively. Higher concentrations of Ca^{2+} and Mg^{2+} at 300 ppm humic acid indicated the increase in dissolved Ca^{2+} and Mg^{2+} by interaction with the dissolved humic acid

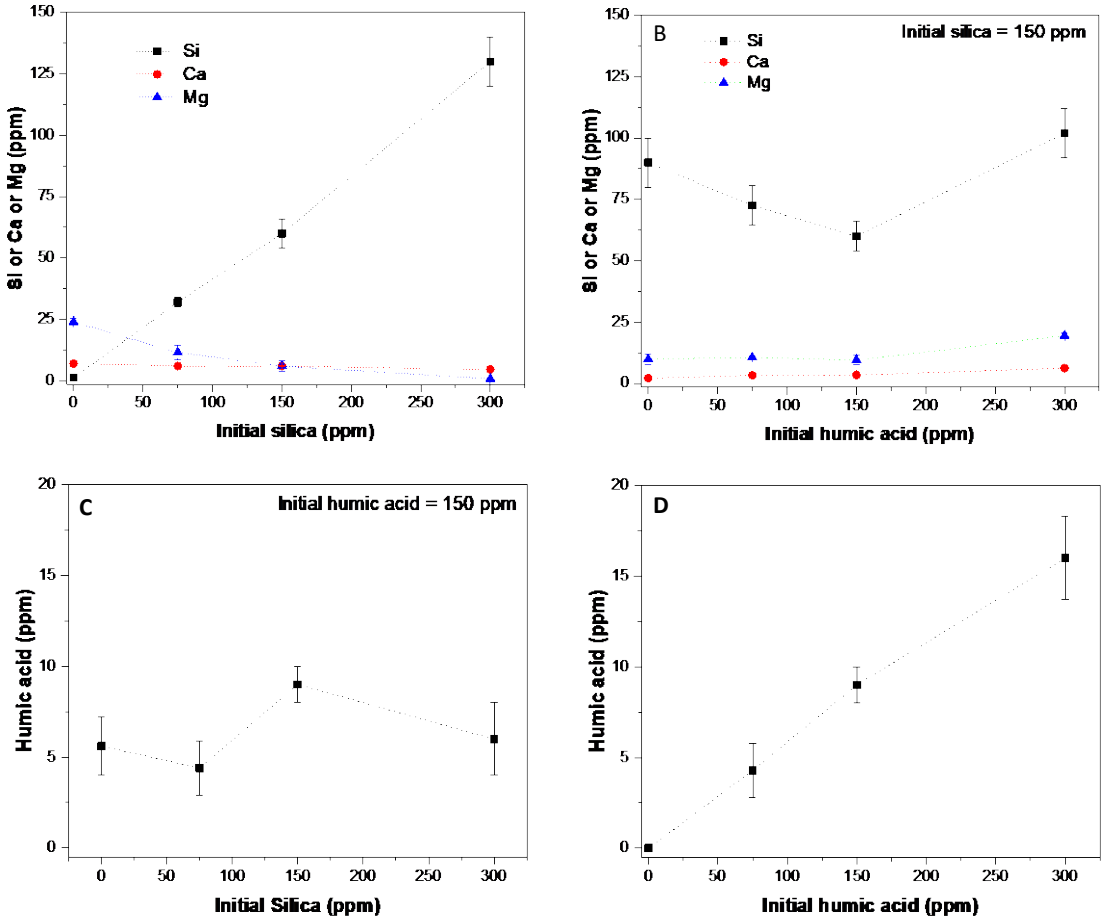

Figure 3.12. ICP measurements of Si, Ca, and Mg in Benchmark water samples of (A) different silica levels (HA = 150 ppm), and (B) different humic acid levels (silica = 150 ppm) after lime softening and coagulation/flocculation process, and corresponding determination of humic acid by UV-visible spectroscopy at three wavelengths in water samples with different initial (C) silica levels (humic acid = 150 ppm) (D) humic acid levels (silica = 150 ppm) .

The corresponding removal of humic acid after coagulation was determined by UV-visible spectroscopy. The concentration of humic acid remaining in the solution was measured by averaging three measurements at 350, 400 and 500 nm. As shown in **Figure 3.12C**, the humic acid concentration was not directly affected by the starting silica concentration and the average humic acid concentration after coagulation was between 5 to 10 ppm which corresponded to about 95% removal. Humic acid removal study at different humic acid concentrations is shown in **Figure**

3.12D. As the initial humic acid concentration increased from 0 to 300 ppm, the residual humic acid after coagulation increased as well. However, it is clear that 95% of humic acid is removed during the process.

3.3.11 Insights on the factors impacting coagulant dose

Overall, dissolved organic matter (represented by HA) and silica strongly influenced the coagulant dose. Therefore, warm lime softening performance in terms of silica and HA reduction was further evaluated using the benchmark water samples in **Table 3.1** with varied concentrations of silica and HA, and treated with the optimum coagulant dose determined by the zeta potential measurements. **Figure 3.13A** shows the remaining concentration of silica after the WLS treatment as a function of the initial concentration of silica. The MgO concentration was fixed (150 ppm) in all the cases and thus, MgO: silica ratio decreased with increasing silica concentration. For the tested initial silica concentrations (i.e. 75, 150, 300 ppm), a similar silica reduction rate (about 60%) was achieved. HA removal at different initial HA concentration is shown in **Figure 3.13B**. It can be seen that 95% HA removal was achieved for all the tested initial HA concentrations. This confirms that there is a strong relationship between silica and cationic polymer coagulant, and between HA and cationic polymer coagulant during the coagulation-flocculation process. Note that the water soluble organic fraction in SAGD waters is complex, and the HA respresentation used in this report is acknowledged to be a simplification of the organic fraction seen in industry. For example, organics reduction in industry across a lime softening process is typically no more than 10% of influent levels.

The schematic in **Figure 3.13C** shows the dominant particles present in SAGD produced water and potential interactions among dissolved and non-dissolved particles in the WLS. Those interactions can be due to van der Waals attraction, electrostatic interactions, hydrogen bonding, hydrophobic interactions, and/or chemical reactions depending on the chemical structures (Israelachvili 1992). $CaCO_3$ and $Mg(OH)_2$ precipitate through lime and soda ash treatment in the WLS. The sign and magnitude of their surface charges depend on the concentration of dissolved ions in the solution (Ca^{2+}, Mg^{2+}, HCO_3^-, CO_3^{2-}, OH^-) (Zhang et al. 2020). $CaCO_3$ and $Mg(OH)_2$ particles interact with each other, and they also interact with other particles carrying negative charges such as HA, silica, and clay in the system (Zhang et al. 2020). The surface charge densities and particle structures of HA, silica and clay are impacted by each other and other particles in the system as discussed above in detail. MgO mainly interacts with silica but may interact with HA as well considering the electrostatic attraction between them. The high molecular weight cationic coagulant EPI-DMA can interact with particles in the system through the electrostatic patch and bridging mechanisms (Bratby 2006; Ji et al. 2013).

The coagulant dose increases strongly and linearly with the concentration of organic matter (represented by HA) and silica in the influent, consistent with our previous observations (Zhang et al. 2020), where HA and silica easily shift the charges of the system to negative. The impact of clay is not significant at the concentrations that would be expected to occur in a SAGD WLS. The impact of Ca^{2+}, Mg^{2+}, and HCO_3^- is marginal, consistent with the previous observation in a simplified system (Zhang et al. 2020), especially in complex SAGD produced water which is dominated by negative charges due to high concentration of HA and silica. There is a slow but steady increase in the coagulant dose with the addition of dry chemicals (soda ash and lime). The

addition of MgO does not impact the coagulant dose. Overall, the variations of influent organic matter and silica will drive coagulant dose significantly, while the variations of dry chemical addition except lime will not. These results will be highly relevant to water treatment facilities where solution conditions change need to be optimized for effective removal of suspended organic and inorganic particles. These results indicate the influence of organic matter and silica for optimizing the WLS process and saving operating cost.

It is worth noting that the findings have some limitations and may not be directly applicable in field work at all locations. In this study, the conventional bench-scale jar tester was used to study the interactions between the coagulant and each component in the WLS. Throughout the experiments, temperature control was achieved by a separated water bath, and $CaCO_3$ and $Mg(OH)_2$ particles were freshly generated. However, in full-scale operating SAGD WLS units, sludge is recycled back into the precipitation system, and the particles present in the softener are a mixture of freshly-precipitated and preformed, which differs from the experimental set-up used in this study. This should be taken into consideration because different electrokinetic properties of freshly precipitated and preformed $CaCO_3$ and $Mg(OH)_2$ particles were observed in our previous study (Zhang et al. 2020). In addition, the complex fluid dynamics in full-scale units may impact the process efficiency as well.

Future experimental designs that mimic the WLS sludge recycling process are now being explored. Future experiments are also planned to assess the influence of lime particles that may precipitate at higher pH values and also using extracted water-soluble organic fractions from industrial waters versus commercially available HA's. Enabling sludge recycle in an experimental setting will also allow for the study of flocculants in addition to coagulants. A useful deliverable from additional

experimental work that builds on the work presented here would be a model that allows for an estimate of the overall charge balance in the RMZ to help guide coagulant optimization.

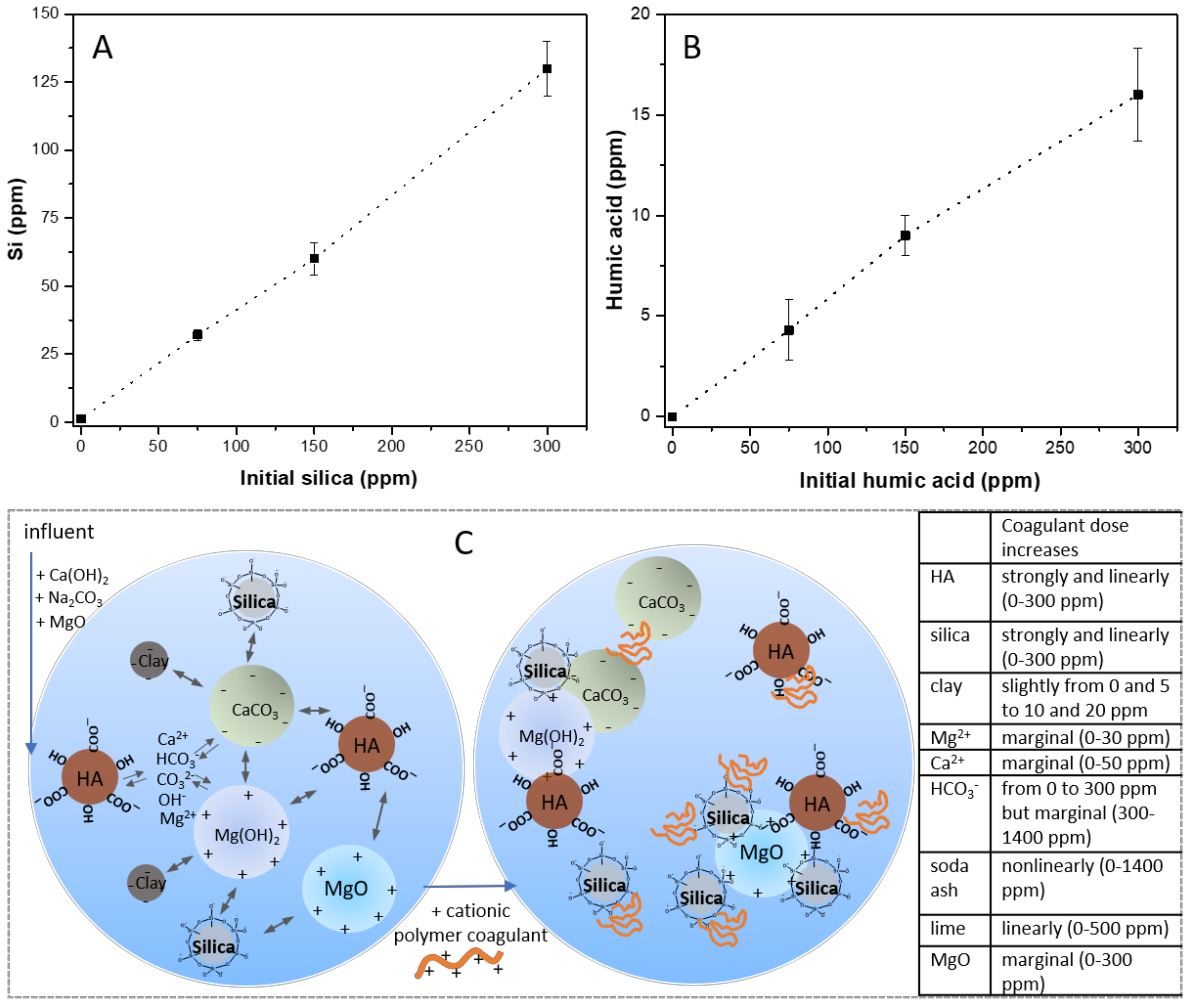

	Coagulant dose increases
HA	strongly and linearly (0-300 ppm)
silica	strongly and linearly (0-300 ppm)
clay	slightly from 0 and 5 to 10 and 20 ppm
Mg^{2+}	marginal (0-30 ppm)
Ca^{2+}	marginal (0-50 ppm)
HCO_3^-	from 0 to 300 ppm but marginal (300-1400 ppm)
soda ash	nonlinearly (0-1400 ppm)
lime	linearly (0-500 ppm)
MgO	marginal (0-300 ppm)

Figure 3.13. Remaining concentrations of supernatant Si and HA in benchmark water samples with varied initial concentration of (A) silica and (B) HA after the warm lime softening process with optimum coagulant dose determined from zeta potential measurements, respectively, and (C) schematic of the interactions in the warm lime softener strongly influenced by HA and silica in the system

3.4. Conclusion

- For WLS treatment of synthetic SAGD produced water, the dose of polymeric quaternary ammonium coagulant (EPI-DMA) was influenced more by the variations of organic matter

(represented by HA) and silica in the feed water and less by the variations of dry chemical addition.

- HA and silica in the inlet water strongly and linearly influenced the dose of coagulant within the tested concentration range of 0-300 ppm, following the linear equation of $Y_{coagulant} = 29 + 0.703X_{HA}$ and $Y_{coagulant} = 52 + 0.537X_{silica}$, respectively. This is related to their high negative charge density.

- Coagulant dose increased with increasing lime addition (0-500 ppm) but not significantly.

- Coagulant dose decreased marginally upon increasing MgO addition (0-300 ppm).

- Increasing concentrations of divalent ions Mg^{2+} (0-30 ppm) and Ca^{2+} (0-50 ppm) marginally impacted the coagulant dose.

- Coagulant dose increased with the addition of soda ash (0-1400 ppm). A significant increase was seen after the initial addtion of bicarbonate from 0 to 300 ppm, but the increase was only marginal from 300-1400 ppm. Carbonate and bicarbonate ions increased the overall negative charge of the suspended particles due to adsorption of these ions on colloidal particles which results in increased coagulant demand.

- Bentonite clay did not show a significant effect on coagulant dose up to 5 ppm but did show a slight increase after 10 ppm. Clay particles are negatively charged and thus an increase in coagulant dose with increasing concentration of clay is expected

Chapter 4 Conclusions and Future Work

4.1 Conclusions

WLS is commonly used to reduce hardness, silica, and a small fraction of organic matter in PW from a SAGD facility, typically involving the formation of $CaCO_3$ and $Mg(OH)_2$ precipitates through lime, MgO, and soda ash, coagulant and flocculant addition. Significant effort has been made to measure and understand the surface charge of $CaCO_3$ and $Mg(OH)_2$ particles. However, there are very few studies on the zeta potential of $CaCO_3$ and $Mg(OH)_2$ particles at conditions relevant to WLS operation. Additionally, there is also a lack of study on systematic high temperature jar testing to specifically exam the impact of feed water quality deviation on coagulant demand. Therefore, this study aims to

1. Understand the interactions and electrokinetic properties (i.e. zeta potential) of $CaCO_3$ and $Mg(OH)_2$ particles under various experimental parameters such as pH, temperature, aging, inorganic carbon (CO_3^{2-}/HCO_3^-), and divalent cations (Ca^{2+}/Mg^{2+}). The interactions between humic acid (mimicking natural organic matter), silicate (representing silica), clay (mimicking suspended solids) and $CaCO_3$/$Mg(OH)_2$ particles were studied, as well as the interactions between $CaCO_3$ and $Mg(OH)_2$. Visual MINTEQ modeling was used to predict precipitates as a function of solution chemistry and assist with data interpretation
2. Understand the impact of solution chemistry on polyamine coagulant/flocculant demand for treating synthetic SAGD PW. Solution chemistry was altered by varying the concentrations of magnesium, calcium, sodium bicarbonate ($NaHCO_3$), clay (mimicking suspended solids), Na_2SiO_3 (representing silica), and humic acid (mimicking dissolved organic matter) to simulate potential contaminant spikes. The impact of the concentrations

of soda ash, lime, and MgO was also studied. Zeta potential measurements were used to determine the optimum coagulant dosage for each experiment.

The electrokinetic study suggested the importance of describing and understanding an aqueous system regarding the ions and functional groups present when examining the zeta potential of particles. It is also critical to review if other particles may form as a result of changes in water chemistry such as pH. Based on the results, $CaCO_3$ and $Mg(OH)_2$ particles can be either positively or negatively charged. For both particles, the presence of PDIs has a significant impact on their surface charges mainly by the absorption of ions on the surface sites and the alteration of the functional groups. For $Mg(OH)_2$ particles, pH was found to be equally important as PDIs; however, the zeta potential of $CaCO_3$ particles is believed to be only secondarily impacted by pH values compared to the PDIs. Divalent metal ions were found to be the common PDIs of $CaCO_3$ and $Mg(OH)_2$ particles which agreed with most literature. $Mg(OH)_2$ particles were found to be mostly positively charged under WLS pH and temperature ranges, whereas CaCO3 particles were found to be mostly negatively charged. For binary systems, the additions of silica, HA, and clay were found to dominate the system with negative charges. For the mixture of $Mg(OH)_2$ and $CaCO_3$ particles, the charge of the system was reversed to positive and became more positive with the increasing molar ratio of $Mg(OH)_2$ and $CaCO_3$. Strong particle interactions were also observed in the binary systems.

The coagulation study was performed at 65 ℃ to simulate the WLS operating conditions and suggested that Humic acid and silica strongly influenced the dose of the coagulant. There was a near-linear dependence of the coagulant dose on humic acid and silica concentration. This is due to the negatively charged functional groups, high charge density, and preference for accumulating

at the solid/liquid phase. The coagulant demand also increased with the lime concentration, which was ascribed to the increase in pH of the system with increasing lime concentration. Similarly, carbonate ions also increased coagulant demand. However, bicarbonate ions and dissolved hardness (Ca and Mg) showed insignificant impacts on the coagulant demand.

WLS is complicated in terms of water chemistry and is difficult to optimize. This study provides insights into the fundamental electrokinetic properties of the two common softening particles and suggests that the presence of organic matter and silica can have significant effects on coagulant demand and clarification/sedimentation performance. It also suggests that the dose of other chemicals such as lime and soda ash can have a mild impact on the coagulant demand. Therefore, the operation of a WLS process should particularly focus on dissolved organic matter and silica content monitoring while ensuring optimum doses of other chemicals. Compared to the traditional jar testing and turbidity analysis, the use of zeta potential measurement could be beneficial when it comes to chemical selection and optimum dose determination and can provide more accurate and representative information for field operation.

4.2 Future Work

In the WLS operation, sludge is continuously recycled back to the rapid mixing zone for seeding. The effect of sludge recirculation on the coagulant dose and system charge can be studied in terms of recycle ratio and sludge aging to provide further understandings for field operation. The experiment can be designed by utilizing the 3D printing technology to build a bench-top scale clarifier that reassembles WLS configuration. In this study, temperature and aging were shown to impact the charge of particles. Further experiments can be conducted to qualitatively assess their impact on coagulant demand which could help better field testing protocols.

Synthetic water samples were used for the coagulation study in this work which do not fully represent the characteristics of a field SAGD PW. More testing can be performed using real SAG PW samples to provide more accurate and representative results that could provide direct feedback to field operation.

Although MINTEQ is not specific for SAGD PW modelling but could be a useful tool to help understand chemical speciation in SAGD conditions. Further studies can be done to understand the feasibility of using MINTEQ to model SAGD PW and ultimately to optimize WLS operation.

References

Adusei-Gyamfi, Junias, Baghdad Ouddane, Luuk Rietveld, Jean Paul Cornard, and Justine Criquet. 2019. "Natural Organic Matter-Cations Complexation and Its Impact on Water Treatment: A Critical Review." *Water Research*. https://doi.org/10.1016/j.watres.2019.05.064.

Alroudhan, A., J. Vinogradov, and M. D. Jackson. 2016. "Zeta Potential of Intact Natural Limestone: Impact of Potential-Determining Ions Ca, Mg and SO4." *Colloids and Surfaces A: Physicochemical and Engineering Aspects* 493: 83–98. https://doi.org/10.1016/j.colsurfa.2015.11.068.

Angelico, Ruggero, Andrea Ceglie, Ji Zheng He, Yu Rong Liu, Giuseppe Palumbo, and Claudio Colombo. 2014. "Particle Size, Charge and Colloidal Stability of Humic Acids Coprecipitated with Ferrihydrite." *Chemosphere*. https://doi.org/10.1016/j.chemosphere.2013.10.092.

ASTM. 2012. "Standard Guide for Measurement of Electrophoretic Mobility and Zeta Potential of Nanosized Biological Materials." West Conshohocken.

Au, Pek Ing, and Yee Kwong Leong. 2013. "Rheological and Zeta Potential Behaviour of Kaolin and Bentonite Composite Slurries." *Colloids and Surfaces A: Physicochemical and Engineering Aspects*. https://doi.org/10.1016/j.colsurfa.2013.06.039.

AWWA. 1990. *Water Quality and Treatment: A Handbook of Community Water Supplies*. *Environmental Protection*. 4th editio.

———. 1999. *Water Quality and Treatment: A Handbook of Community Water Supplies*. *Environmental Protection*. Vol. 331. New York: McGraw Hill. http://uclibs.org/PID/106321.

Behrman, A. S., and H. Gustafson. 1940. “Removal of Silica from Water.” *Industrial and Engineering Chemistry* 32 (4): 468–72. https://doi.org/10.1021/ie50364a006.

Black, A. P., and Russell F. Christman. 1961. “Electrophoretic Studies of Sludge Particles Produced in Lime-Soda Softening.” *Journal - American Water Works Association* 53 (6): 737–47. https://doi.org/10.1002/j.1551-8833.1961.tb00709.x.

Bob, Mustafa, and Harold W. Walker. 2001. “Enhanced Adsorption of Natural Organic Matter on Calcium Carbonate Particles through Surface Charge Modification.” *Colloids and Surfaces A: Physicochemical and Engineering Aspects*. https://doi.org/10.1016/S0927-7757(01)00760-9.

Brady, Patrick V., and John V. Walther. 1989. “Controls on Silicate Dissolution Rates in Neutral and Basic PH Solutions at 25°C.” *Geochimica et Cosmochimica Acta*. https://doi.org/10.1016/0016-7037(89)90160-9.

Bratby, John. 2006. *Coagulation and Flocculation in Water and Wastewater Treatment*. *IWA Publishing*. https://doi.org/10.2166/9781780407500.

Bridle, M. 2005. “Treatment of SAGD-Produced Waters without Lime Softening.” In *SPE/PS-CIM/CHOA International Thermal Operations and Heavy Oil Symposium Proceedings*. https://doi.org/10.2118/97686-ms.

Butler, R. M. 1994. “Steam-Assisted Gravity Drainage: Concept, Development, Performance and Future.” *Journal of Canadian Petroleum Technology*, no. 61: 44–50. https://doi.org/10.2118/94-02-05.

Coto, B., C. Martos, J. L. Peña, R. Rodríguez, and G. Pastor. 2012. “Effects in the Solubility of CaCO 3: Experimental Study and Model Description.” *Fluid Phase Equilibria*. https://doi.org/10.1016/j.fluid.2012.03.020.

D.F. Evans, H. Wennerström. 1999. *The Colloidal Domain: Where Physics, Chemistry, Biology, and Technology Meet*. Edited by second ed. *Choice Reviews Online*. New York: Wiley-VCH. https://doi.org/10.5860/choice.37-0334.

Derkani, Maryam H., Ashleigh J. Fletcher, Maxim Fedorov, Wael Abdallah, Bastian Sauerer, James Anderson, and Zhenyu J. Zhang. 2019. "Mechanisms of Surface Charge Modification of Carbonates in Aqueous Electrolyte Solutions." *Colloids and Interfaces*. https://doi.org/10.3390/colloids3040062.

Duman, Osman, and Sibel Tunç. 2009. "Electrokinetic and Rheological Properties of Na-Bentonite in Some Electrolyte Solutions." *Microporous and Mesoporous Materials* 117 (1–2): 331–38. https://doi.org/10.1016/j.micromeso.2008.07.007.

Environmental Protection Agency. 2002. *Water Treatment Manuals: Coagulation, Flocculation & Clarification*.

Eriksson, Rasmus, Juha Merta, and Jarl B. Rosenholm. 2007. "The Calcite/Water Interface. I. Surface Charge in Indifferent Electrolyte Media and the Influence of Low-Molecular-Weight Polyelectrolyte." *Journal of Colloid and Interface Science*. https://doi.org/10.1016/j.jcis.2007.04.034.

Ersoy, Bahri, and Mehmet S. Çelik. 2002. "Electrokinetic Properties of Clinoptilolite with Mono- and Multivalent Electrolytes." *Microporous and Mesoporous Materials*. https://doi.org/10.1016/S1387-1811(02)00433-X.

Fatema, Jannat. 2014. "Characterization of Silica and Dissolved Organic Matter Aggregation in SAGD Produced Water." University of Alberta. https://doi.org/10.1227/00006123-197907010-00116.

Fatema, Jannat, Subir Bhattacharjee, David Pernitsky, and Abhijit Maiti. 2015. "Study of the

Aggregation Behavior of Silica and Dissolved Organic Matter in Oil Sands Produced Water Using Taguchi Experimental Design." *Energy and Fuels* 29 (11): 7465–73. https://doi.org/10.1021/acs.energyfuels.5b01223.

Feng, Bo, Yiping Lu, Qiming Feng, and Hao Li. 2012. "Solution Chemistry of Sodium Silicate and Implications for Pyrite Flotation." *Industrial and Engineering Chemistry Research*. https://doi.org/10.1021/ie301307a.

Foxall, Thomas, Gordon C. Peterson, Henry M. Rendall, and Alec L. Smith. 1979. "Charge Determination at Calcium Salt/Aqueous Solution Interface." *Journal of the Chemical Society, Faraday Transactions 1: Physical Chemistry in Condensed Phases* 75 (2): 1034–39. https://doi.org/10.1039/F19797501034.

Ghernaout, Djamel, Noureddine Elboughdiri, Saad Ghareba, and Alsamani Salih. 2020. "Coagulation Process for Removing Algae and Algal Organic Matter—An Overview." *OALib*. https://doi.org/10.4236/oalib.1106272.

Gustafsson, Jon Petter. 2001. "Modeling the Acid-Base Properties and Metal Complexation of Humic Substances with the Stockholm Humic Model." *Journal of Colloid and Interface Science*. https://doi.org/10.1006/jcis.2001.7871.

Heins, W. F. 2009. "Technical Advancements in SAGD Evaporative Produced Water Treatment." *Journal of Canadian Petroleum Technology*. https://doi.org/10.2118/130442-PA.

Heins, W., and Dan Peterson. 2005. "Use of Evaporation for Heavy Oil Produced Water Treatment." *Journal of Canadian Petroleum Technology*. https://doi.org/10.2118/05-01-01.

Iler, Ralph K. 1979. *Chemistry of Silica - Solubility, Polymerization, Colloid and Surface Properties and Biochemistry*.

Israelachvili, Jacob N. 1992. *Electrostatic Forces between Surfaces in Liquids*. *Intermolecular and Surface Forces*. https://doi.org/10.1017/CBO9781107415324.004.

Ji, Yaguan, Qingye Lu, Qingxia Liu, and Hongbo Zeng. 2013. "Effect of Solution Salinity on Settling of Mineral Tailings by Polymer Flocculants." *Colloids and Surfaces A: Physicochemical and Engineering Aspects*. https://doi.org/10.1016/j.colsurfa.2013.04.006.

Karim, Omar. 2018. "Development of Polyacrylamide Composite Hydrogel for Removal of Humic Acid Based on Interaction Studies." https://doi.org/10.11575/PRISM/33128.

Knight, James T. 1981. "CHEMISTRY OF SIDESTREAM SOFTENING AND SILICA REDUCTION." *Journal of the Cooling Tower Institute*.

Kuwatsuka, Shozo, Kiyoshi Tsutsuki, and Kyoichi Kumada. 1978. "Chemical Studies on Soil Humic Acids: Elementary Composition of Humic Acids." *Soil Science and Plant Nutrition* 24 (3): 337–47. https://doi.org/10.1080/00380768.1978.10433113.

Larson, T. E., and A. M. Buswell. 1940. "Water Softening: Sign of the Charge on Colloidal Particles of Hydrous Alumina, Hydrous Magnesium, and Calcium Carbonate." *Industrial and Engineering Chemistry*. https://doi.org/10.1021/ie50361a030.

Latour, Isabel, Ruben Miranda, and Angeles Blanco. 2014. "Silica Removal in Industrial Effluents with High Silica Content and Low Hardness." *Environmental Science and Pollution Research*. https://doi.org/10.1007/s11356-014-2906-8.

Maan, Omar, Jun Huang, Hongbo Zeng, and Qingye Lu. 2018. "Probing Molecular Interactions between Humic Acid and Surface-Grafted Polyacrylamide Using Quartz Crystal Microbalance with Dissipation and Atomic Force Microscopy: Implications for Environmental Remediation." *Environmental Chemistry*. https://doi.org/10.1071/EN18079.

Maan, Omar, Ping Song, Ningxin Chen, and Qingye Lu. 2019. "An In Situ Procedure for the

Preparation of Zeolitic Imidazolate Framework-8 Polyacrylamide Hydrogel for Adsorption of Aqueous Pollutants." *Advanced Materials Interfaces*. https://doi.org/10.1002/admi.201801895.

Mahani, Hassan, Arsene Levy Keya, Steffen Berg, Willem Bart Bartels, Ramez Nasralla, and William R. Rossen. 2015. "Insights into the Mechanism of Wettability Alteration by Low-Salinity Flooding (LSF) in Carbonates." *Energy and Fuels*. https://doi.org/10.1021/ef5023847.

Mahrouqi, Dawoud Al, Jan Vinogradov, and Matthew D. Jackson. 2016. "Temperature Dependence of the Zeta Potential in Intact Natural Carbonates." *Geophysical Research Letters*. https://doi.org/10.1002/2016GL071151.

———. 2017. "Zeta Potential of Artificial and Natural Calcite in Aqueous Solution." *Advances in Colloid and Interface Science*. https://doi.org/10.1016/j.cis.2016.12.006.

Matilainen, Anu, Mikko Vepsäläinen, and Mika Sillanpää. 2010. "Natural Organic Matter Removal by Coagulation during Drinking Water Treatment: A Review." *Advances in Colloid and Interface Science*. https://doi.org/10.1016/j.cis.2010.06.007.

McLaughlin, William J., Joe L. White, and Stanley L. Hem. 1993. "Heterocoagulation in Magnesium Hydroxide and Aluminum Hydroxycarbonate Suspensions." *Journal of Colloid And Interface Science* 157 (1): 113–23. https://doi.org/10.1006/jcis.1993.1164.

Mercer, Kenneth L., Yi Pin Lin, and Philip C. Singer. 2005. "Enhancing Calcium Carbonate Precipitation by Heterogeneous Nucleation during Chemical Softening." *Journal / American Water Works Association*. https://doi.org/10.1002/j.1551-8833.2005.tb07545.x.

Mohammadtabar, Farshad, Rajesh G. Pillai, Behnam Khorshidi, Armin Hayatbakhsh, and Mohtada Sadrzadeh. 2019. "Efficient Treatment of Oil Sands Produced Water: Process

Integration Using Ion Exchange Regeneration Wastewater as a Chemical Coagulant." *Separation and Purification Technology*. https://doi.org/10.1016/j.seppur.2019.03.070.

Moulin, P., and H. Roques. 2003. "Zeta Potential Measurement of Calcium Carbonate." *Journal of Colloid and Interface Science* 261 (1): 115–26. https://doi.org/10.1016/S0021-9797(03)00057-2.

Natural Resouces Canada. 2020. "What Are the Oil Sands?" 2020. https://www.nrcan.gc.ca/our-natural-resources/energy-sources-distribution/clean-fossil-fuels/what-are-oil-sands/18089.

Natural Resources Canada. 2013. "Technical Overview." 2013. https://www.nrcan.gc.ca/our-natural-resources/energy-sources-distribution/clean-fossil-fuels/technical-overview/5851.

Nordström, Jonas, Erik Nilsson, Patrik Jarvol, Moheb Nayeri, Anders Palmqvist, Johan Bergenholtz, and Aleksandar Matic. 2011. "Concentration- and PH-Dependence of Highly Alkaline Sodium Silicate Solutions." *Journal of Colloid and Interface Science* 356 (1): 37–45. https://doi.org/10.1016/j.jcis.2010.12.085.

Oliver, Barry G., Earl M. Thurman, and Ronald L. Malcolm. 1983. "The Contribution of Humic Substances to the Acidity of Colored Natural Waters." *Geochimica et Cosmochimica Acta*. https://doi.org/10.1016/0016-7037(83)90218-1.

Ostovar, Mohamad, and Mohamad Amiri. 2013. "A Novel Eco-Friendly Technique for Efficient Control of Lime Water Softening Process." *Water Environment Research*. https://doi.org/10.2175/106143013x13807328848333.

Otsuki, Akira, and Neil Lonio Hayagan. 2020. "Zeta Potential of Inorganic Fine Particle—Na-Bentonite Binder Mixture Systems." *Electrophoresis*. https://doi.org/10.1002/elps.202000136.

Parks, George A. 1965. "The Isoelectric Points of Solid Oxides, Solid Hydroxides, and Aqueous

Hydroxo Complex Systems." *Chemical Reviews* 65 (2): 177–98. https://doi.org/10.1021/cr60234a002.

Parsons, Simon A., and Bruce Jefferson. 2009. *Introduction to Potable Water Treatment Processes*. *Introduction to Potable Water Treatment Processes*. https://doi.org/10.1002/9781444305470.

Pate, K., and P. Safier. 2016. "Chemical Metrology Methods for CMP Quality." In *Advances in Chemical Mechanical Planarization (CMP)*. https://doi.org/10.1016/B978-0-08-100165-3.00012-7.

Pedenaud, Pierre, Caroline Goulay, Fabien Pottier, Olivier Garnier, and Bernard Gauthier. 2006. "Silica-Scale Inhibition for Steam Generation in OTSG Boilers." *SPE Production and Operations*. https://doi.org/10.2118/86934-pa.

Perdicakis, Basil, Mick McGregor, Matthew Petersen, and Anthony J. (A.J.) Gerbino. 2019. "High Temperature Reverse Osmosis Membrane SAGD Process Design Assessment." In *International Water Conference*.

Pernitsky, David, Gabe Maul, Keri Seely, Basil Perdicakis, Adrian Revington, and Anita Selinger. 2018. "Zeta Potential for Optimizing Coagulation at Industrial Water Treatment Plants." In *Zeta Potential for Optimizing Coagulation at Industrial Water Treatment Plants*.

Pillai, Rajesh G., Ni Yang, Steven Thi, Jannat Fatema, Mohtada Sadrzadeh, and David Pernitsky. 2017. "Characterization and Comparison of Dissolved Organic Matter Signatures in Steam-Assisted Gravity Drainage Process Water Samples from Athabasca Oil Sands." *Energy and Fuels*. https://doi.org/10.1021/acs.energyfuels.7b00483.

Razi, Maryam, Shayandev Sinha, Prashant R. Waghmare, Siddhartha Das, and Thomas Thundat. 2016. "Effect of Steam-Assisted Gravity Drainage Produced Water Properties on Oil/Water

Transient Interfacial Tension." *Energy and Fuels* 30 (12): 10714–20. https://doi.org/10.1021/acs.energyfuels.6b01686.

Russell, Caroline G., Desmond F. Lawler, and Gerald E. Speitel. 2009. "NOM Coprecipitation with Solids Formed during Softening." *Journal / American Water Works Association*. https://doi.org/10.1002/j.1551-8833.2009.tb09879.x.

Russell, Caroline G., Desmond F. Lawler, Gerald E. Speitel, and Lynn E. Katz. 2009. "Effect of Softening Precipitate Composition and Surface Characteristics on Natural Organic Matter Adsorption." *Environmental Science and Technology* 43 (20): 7837–42. https://doi.org/10.1021/es900991n.

Sawyer, C N, and P L McCarty. 1978. *Chemistry for Environmental Engineering*. *McGraw-Hill Series in Water Resources and Environmental Engineering*.

Schott, Hans. 1981. "Electrokinetic Studies of Magnesium Hydroxide." *Journal of Pharmaceutical Sciences* 70 (5): 486–89. https://doi.org/10.1002/jps.2600700505.

Skoglund, Sara, Jonas Hedberg, Elena Yunda, Anna Godymchuk, Eva Blomberg, and Inger Odnevall Wallinder. 2017. "Difficulties and Flaws in Performing Accurate Determinations of Zeta Potentials of Metal Nanoparticles in Complex Solutions - Four Case Studies." *PLoS ONE*. https://doi.org/10.1371/journal.pone.0181735.

Skybová, M., Ľ Turčániová, S. Čuvanová, A. Zubrik, S. Hredzák, and Ľ Hudymáčová. 2007. "Mechanochemical Activation of Humic Acids in the Brown Coal." *Journal of Alloys and Compounds*. https://doi.org/10.1016/j.jallcom.2006.08.310.

Somasundaran, P., and G. E. Agar. 1967. "The Zero Point of Charge of Calcite." *Journal of Colloid And Interface Science*. https://doi.org/10.1016/0021-9797(67)90241-X.

Stipp, S. L.S. 1999. "Toward a Conceptual Model of the Calcite Surface: Hydration, Hydrolysis,

and Surface Potential." *Geochimica et Cosmochimica Acta*. https://doi.org/10.1016/S0016-7037(99)00239-2.

Stipp, Susan L., and Michael F. Hochella. 1991. "Structure and Bonding Environments at the Calcite Surface as Observed with X-Ray Photoelectron Spectroscopy (XPS) and Low Energy Electron Diffraction (LEED)." *Geochimica et Cosmochimica Acta*. https://doi.org/10.1016/0016-7037(91)90142-R.

Stumm, Werner. 1992. *Surface Charge and the Electric Double Layer*. *Chemistry of the Solid-Water Interface: Processes at the Mineral-Water and Particle-Water Interface in Natural Systems*.

Szyguła, Agata, Eric Guibal, Montserrat Ruiz, and Ana Maria Sastre. 2008. "The Removal of Sulphonated Azo-Dyes by Coagulation with Chitosan." *Colloids and Surfaces A: Physicochemical and Engineering Aspects*. https://doi.org/10.1016/j.colsurfa.2008.08.001.

Thompson, Dudley William, and Pamela Gillian Pownall. 1989. "Surface Electrical Properties of Calcite." *Journal of Colloid And Interface Science*. https://doi.org/10.1016/0021-9797(89)90147-1.

U.S. Environmental Protection Agency. 1991. *MINTEQA2/PRODEFA2, A GEOCHEMICAL ASSESSMENT MODEL FOR ENVIRONMENTAL SYSTEMS: VERSION 3.0 USER'S MANUAL*. ATHENS,.

Wang, Yuanfang, Baoyu Gao, Qinyan Yue, Xiao Zhan, Xiaohui Si, and Chunxiao Li. 2009. "Flocculation Performance of Epichlorohydrin-Dimethylamine Polyamine in Treating Dyeing Wastewater." *Journal of Environmental Management*. https://doi.org/10.1016/j.jenvman.2009.09.012.

Wells, R.C. 1915. "The Solubility of Calcite in Water in Contact with the Atmosphere, and Its

Variation with Temperature Wells R.C." *J.Wash. Aca. Sci.*, 617–22.

Wolthers, Mariëtte, Laurent Charlet, and Philippe Van Cappellen. 2008. "The Surface Chemistry of Divalent Metal Carbonate Minerals: A Critical Assessment of Surface Charge and Potential Data Using the Charge Distribution Multi-Site Ion Complexation Model." *American Journal of Science*. https://doi.org/10.2475/08.2008.02.

Yin, Chun Yang. 2010. "Emerging Usage of Plant-Based Coagulants for Water and Wastewater Treatment." *Process Biochemistry*. https://doi.org/10.1016/j.procbio.2010.05.030.

Yoon, Seong Hoon, Chung Hak Lee, Kyu Jin Kim, and Anthony G. Fane. 1998. "Effect of Calcium Ion on the Fouling of Nanofilter by Humic Acid in Drinking Water Production." *Water Research* 32 (7): 2180–86. https://doi.org/10.1016/S0043-1354(97)00416-8.

Yue, Q. Y., B. Y. Gao, Y. Wang, H. Zhang, X. Sun, S. G. Wang, and Roy R. Gu. 2008. "Synthesis of Polyamine Flocculants and Their Potential Use in Treating Dye Wastewater." *Journal of Hazardous Materials* 152 (1): 221–27. https://doi.org/10.1016/j.jhazmat.2007.06.089.

Zeng, Teng, Russell Jingxian Li, and William A. Mitch. 2016. "Structural Modifications to Quaternary Ammonium Polymer Coagulants to Inhibit N-Nitrosamine Formation." *Environmental Science and Technology*. https://doi.org/10.1021/acs.est.6b00602.

Zhang, Lu, Dinesh Mishra, Kailun Zhang, Basil Perdicakis, David Pernitsky, and Qingye Lu. 2020. "Electrokinetic Study of Calcium Carbonate and Magnesium Hydroxide Particles in Lime Softening." *Water Research*. https://doi.org/10.1016/j.watres.2020.116415.

Zhou, Jingjing, Wenjing Zhang, Dan Liu, Zhuo Wang, and Shuo Li. 2017. "Influence of Humic Acid on the Transport and Deposition of Colloidal Silica under Different Hydrogeochemical Conditions." *Water (Switzerland)* 9 (1).

https://doi.org/10.3390/w9010010.

Zueva, S. B., P. Macolino, A. L. Manciulea, and F. Vegliò. 2015. “Polyamine Flocculation Applied to Household Batteries Recycling.” *Journal of Material Cycles and Waste Management*. https://doi.org/10.1007/s10163-014-0265-7.

Appendix A1: Statement of Contribution

The contributions of the authors for each publication and manuscript are listed below:

Electrokinetic Study of Calcium Carbonate and Magnesium Hydroxide Particles in Lime Softening

Dr. Dinesh Misha, Kailun Zhang, and I were co-primary authors of this publication. I developed the methodology and protocol for the research work including procedures for water sample preparation, operation and set-up of zeta potential analyzer, and integration of chemistry modelling for data interpretation. I also composed the manuscript and analyzed results from the experiments performed. Dr. Dinesh Mishra provided guidance on shaping the research, assisted with performing measurements and setting up models, interpreting chemistry modelling results, as well as undertook editorial work on the manuscripts. Kailun Zhang aided in carrying out a portion of experiments to validate measurements. Dr. David Pernitsky and Dr. Basil Perdicakis provided suggestions during the project work and critical feedback during the revisions of the manuscripts. Dr. Qingye Lu supervised the findings of the work, supported the design and implementation of the research, and revised the manuscript which greatly improved the quality of the publication.

Impact of Solution Feed Deviations on Polymer Coagulant Dose in Synthetic SAGD Produced Water

Dr. Dinesh Misha and I were co-primary authors of this publication. I developed the methodology and protocol for the research work including procedures for SAGD synthetic water sample preparation, operation and control of the programmable jar tester, and chemical dosing calculation. I also composed the manuscript and analyzed results from the experiments performed. Dr. Dinesh

Mishra assisted with jar testing and result interpretation, carried out ICP measurements, and undertook editorial work on the manuscripts. Kailun Zhang aided in carrying out a portion of during jar test experiments. Dr. David Pernitsky and Dr. Basil Perdicakis provided suggestions during the project work and critical feedback during the revisions of the manuscripts. Dr. Qingye Lu supervised the findings of the work, supported the design and implementation of the research, and revised the manuscript.

Publications

Zhang, L., Mishra, D., Zhang, K., Perdicakis, B., Pernitsky, D., & Lu, Q. (2020). Electrokinetic study of calcium carbonate and magnesium hydroxide particles in lime softening. *Water Research*. https://doi.org/10.1016/j.watres.2020.116415

Copyright Permissions

ELSEVIER

Dear Lu Zhang,

Thank you for your query.

Please note that, as one of the authors of this article, you retain the right to reuse it in your thesis/dissertation. You do not require formal permission to do so. You are permitted to post this Elsevier article online if it is embedded within your thesis. You are also permitted to post your Author Accepted Manuscript online.

However posting of the final published article is prohibited.

*"As per our Sharing Policy, authors are permitted to post the Accepted version of their article on their institutional repository – as long as it is for **internal institutional use only.***

It can only be shared publicly on that site once the journal-specific embargo period has lapsed. For a list of embargo periods please see: Embargo List.

You are not permitted to post the Published Journal Article (PJA) on the repository."

Please feel free to contact me if you have any queries.

Regards,

Kaveri

Permissions Helpdesk
ELSEVIER |Operations

PERMISSION OF CO-AUTHORS

Lu Zhang	*SIGNATURE COVERED AS PER REQUIREMENT SET BY THE FACULTY OF GRADUATE STUDY*
NAME OF COPYRIGHT AUTHOR	**SIGNATURE OF COPYRIGHT AUTHOR**

We, the undersigned, hereby grant permission to Lu Zhang to include the following two manuscripts in his Master of Engineering thesis:

1. **Lu Zhang, Dinesh Mishra, Kailun Zhang, Basil Perdicakis, David Pernitsky, and Qingye Lu, "Electrokinetic Study of Calcium Carbonate and Magnesium Hydroxide Particles in Lime Softening" in Water Research, 2020, 186, 116415 (doi.org/10.1016/j.watres.2020.116415).**
2. **Lu Zhang, Dinesh Mishra, Kailun Zhang, Basil Perdicakis, David Pernitsky, and Qingye Lu, "Impact of Influent Deviations on Polymer Coagulant Dose in Warm Lime Softening of Synthetic SAGD Produced Water"**

NAMES OF CO-AUTHORS	**SIGNATURE OF CO-AUTHORS**
Dinesh Mishra	*SIGNATURE COVERED AS PER REQUIREMENT SET BY THE FACULTY OF GRADUATE STUDY*
Kailun Zhang	*SIGNATURE COVERED AS PER REQUIREMENT SET BY THE FACULTY OF GRADUATE STUDY*
Qingye Lu	*SIGNATURE COVERED AS PER REQUIREMENT SET BY THE FACULTY OF GRADUATE STUDY*
David Pernitsky	*SIGNATURE COVERED AS PER REQUIREMENT SET BY THE FACULTY OF GRADUATE STUDY*
Basil Perdicakis	*SIGNATURE COVERED AS PER REQUIREMENT SET BY THE FACULTY OF GRADUATE STUDY*